Signal Processing of FMCW Synthetic Aperture Radar Data

The pictures on the cover are FMCW SAR images produced with and without using the range frequency non-linearity correction algorithm developed by the author. (See also figure 7.11 of this thesis).

Signal Processing of FMCW Synthetic Aperture Radar Data

Proefschrift

ter verkrijging van de graad van doctor
aan de Technische Universiteit Delft,
op gezag van de Rector Magnificus prof.dr.ir. J.T. Fokkema,
voorzitter van het College voor Promoties,
in het openbaar te verdedigen op maandag 2 oktober 2006 om 15:00 uur

door

Adriano META
Laurea di dottore in Ingegneria delle Telecomunicazioni
Universita’ degli Studi di Roma “La Sapienza”

geboren te Pontecorvo, Italië.

Dit proefschrift is goedgekeurd door de promotor:
Prof.ir. P. Hoogeboom
Prof.dr.ir. L.P. Ligthart

Samenstelling promotiecomissie:

Rector Magnificus,	voorzitter
Prof.ir. P. Hoogeboom	Technische Universiteit Delft, promotor
Prof.dr.ir. L.P. Ligthart,	Technische Universiteit Delft, promotor
Prof.dr. C. Baker,	University College London
Prof.dr. A. Moreira,	DLR Institut für Hochfrequenztechnik und Radarsysteme
Prof.dr. S. Vassiliadis,	Technische Universiteit Delft
Dr.ir. R.F. Hanssen,	Technische Universiteit Delft
Drs. W. Pelt,	Ministerie van Defensie

This research was supported by the Dutch Technology Foundation STW, applied science division NWO and the technology programme of the Ministry of Economic Affairs. The project was granted under number DTC.5642.
The work was furthermore supported by TNO Defence, Security and Safety.

ISBN 907692810X
Signal Processing of FMCW Synthetic Aperture Radar Data.
Dissertation at Delft University of Technology.
Copyright © 2006 by A. Meta.

All rights reserved. No parts of this publication may be reproduced or transmitted in any form or by any means, electronic or mechanical, including photocopy, recording, or any information storage and retrieval system, without permission in writing from the author.

to our little Andrea

Contents

1 Introduction **1**
1.1 Research motivation . . . 2
1.2 Research objectives . . . 2
1.3 Novelties and main results . . . 3
1.4 Outline of the thesis . . . 4
References . . . 5

2 FMCW radar and SAR overview **7**
2.1 The FMCW radar principle . . . 7
2.2 The Synthetic Aperture Radar principle . . . 9
2.2.1 Range migration . . . 10
2.2.2 Motion errors . . . 10
References . . . 11

3 Range processing in FMCW **13**
3.1 Introduction . . . 13
3.2 Linear deramped FMCW signals . . . 14
3.2.1 Stationary targets . . . 15
3.2.2 Moving targets . . . 16
3.3 Non-linearities in FMCW signals . . . 16
3.4 Non-linearity correction . . . 17
3.4.1 Algorithm overview . . . 19
3.4.2 Analytical development . . . 21
3.4.3 Simulation . . . 22
3.4.4 Frequency non-linearity estimation . . . 24
3.5 Linear SFCW signal . . . 25
3.6 Randomized non-linear SFCW . . . 26
3.6.1 Non linear deramping technique . . . 26
3.6.2 Stationary targets . . . 28
3.6.3 Moving targets . . . 29
3.6.4 Influence of hardware non ideality . . . 31
3.7 Summary . . . 32

References . . . 33

4 Cross-range imaging with FMCW SAR 35
4.1 Introduction . . . 35
4.2 Signal processing aspects . . . 36
4.3 Analytical development . . . 39
4.4 Stripmap FMCW SAR simulation . . . 40
4.5 Spotlight FMCW SAR . . . 41
4.6 Digital beam forming FMCW SAR . . . 42
4.7 Summary . . . 46
References . . . 46

5 Moving Targets and FMCW SAR 49
5.1 Introduction . . . 49
5.2 Moving target Doppler spectrum . . . 50
5.3 MTI with linear triangular FMCW SAR . . . 51
5.4 MTI with randomized non-linear SFCW SAR . . . 55
5.5 Summary . . . 60
References . . . 60

6 FMCW SAR demonstrator system 61
6.1 Introduction . . . 61
6.2 Front-end . . . 62
6.2.1 Steering signal . . . 63
6.2.2 Predistorted linearization . . . 63
6.3 Noise power calculation . . . 67
6.3.1 Thermal noise . . . 68
6.3.2 Phase noise . . . 69
6.3.3 Quantization noise . . . 70
6.3.4 Total noise . . . 70
6.4 Experimental tests . . . 70
6.4.1 Noise laboratory measurements . . . 71
6.4.2 Phase measurements . . . 71
6.5 Summary . . . 71
References . . . 72

7 Flight test campaign results 73
7.1 Introduction . . . 73
7.2 Overview of the flight campaign . . . 74
7.3 Non-linearities correction . . . 78
7.3.1 First example . . . 78
7.3.2 Second example . . . 81
7.3.3 Third example . . . 83

7.4 High resolution images . . . 85
7.5 Medium resolution images . . . 87
7.6 Low resolution image . . . 90
7.7 Resolution comparison . . . 92
7.8 Triangular FMCW SAR test . . . 95
7.9 Summary . . . 98
References . . . 98

8 Conclusions and discussion **99**
8.1 Contributions of this research . . . 99
8.2 Recommendations . . . 100
8.3 Related works at other institutes . . . 101
References . . . 101

A Non-linear Frequency Scaling Algorithm for FMCW SAR data **103**
A.1 Introduction . . . 103
A.2 Deramped non-linear FMCW SAR signal . . . 104
A.3 Frequency non-linearity, Doppler shift and range cell migration correction . . . 106
A.4 Summary . . . 107
References . . . 107

List of acronyms **109**

List of symbols **111**

Summary **115**

Samenvatting **117**

Author's publications **119**

Acknowledgements **121**

About the author **123**

Chapter 1

Introduction

In the field of airborne earth observation, there is special attention for compact, cost effective, high resolution imaging sensors. Such sensors are foreseen to play an important role in small-scale remote sensing applications, such as the monitoring of dikes, watercourses, or highways. Furthermore, such sensors are of military interest; reconnaissance tasks could be performed with small unmanned aerial vehicles (UAVs), reducing in this way the risk for one's own troops.

In order to be operated from small, even unmanned, aircrafts, such systems must consume little power and be small enough to fulfill the usually strict payload requirements. Moreover, to be of interest for the civil market, a reasonable cost is mandatory.

Radar-based sensors have advantages over optical systems in their all weather capability and in the possibility to operate through smoke and at night. However, radar sensors used for imaging purposes exhibit relative low resolution in the cross-range or azimuth dimension, and furthermore it gets coarser with increasing distance due to the constant antenna beamwidth. This limitation is overcome by *Synthetic Aperture Radar* (SAR) techniques. Such techniques have already been successful employed in the field of radar earth observation by using coherent pulse radars. However, pulse radar systems are usually very complex instruments, and neither low cost nor compact. The fact that they are quite expensive makes them less suitable for low-cost, civil applications, while their bulkiness could prevent them from being chosen for UAV or small aircraft solutions.

Frequency Modulated Continuous Wave (FMCW) radar systems are, instead, generally compact and relatively cheap to purchase and to exploit. FMCW radars consume little power and, due to the fact that they are continuously operating, they can transmit a modest power, which makes them very interesting for military applications. Consequently, FMCW radar technology is of interest for both civil and military airborne earth observation applications, specially in combination with high resolution SAR techniques. The novel combination of FMCW technology and SAR techniques leads to the development of a small, lightweight, and cost-effective high resolution imaging sensor.

1.1 Research motivation

SAR techniques have been successfully applied in combination with coherent pulse radars. Also the concept of synthetic aperture with FMCW sensors has already been put forward in literature, [1] [2], and some experimental systems have been described, [3] [4]. However, the practical feasibility of an *airborne FMCW SAR was not evident*; the experimental sensors described in literature were, in fact, radars mounted on rail supports operating in ground SAR configurations and at short distances. These FMCW radars could perform measurements in each position of the synthetic aperture and then be moved to the next one. As in conventional pulse SAR systems, the stop-and-go approximation could be used; such an approximation assumes the radar platform stationary during the transmission of the electromagnetic pulse and the reception of the corresponding echo. The approximation is valid for conventional pulse systems because the duration of the transmitted waveform is relatively short and, of course, is also valid for ground FMCW SAR where the radar can be actually fixed in a predetermined position while making the measurements. For airborne FMCW radars, however, the stop-and-go approximation can be not valid anymore because the platform is actually moving while continuously transmitting. A complete model for the deramped FMCW SAR signal derived without using the stop-and-go approximation *was missing in the literature.*

In addition to the particular signal aspects relative to the combination of FMCW technology and SAR techniques, the use of FMCW radars for high resolution and long range applications was not evident. In practical FMCW sensors, in fact, the presence of unwanted non-linearities in the frequency modulation severely degrades the radar performances for large distances. Again, proper processing methods to overcome such limitation due to frequency non-linearities *were not available* to the scientific community.

Therefore, the area of FMCW SAR airborne observation and related signal processing aspects was a very novel field of research. At the International Research Centre for Telecommunications and Radar (IRCTR) of the Delft University of Technology, a project was initiated to investigate the feasibility of FMCW SAR in the field of airborne earth observation and to develop proper processing algorithms to fully exploit the capability of such sensors.

1.2 Research objectives

Following from the motivations previously discussed, the first main objective of the project was to develop special processing SAR algorithms which could take into account the peculiar characteristics of an FMCW sensor. The features of major interest were: the presence of frequency non-linearities in the transmitted waveform and the fact that the FMCW sensor is continuously transmitting. The non-linearities represent a difference between an ideal and actual system, while the continuous motion has to be faced even when using sensors with performance close to the ideal. In the literature, some non-linearity correction algorithms were available, however they work only for very limited range intervals and, furthermore, require a reference point in each interval. For larger distance applications, as in the case for SAR, the use of these algorithms is not efficient neither robust. In FMCW SAR, the

fact that the radar is continuously transmitting while moving means that the stop-and-go approximation used for the derivation of conventional SAR algorithms could not be anymore valid. These aspects needed to be analyzed and solutions had to be provided.

The continuous transmission, on the other hand, can be used as an advantage in different other applications, as Moving Target Indication (MTI). In fact, in FMCW sensors, the pulse duration is considerably longer than in pulse radars, and therefore a better range frequency resolution is possible. The combination of this property and the possibility of using different kind of modulations (linear and non-linear) was investigated to see whether some FMCW SAR properties could be used to enhance the indication of moving targets.

The other main objective of the project was to show the practicability of FMCW SAR under operational circumstances. Therefore, concurrently with the signal processing algorithms elaboration, the development of a fully operational airborne demonstrator system and an X-band radar front-end was started at the Delft University of Technology. A complete and detailed sensor model was required in order to estimate and analyze the performances of the system during the operational mode. In addition, the demonstrator system had to prove that an FMCW SAR sensor can indeed be operated in an efficient and cost effective manner from a very small airborne platform. The work for the initial requirements to the FMCW SAR system, the acquisition design and the development of the controlling software has been done by dr.ir. J.J.M. de Wit within the framework of the project [5]. This part will not be treated in this thesis.

1.3 Novelties and main results

Corresponding to the objectives set by the research project, the following novelties and main results have been reached and are presented in this thesis:

- *Non-linearity correction.* The author has developed a very innovative processing solution, which completely solves the problem of the presence of frequency non-linearities in FMCW SAR. It corrects for the non-linearity effects for the whole range profile in one step, and it allows perfect range focusing, independently of the looking angle. The proposed method operates directly on the deramped data and it is very computationally efficient (Chapter 3, Section 3.4).

- *Deramping technique for non-linear Stepped Frequency Continuous Wave (SFCW) signals.* An extension to non-linear continuous signals of the deramping technique, commonly used in linear FMCW sensors, has been developed. With the proposed extension, the great reduction in terms of sampling requirements can be achieved also when using non-linear waveforms, at the cost of increased computation (Chapter 3, Section 3.6.1).

- *A complete FMCW SAR signal model.* The author has derived a detailed analytical model for the FMCW SAR signal in the two-dimensional frequency domain. Based

on this model, proper algorithms are developed which guarantee the best performances when processing FMCW SAR data (Chapter 4).

- *MTI with slope diversity in linear FMCW SAR.* The author has exploited the possibility of using triangular modulation for MTI by producing two images, respectively with the upslope and downslope part of the transmitted waveform. Based on the FMCW SAR signal model, interferometric techniques on the pair of images can be used to help distinguishing moving targets from stationary clutter (Chapter 5, Section 5.3).

- *MTI with randomized SFCW SAR.* Based on the non-linear deramping technique previously proposed, the author has analyzed how randomized non-linear SFCW SAR can be used for MTI purposes (Chapter 5, Section 5.4).

- *Detailed system model.* A complete model description of the X-band FMCW SAR front-end system developed at the IRCTR, Delft University of Technology, has been provided. The system has been extensively tested by the author together with P. Hakkart and W.F. van der Zwan through ground and laboratory measurements, the results showing very good consistency with the developed model (Chapter 6).

- *First demonstration of an X-band FMCW SAR.* A flight test campaign has been organized during the last part of 2005. The results were very successful. The feasibility of an operational cheap FMCW SAR under practical circumstances has been proved.

- *High resolution FMCW SAR images.* Thanks to the special algorithms developed, FMCW SAR images with 45 cm times 25 cm resolution (including windowing) have been obtained for the first time.

1.4 Outline of the thesis

The remaining of this thesis is divided in seven chapters: in the first four, the theory of FMCW SAR is introduced. Subsequently, the experimental system built at the IRCTR is described; the methods previously developed are validated by processing real FMCW SAR data collected during the flight test campaign organized in the last part of 2005. The thesis is organized as follows:

Chapter 2 provides a short overview of the FMCW radar and SAR principles. It introduces aspects which are then more deeply analyzed and discussed in the subsequent chapters.

Chapter 3 deals with the range processing of FMCW data and presents a novel processing solution, which completely solves the frequency non-linearity problem. It corrects for the non-linearity effects for the whole range profile and Doppler spectrum in one step, it operates directly on the deramped data and it is very computationally efficient. Non-linear SFCW modulation is also treated in the chapter; a novel deramping technique extended to the case of non-linear signals is introduced. With the extended deramping

technique proposed here, a reduced sampling frequency as for the linear case can be used also for randomized SFCW signals, at the cost of increased computation.

Chapter 4 derives a complete analytical model of the FMCW SAR signal description in the two-dimensional frequency domain, starting from the deramped signal and without using the stop-and-go approximation. The model is then applied to stripmap, spotlight and single transmitter/multiple receiver Digital Beam Forming (DBF) synthetic aperture operational modes. Specially in the last two cases, the effects of the motion during the transmission and reception of the pulse can become seriously degrading for the SAR image quality, if not compensated.

Chapter 5 exploits the peculiar characteristics of the complex FMCW SAR image for Moving Target Indication purposes. Two MTI methods are proposed in the chapter. The first is based on the frequency slope diversity in the transmitted modulation by using linear triangular FMCW SAR. The second makes use of the Doppler filtering properties of randomized SFCW modulations.

Chapter 6 describes the X-band radar front-end developed at the Delft University of Technology. A detailed system model is provided in order to estimate and analyze the performance of the demonstrator system. Laboratory and ground based measurements show very good consistency with the calculated values, validating the model description.

Chapter 7 presents the results obtained from the FMCW SAR flight test campaign organized during the last part of 2005. Thanks to the special algorithms which have been developed during the research project and described in the previous chapters, FMCW SAR images with a measured resolution up to 45 cm times 25 cm (including windowing) were obtained for the first time. Several tests performed during the flight campaign (imaging at different resolutions, varying the incident angle, MTI experiment) are reported and discussed.

Chapter 8 summarizes the main results of the study which have led to this thesis; additionally, it draws conclusions and gives some recommendations for future work. Finally, as a demonstration of the increasing interest in FMCW SAR from the scientific and industry community, the chapter reports some related works started at other institutes.

References

[1] H. D. Griffiths, "Synthetic Aperture Processing for Full-Deramp Radar," *IEE Electronic Letters*, vol. 24, no. 7, pp. 371–373, Mar. 1988.

[2] M. Soumekh, "Airborne Synthetic Aperture Acoustic Imaging," *IEEE Trans. on Image Processing*, vol. 6, no. 11, pp. 1545–1554, Nov. 1997.

[3] G. Connan, H. D. Griffiths, P. V. Brennan, D. Renouard, E. Barthlmy, and R. Garello, "Experimental Imaging of Internal Waves by a mm-Wave Radar," in *Proc. MTS/IEEE Oceans '98*, Nice, France, Sept. 1998, pp. 619–623.

[4] Y. Yamaguchi, "Synthetic Aperture FM-CW Radar Applied to the Detection of Objects Buried in Snowpack," *IEEE Trans. Geosci. Remote Sensing*, vol. 32, no. 1, pp. 11–18, Jan. 1994.

[5] J. J. M. de Wit, *Development of an Airborne Ka-Band FM-CW Synthetic Aperture Radar*. Delft University of Technology, Ph. D. thesis, 2005.

Chapter 2

FMCW radar and SAR overview

The chapter provides a short overview of the FMCW radar and SAR principles; it introduces aspects which are then deeply analyzed and discussed in the following of the thesis.

2.1 The FMCW radar principle

FMCW is a continuous wave (CW) radar which transmits a frequency modulated (FM) signal [1]. In linear FMCW radars, the used modulation is usually a sawtooth. The ramp is also known as a chirp, fig. 2.1(a). Objects illuminated by the antenna beam scatter part of the transmitted signal back to the radar, where a receiving antenna collects this energy. The time the signal travels to an object, or target, at a distance r and comes back to the radar is given by:

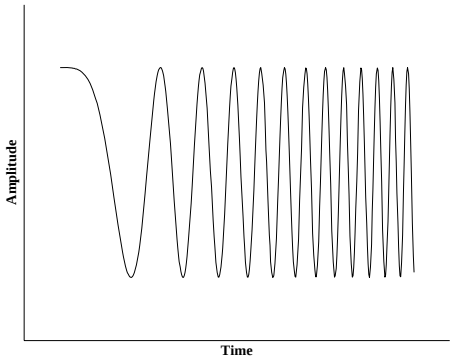
$$\tau = \frac{2r}{c} \tag{2.1}$$

where c is the speed of light. In a homodyne FMCW receiver, the received signal is mixed with a replica of the transmitted waveform and low pass filtered. This process is usually called stretching or deramping. The resulting output is called the beat (or intermediate frequency) signal. From fig. 2.1(b), it can be seen that the frequency of the beat signal is directly proportional to the target time delay, and hence to the distance. The beat frequency is expressed as:

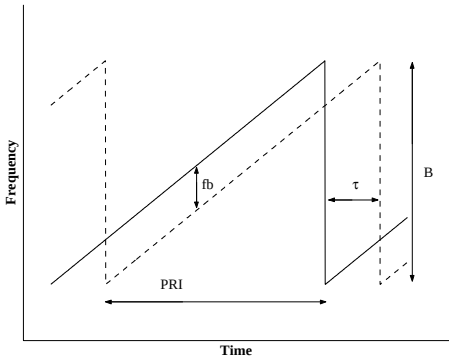
$$f_b = \frac{B}{PRI}\tau \tag{2.2}$$

where B is the transmitted bandwidth given by the frequency sweep and PRI is the pulse repetition interval. In order to compress the range response, a Fourier transform is performed on the beat signal (fig. 2.1(c)), making the signal content available in the frequency domain. The response of a single target is qualitatively shown in fig. 2.1(d). A practical resulting signal from an FMCW sensor is the superposition of different sinusoidal signals, corresponding to the environment being illuminated by the radar waves. In this case, the sidelobes of a strong target response could cover the signal of a weaker scatterer. Windowing the signal before

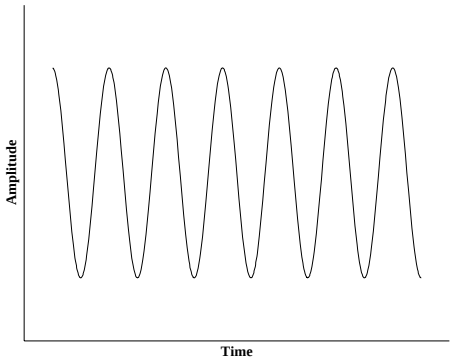
applying the Fourier transform can reduce the sidelobe level at the expense of a broadening of the main lobe. If a target is moving while being illuminated by the radar, its radial velocity



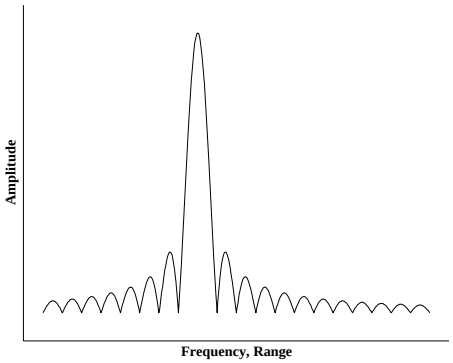
(a) Amplitude plot of a chirp signal. The frequency is linearly increasing with time



(b) Frequency plot of the chirp signal. The received signal (dashed) is a delay version of the transmitted (solid)



(c) Beat signal representation in the time domain. The signal frequency is proportional to the scatterer distance.



(d) Beat signal representation in the frequency domain. The frequency axis can be directly associated with range.

Figure 2.1: Overview of the linear FMCW radar principle.

component causes an additional Doppler frequency shift superimposed on the beat frequency due to the actual distance, leading to an invalid range measurement. The Doppler shift is given by:

$$f_D = \frac{2v_r}{\lambda} \tag{2.3}$$

where v_r is the velocity in the radial direction and λ is the wavelength of the transmitted signal.

2.2 The Synthetic Aperture Radar principle

In conventional Real Aperture Radar (RAR) systems, the azimuth resolution deteriorates with increasing distances due to the constant antenna beamwidth. The RAR azimuth resolution $\delta az_{RAR}$is given as:

$$\delta az_{RAR} \approx \theta_{az} R \tag{2.4}$$

in which θ_{az} is the azimuth 3-dB antenna beamwidth and R is the target distance. It can be noticed that in RAR systems the azimuth resolution is range dependent. The antenna beamwidth is related to the antenna length l_{az} by:

$$\theta_{az} \approx \frac{\lambda}{l_{az}} \tag{2.5}$$

As can be seen from (2.4) and (2.5), the azimuth resolution improves as the antenna length increases. In synthetic aperture radar a large antenna length is synthesized by making use of the motion of the radar platform [2]. The platform on which the SAR is mounted is usually an aircraft or satellite. In order to review the SAR principle we will use a stripmap configuration. Its geometry and the radar position relative to the ground is shown in fig. 2.2. A burst of pulses

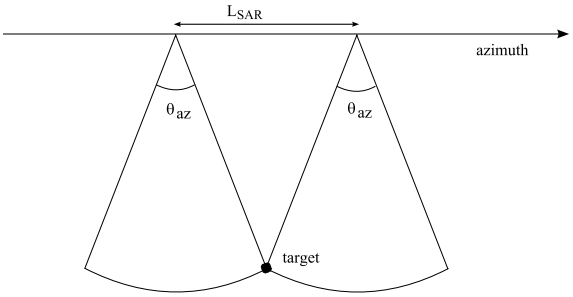


Figure 2.2: Stripmap SAR geometry.

is transmitted by the side-looking antenna pointed to the ground and the backscattered power of each pulse is collected. The SAR is a coherent system, which means it retains the amplitude and phase of the responses at each position as the radar moves. Due to the radar platform motion, a stationary target is seen from different angles, which determines a variation of the radial velocity between the radar and the target. The Doppler shift induced by the radial velocity varies approximately linearly with time (at least for narrow beamwidth systems),

therefore the collected target response exhibits a Doppler bandwidth which is determined by the variation of the angle under which the target is illuminated by the antenna beamwidth:

$$B_D = f_{D_{max}} - f_{D_{min}} \approx \frac{2v}{\lambda} \sin \theta_{az} \tag{2.6}$$

where v is radar velocity. As in conventional pulse compression techniques, this frequency bandwidth determines a temporal resolution equal to:

$$\delta T = \frac{1}{B_D} \tag{2.7}$$

The temporal resolution is directly related to the obtainable SAR along-track resolution by the aircraft velocity:

$$\delta az = v\delta T = \frac{v}{B_D} \tag{2.8}$$

$$= \frac{\lambda}{2 \sin \theta_{az}} \approx \frac{\lambda}{2\theta_{az}} = \frac{l_{az}}{2} \tag{2.9}$$

These are two important expressions for the theoretical azimuth resolution obtainable with a SAR system. Equation (2.9) states that the SAR azimuth resolution is independent of the range and it improves by decreasing the antenna length. This can be intuitively explained because a smaller antenna has a larger beamwidth and therefore a larger Doppler bandwidth is available, as described by the other expression for the azimuth resolution, (2.8). However, reducing the antenna size also decreases its gain.

2.2.1 Range migration

One consideration has to be made about the theoretical SAR resolution. In order to achieve the maximum resolution, the full Doppler bandwidth has to be processed. As the platform moves by, the distance between the target and the radar changes, producing the signal Doppler bandwidth. This range variation can be larger than the range resolution, causing the target response to migrate through different resolution cells. This phenomenon is called Range Cell Migration (RCM). Furthermore, the range migration depends on the distance and this is what makes the SAR reconstruction an inherent two-dimensional inversion problem. Range migration correction is an important step in SAR processing algorithms in order to produce high quality images, and the way it is performed distinguishes one algorithm from one other. We will see in chapter 4 how FMCW signals can influence the range migration correction step when compared to conventional pulse SAR systems.

2.2.2 Motion errors

Synthetic aperture techniques simulate a long array antenna by means of the radar motion. However, in order to achieve the theoretical resolution, the platform motion has to be accurately known. Motion errors distort the phase history of the received signal; furthermore, they cause the amplitude response to move along a different path compared to the ideal range

migration path that it would have when no motion errors were present. Failing in correctly removing motion error distortions causes resolution degradation both in range (because all the target energy will not be confined to one resolution cell) and in cross-range (because the signal phase history will be different from the phase of the reference function). SAR systems are provided with motion sensors in order to reconstruct the platform path; however, usually the accuracy of the reconstructed path is not sufficient in order to get the maximum achievable SAR resolution. Motion data are used to perform a first removal of the motion error effects, and then SAR algorithms process the collected raw data to produce SAR images. Next, autofocus techniques, working directly on the produced complex SAR product, are used to eliminate the residual phase errors, leading therefore to a better focused image.

References

[1] M. I. Skolnik, *Introduction to Radar Systems*. McGraw-Hill, Inc., 1980.

[2] J. C. Curlander and R. N. McDonough, *Synthetic Aperture Radar : Systems and Signal Processing*. John Wiley & Sons, Inc., 1991.

Chapter 3

Range processing in FMCW

The chapter deals with range processing of FMCW data. Using linear modulation, the range compression is achieved by deramping techniques. However, one limitation is the well known presence of non-linearities in the transmitted signal. This results in contrast and range resolution degradation, especially when the system is intended for long range applications. The chapter presents a novel processing solution, which completely solves the non-linearity problem. It corrects for the non-linearity effects for the whole range profile and Doppler spectrum in one step, differently from the algorithms described in literature so far, which work only for very short range intervals. The proposed method operates directly on the deramped data and it is very computationally efficient. Non linear SFCW modulation is also treated in this chapter; a novel deramping technique extended to the case of non linear signals is introduced. The extended deramping technique proposed here allows to use a reduced sampling frequency as for the linear case also for randomized SFCW signals, at the cost of increased computation.

3.1 Introduction

In FMCW sensors, the radar is continuously transmitting and frequency modulation on the transmitted signal is used to measure the distance of a scattering object. In linear FMCW, the deramping technique is often adopted for range processing in order to drastically reduce the sampling frequency. However, such a technique properly works only if the signal frequency ramp is linear. The presence of non-linearities in the transmitted waveform deteriorates the range resolution when the deramping technique is used, because non-linearities spread the target energy through different frequencies [1] [2]. This problem was actually limiting the use of high resolution FMCW systems to short range applications, specially when using cheap component solutions.

A new algorithm has been invented which completely removes the non-linearity effects in the range response. While existing algorithms work only for limited range intervals, the proposed method is effective for the whole range profile and it is very computationally efficient.

The novel method is based on the fact that the deramping accounts for the compression

of the linear part of the signal; therefore, the only part which still needs to be processed with a reference function is the non linear term. Depending on the non-linearity bandwidth, the sampling frequency has to be increased (if necessary) only to satisfy the Nyquist requirements for the non linear term. In order to correct for the spreading in the range profile by a single reference function, the algorithm makes the non-linearity effects range independent.

Another novel aspect discussed in the chapter is the extension of the deramping technique to non-linear signals. Linear frequency modulation offers the advantage of using deramping technique and therefore reducing the sampling requirements. Range information is obtained performing a Fast Fourier Transform (FFT) on the collected data [3]. However, if the signal is not linear (as it is the case for randomized stepped frequency modulation), the FFT on the collected data fails in reconstructing the range information. The data have to be reassembled in order to compensate for the random subpulse sequence order. This operation depends on the target time delay. Moreover, if the delay is larger than the subpulse duration, also a phase shift multiplication is needed. The extended deramping technique proposed here allows to use a reduce sampling frequency as for the linear case also for randomized SFCW signals, at the cost of increased computation.

The following section 3.2 describes the deramped FMCW signal, assuming that the transmitted signal is a linear chirp and then introducing non-linearities in section 3.3. Successively, sections 3.4.1 and 3.4.2 first present an overview of the algorithm and then derive an analytical development assuming the non-linearities as known. Simulation results prove the effectiveness of the proposed method in section 3.4.3. The assumption that the non-linearities are known is overcome in section 3.4.4, where an estimate directly from the deramped data is discussed. This approach offers the advantage that no additional complex circuit in the hardware is required and that it can be applied directly on the collected data. Chapter 7 reports results of the algorithm applied to real data. Successively, in section 3.5 and 3.6 linear and randomized stepped modulation are introduced and a new deramping technique for non-linear SFCW is presented.

3.2 Linear deramped FMCW signals

This section introduces linear FMCW signals and how their properties are exploited by the deramping, or stretching, technique in order to perform the range compression. Usually, the range compression is obtained through matched filtering operation. After a transmitted waveform is sent, the received signal is sampled with a frequency satisfying the Nyquist theorem and successively convoluted with a replica of the transmitted signal. However, when linear frequency modulated signals are used, under certain circumstances discussed in the following section, the deramping technique allows much lower sampling requirements, leading to a smaller data rate to be handled and to a simpler circuitry. In the following, stationary and moving target cases are analyzed.

3.2.1 Stationary targets

When a linear frequency modulation is applied to continuous wave radars, the transmitted signal can be expressed as:

$$s_{t\ lin}(t) = \exp(j2\pi(f_c t + \frac{1}{2}\alpha t^2)) \tag{3.1}$$

where f_c is the carrier frequency, t is the time variable varying within the Pulse Repetition Interval (PRI) and α is the frequency sweep rate equal to the ratio of the transmitted bandwidth B and the PRI. The received signal is a delayed version of the transmitted (amplitude variations are not considered in the derivation):

$$s_{r\ lin}(t) = \exp(j2\pi(f_c(t-\tau) + \frac{1}{2}\alpha(t-\tau)^2)) \tag{3.2}$$

where τ is the time delay. The transmitted and received signals are then mixed, generating the intermediate frequency (or beat) signal:

$$s_{if\ lin}(t) = \exp(j2\pi(f_c\tau + \alpha t\tau - \frac{1}{2}\alpha\tau^2)) \tag{3.3}$$

The beat signal is a sinusoidal signal with frequency proportional to the time delay, and therefore to the target range:

$$f_b = \alpha\tau = \frac{2\alpha}{c}r \tag{3.4}$$

The range resolution is directly proportional to the frequency resolution δf_b, and therefore inversely to the observation time:

$$\delta r = \frac{\delta f_b c}{2\alpha} = \frac{c}{2PRI\,\alpha} = \frac{c}{2B} \tag{3.5}$$

and, of course, it just depends on the processed bandwidth. It is important to note that the sampling requirements are not dictated by the transmitted bandwidth, but by the maximum range of interest, or, more precisely, by the range interval Δr which has to be measured. In fact, the bandwidth B_{IF} of the intermediate frequency signal is given by:

$$B_{IF} = f_{b_{max}} - f_{b_{min}} = \alpha(\tau_{max} - \tau_{min}) = \frac{2\alpha}{c}(r_{max} - r_{min}) = \frac{2\alpha}{c}\Delta r \tag{3.6}$$

The maximum unambiguous range R_u is determined by the sampling frequency f_s, because it limits the maximum measurable beat frequency. If a complex sampling frequency is considered, from (3.4) follows:

$$R_u = \frac{f_s c}{2\alpha} \tag{3.7}$$

This is the main difference compared to conventional pulse systems where the unambiguous range is determined by the PRI. However, with FMCW sensors, the first part of the beat signal is discarded, for the presence of high frequency components, and the ranges of interest are limited in such a way that the processed part of the beat signal is not less than 80% of the total pulse duration [4]. This in order to guarantee enough signal to noise ratio and resolution.

3.2.2 Moving targets

This section analyzes the response of a moving target illuminated by a linear FMCW waveform. The difference with the stationary case previously discussed is the fact that the time delay is not constant anymore but it varies with time. Within a single pulse, CW systems offer the advantage of observing the target for a much longer period compared to conventional pulse sensors. This reflects a different response in linear FMCW radars, because the Doppler component within one single pulse could be not negligible. The time delay of a moving target with a constant radial velocity v_r is expressed by:

$$\tau = \frac{2}{c}(r + v_r t) = \tau_0 + \frac{2}{c} v_r t \tag{3.8}$$

where τ_0 is the equivalent constant time delay for a stationary target. Inserting (3.8) in (3.3) yields:

$$s_{if\ lin}(t) = \exp(j2\pi(f_c\tau_0 + (\alpha\tau_0 + \frac{2v_r}{c} f_c - \frac{2\alpha v_r \tau_0}{c})t - \frac{1}{2}\alpha\tau_0^2 + \frac{2\alpha}{c}(v_r - \frac{v_r^2}{c})t^2)) \tag{3.9}$$

The main contribution is the Doppler shift induced in the beat frequency:

$$f_b \approx \alpha\tau_0 + \frac{2v_r}{c} f_c = \alpha\tau_0 + f_D \tag{3.10}$$

where f_D represents the Doppler frequency component, see (2.3). That means, the peak response is shifted with respect to the true position. Also important is to notice that quadratic terms introduce some defocusing in the response; however the peak amplitude is negligibly affected for moderate velocities. This is due to the Doppler tolerant characteristic of linear FM signals. As we will see in section 3.6, non-linear frequency modulations have different properties which can be exploited for moving target indication applications. In linear FMCW, the degradation of the response of a moving object is due to the fact that the target moves through different resolution cells within one single pulse time. Therefore, the degradation depends on the target velocity, the *PRI* and the transmitted bandwidth.

3.3 Non-linearities in FMCW signals

When frequency non-linearities are present in the transmitted signal, the signal modulation is not an ideal chirp anymore; the phase of the signal can be described as the contribution corresponding to an ideal chirp plus a non-linear error function $\epsilon(t)$:

$$s_t(t) = \exp(j2\pi(f_c t + \frac{1}{2}\alpha t^2 + \epsilon(t))) = s_{t\ lin}(t) s_\epsilon(t) \tag{3.11}$$

The last term $s_\epsilon(t)$, accounting for systematic non-linearities of the frequency modulation, limits the performance of conventional FMCW sensors. This phase distortion increases the spectral bandwidth of the response, resulting in range resolution degradation and losses in terms of signal to noise ratio.

The beat signal is represented by:

$$s_{if}(t) = \exp(j2\pi(f_c\tau + \alpha t\tau - \frac{1}{2}\alpha\tau^2 + (\epsilon(t) - \epsilon(t-\tau)))) = s_{if\ lin}(t)s_\epsilon(t)s_\epsilon(t-\tau)^* \quad (3.12)$$

Equation (3.12) differs from (3.3) in the presence of the last term $(\epsilon(t) - \epsilon(t-\tau))$. This difference results in a spreading of the target energy, deteriorating the range resolution and reducing the peak response. The algorithms correcting for the frequency non-linearities available in literature, [5] [6], use the following:

$$\epsilon_{if}(t, \tau_{ref}) = (\epsilon(t) - \epsilon(t - \tau_{ref})) \approx \tau_{ref}\epsilon'(t) \quad (3.13)$$

which is valid for τ quite small. Then, the non-linearities in the beat signal are approximated as:

$$\epsilon_{if}(t, \tau) \approx \epsilon_{if}(t, \tau_{ref})\frac{\tau}{\tau_{ref}} \quad (3.14)$$

This assumption fails when the range interval of interest increases, as it is the case in SAR applications where the swath of interest is much larger compared to short range operation requirements. In fact, the assumption that the non-linearity effects in the intermediate signal linearly depend on the time delay is valid only for small range intervals. The use of methods based on such an approximation, being range dependent, to compensate for frequency non-linearities in FMCW SAR, requires the separate processing of short intervals of the range profiles, and therefore extremely increases the computational load.

Figure 3.1 shows an example where (3.14) does not correctly describe the real situation. It is evident that the resulting non-linearity effects in the intermediate signal of the two targets are not similar; their dependence is not linear, but it depends on the particular shape of the non-linearity in the transmitted signal.

3.4 Non-linearity correction

Non-linearities cause a range resolution and contrast degradation when the deramping technique is used. For an ideal scatterer response, the beat frequency corresponding to the target is not constant, resulting in a more broadened response after a Fourier transform. The non-linearities in the beat signal are the difference between the transmitted and received non-linearities; in the beat signal, their influence is therefore greater for larger distance. For short distance, the transmitted and received non-linearity phase difference is small and results in a compensation in great part of the original non-linearities. This can be seen in fig. 3.1, where the spreading of the beat signal is greater in the target response at larger distance than at closer distance. Hardware and software approaches are known in literature to face the problem. Hardware solutions include the use of a predistorted Voltage Controlled Oscillator (VCO) steering signal to have a linear FM output and complex synthesizer concepts with phase locked loop. However, the former approach fails when the external conditions, i.e. the temperature, changes while the latter requires quite costly devices. The use of Direct Digital

Synthesizer (DDS) offers a quite cost effective solution [7], but the transmitted bandwidth can still be limited when compared to the one obtained directly sweeping the VCO. Different local oscillator could be used to transmit large bandwidth when using DDS solution, however, the system complexity is increased. Software solutions make use of some reference response to estimate the frequency non-linearity directly from the acquired deramped data, and try to compensate them using different methods: resampling of the data in order to have a linear behavior [5], and matched filtering with a function estimated from the reference response [6]. However, these approaches are based on an approximation of the frequency non-linearity function, which limits their applicability to FMCW short range applications.

A novel algorithm has been invented within the framework of this research [8], which completely removes the effects of the non-linearities in the beat signal, independently of the range and Doppler [9]. The proposed method is superior compared to the existing non-

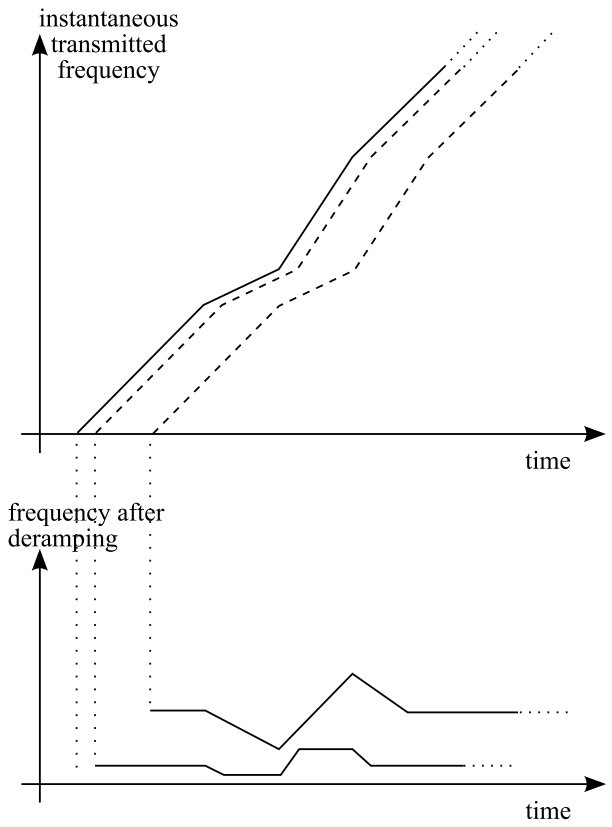


Figure 3.1: Range dependent non-linear effects in the beat frequency signal.

linearity correction algorithms, because it can handle the complete range profile and therefore it is not limited to short range intervals. It is very computational efficient and leads to excellent non-linearity compensation. The following subsections give an overview of the algorithm, followed by an analytical development, simulation results and discussion of some implementation details. The integration of the non-linearity correction in FMCW SAR algorithms is described in appendix A.

3.4.1 Algorithm overview

In this section a heuristic overview of the proposed method is given. In order to have a good understanding of how the algorithm works, it is preferable to have a clear visual representation of which is the distinct transmitted and received non-linearity contribution in the resulting beat signal non-linearities. Therefore, the present explanation uses an example of non-linear FMCW where the non-linearities are localized in a small part of the transmitted signal, as depicted in fig. 3.2. Of course, the algorithm handles also non-linearities whose duration is comparable to the pulse length, as it is in real situations.

The non-linearities present in the beat signal are the result of the interaction between the transmitted and received non-linearities. The removal of the effects induced by the transmit-

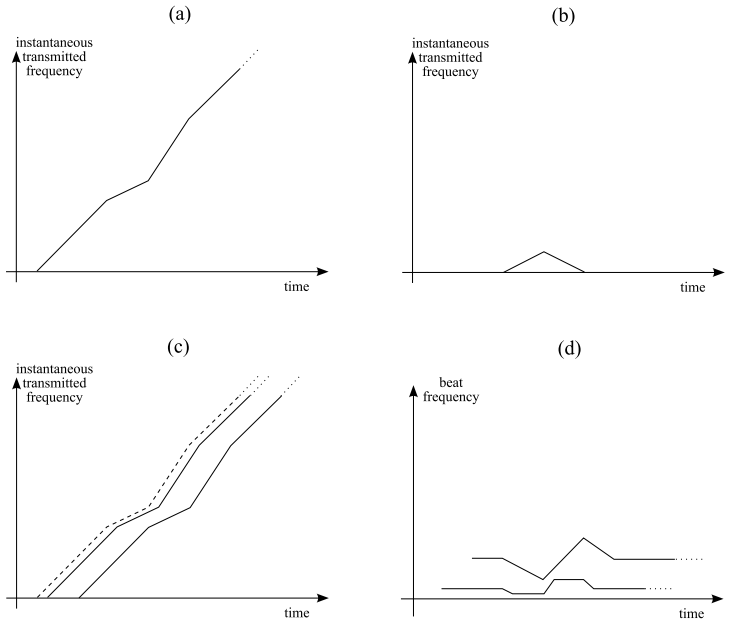


Figure 3.2: Non-linear FMCW signal. The transmitted signal can be thought as the combination of an ideal chirp (a) and a non-linear part (b). The received signal (c) and the transmitted are then mixed, producing the beat signal (d).

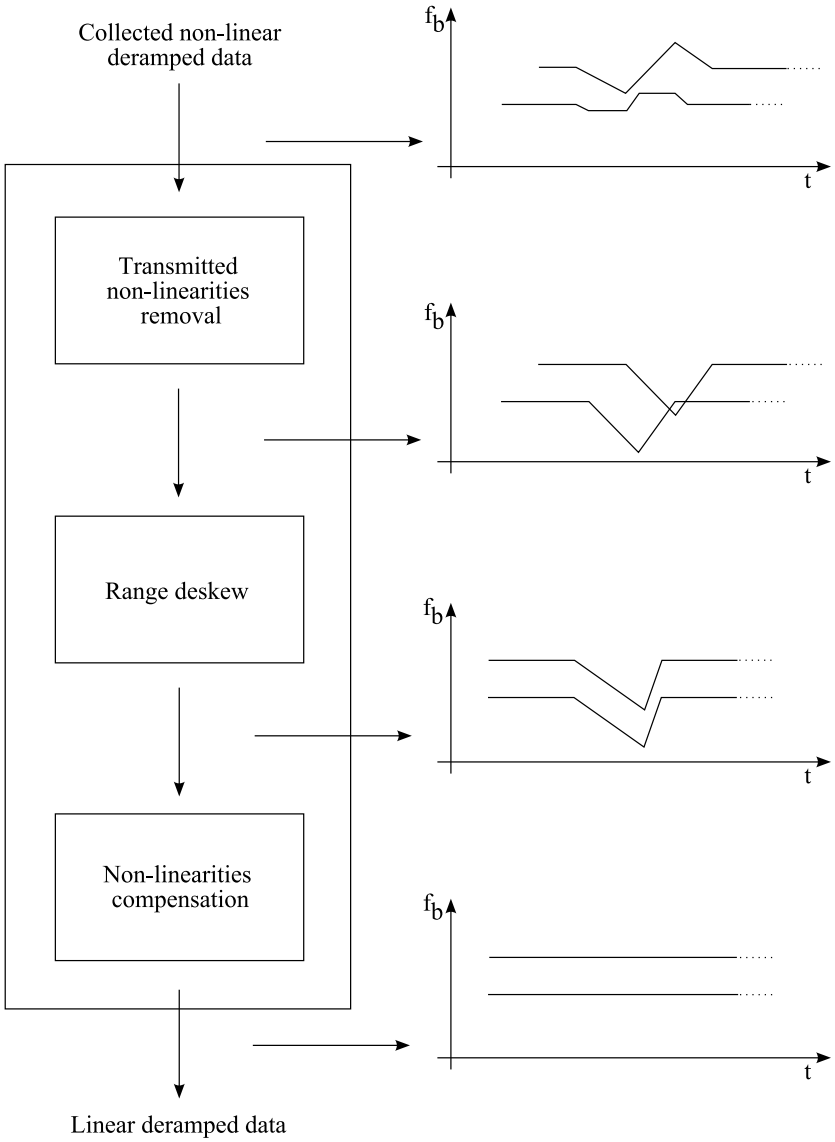


Figure 3.3: Diagram block of the non-linearity correction algorithm.

ted non-linearities is quite simple, because they are the same for all the targets, independently of the range distance. After this step, the remaining non-linearities are due only to the received signal, and therefore have the same shape for all ranges. It is as if the received signal is mixed with an ideal chirp and not with the transmitted signal. However, a straightforward correction is not yet possible; in fact, in the time domain, the non-linearity position depends on the time of arrival of the received signal. This is due to the use of the deramping technique.

In order to remove the non-linearity term with a single reference function, without dividing the range profile in small subparts, every dependence on the time delay needs to be eliminated. The Residual Video Phase (RVP) correction technique is then applied in order to shift in time all the target responses, according to their time of arrival [10]. This effect is obtained through a frequency dependent filter; in fact, the time delay is proportional to the range and therefore to the frequency of the beat signal. Applying RVP correction induces a different time shift at every frequency. This results also in a distortion of the original non-linearities. The non-linearities spread the target response in range and therefore the RVP correction step applies different time shift delay to the energy of the same target. However, all the target responses are affected in the same way, and at this point all the non-linearities can be corrected by a multiplication with a single reference function, obtained by passing the original non-linearity function through the RVP filter. After this last correction, all the non-linearity effects are completely removed, independently of the range for stationary targets. If the frequency non-linearities are such that their Doppler compressed (or expanded) version is quite different from the transmitted, the correction step can be performed in the Doppler domain. A Fourier transform over successive pulses can, in fact, discriminate the responses according their Doppler components and therefore the required Doppler dependent correction can be applied [9]. The resulting beat frequency signal contains only linear frequency terms and its Fourier transform will result in a completely focused range profile.

3.4.2 Analytical development

The beat signal, in the general case when non-linearities are present, is described by (3.12). Assuming the non-linearity function $s_\epsilon(t)$ known (its estimation is discussed in section 3.4.4), the contribution to the beat signal non-linearities of the transmitted non-linearities can be eliminated by the following multiplication:

$$s_{if2} = s_{if} s_\epsilon(t)^* = \exp(j2\pi(f_c\tau + \alpha t\tau - \frac{1}{2}\alpha\tau^2 - \epsilon(t-\tau))) \tag{3.15}$$

The remaining non-linearity term is now present only as part of the received signal. The same technique used for the Residual Video Phase removal can be used to induce a range dependent time shift [10]. After obtaining a range profile Fourier transforming the beat signal, a range dependent phase shift is applied. Subsequently, an inverse Fourier transform is performed to obtain again the beat signal:

$$s_{if3} = \mathcal{F}^{-1}\{\mathcal{F}\{s_{if2}\}\exp(j\pi\frac{f^2}{\alpha})\} \approx \exp(j2\pi(f_c\tau + \alpha t\tau - \epsilon_{RVP}(t))) \tag{3.16}$$

where the last phase term represents the non-linearities after they passed through the RVP filter:

$$s_{\epsilon\ RVP} = \mathcal{F}^{-1}\{\mathcal{F}\{s_\epsilon\}\exp(j\pi\frac{f^2}{\alpha})\} \approx \exp(j2\pi\epsilon_{RVP}(t)) \tag{3.17}$$

Now any non-linearity range dependency has been removed and therefore a simple multiplication with $s_{\epsilon\ RVP}(t)$ completely eliminates any effect of the frequency non-linearity:

$$s_{if4} = s_{if3}s_{\epsilon\ RVP} = \exp(j2\pi(f_c\tau + \alpha t\tau)) \tag{3.18}$$

3.4.3 Simulation

In this section, simulation results are used to validate the analysis previously developed. An FMCW sensor with a transmitted bandwidth of 244 MHz, carrier frequency of 10 GHz and *PRI* of 1.024 ms, resulting in a nominal frequency rate of 250 MHz/ms is simulated. Some non-linearities have been introduced, as shown in fig. 3.4. Simulation results are shown in fig. 3.5, where it can be seen how the algorithm correctly removes the non-linearity effects, independently of the range. The responses of two stationary targets at 999 m and 2001 m have been simulated and the original non-linear range profile is presented in the first row of fig. 3.5. After the removal of the transmitted non-linearities, the energy of the echoes is spread through a much larger bandwidth (second row of fig. 3.5). Finally, after RVP and received non-linearity correction, the target responses are perfectly focused, independently of the range (third row of fig. 3.5). In addition to a better range resolution, the non-linearity correction also improved the response peak level, and hence the signal to noise ratio, by approximately 7 dB and 10 dB for the two targets, respectively.

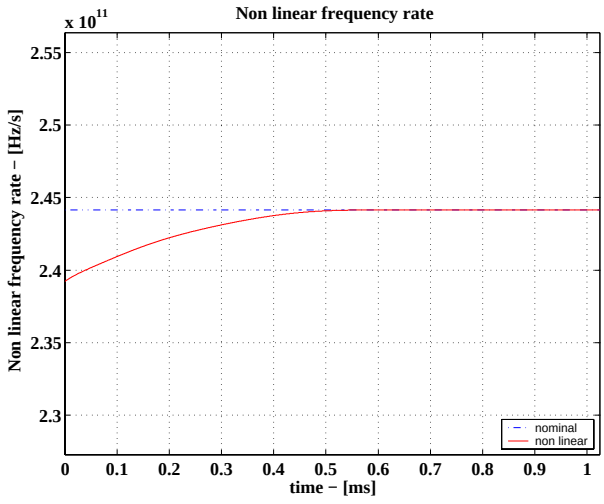


Figure 3.4: Non-linear frequency rate.

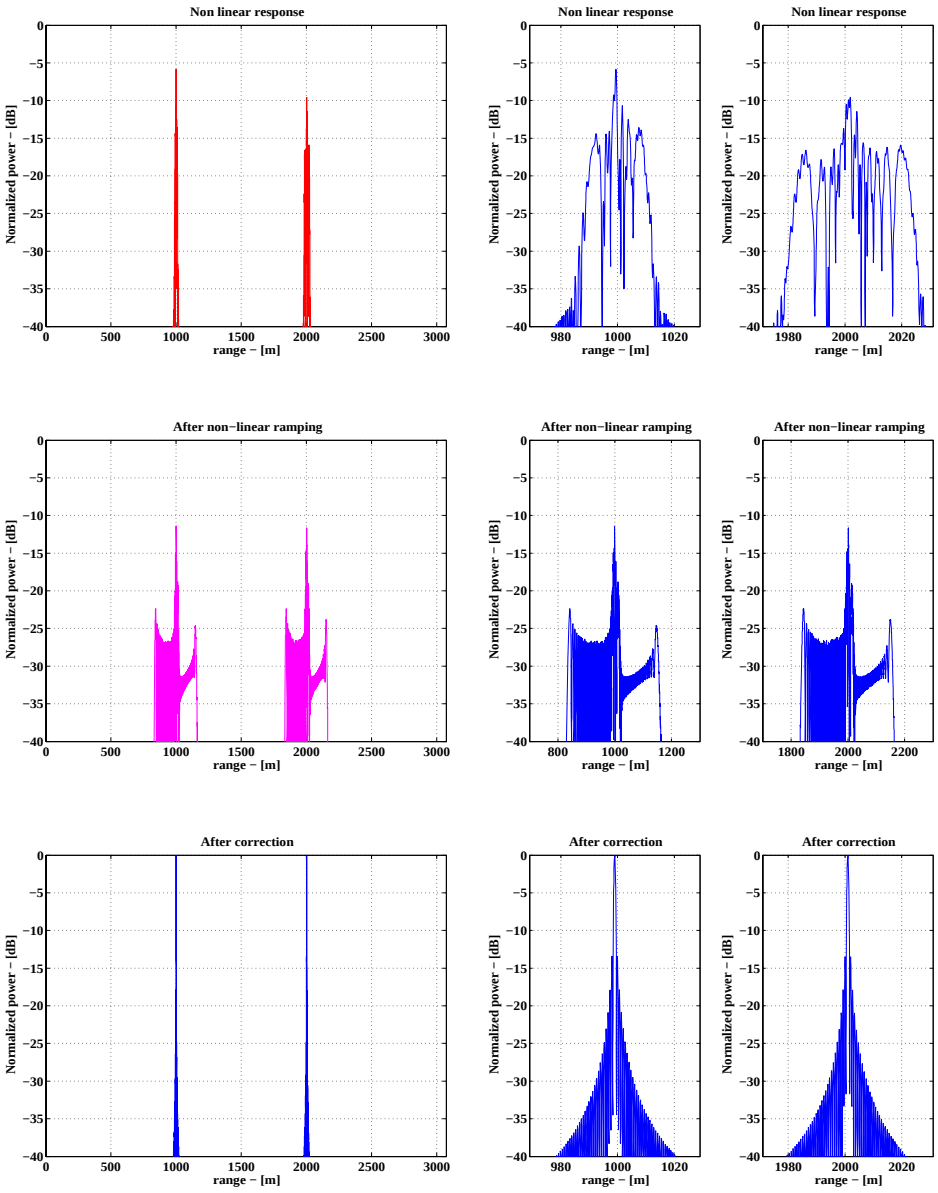
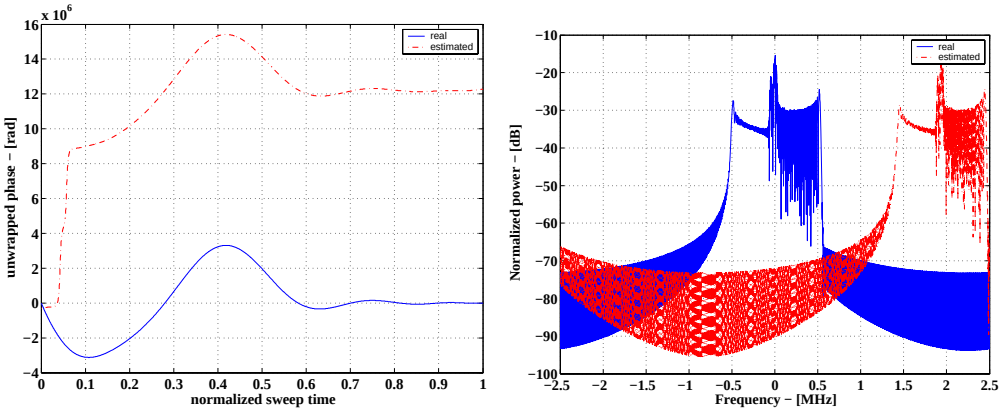


Figure 3.5: Range profile simulation results. The original non-linear responses of two stationary targets is presented in the first row. After the removal of the transmitted non-linearity, the energy of the echoes is spread through a much larger bandwidth (second row). Finally, after RVP and received non-linearity correction, the responses are perfectly focused, independently of the range (third row).



(a) (b)

Figure 3.6: Frequency non-linearity estimation. In (a) the phase estimation (dot-dashed line) is compared with the actual non-linear phase (solid line) of the error derivative, while in (b) the corresponding spectra of the non-linear terms are plotted.

3.4.4 Frequency non-linearity estimation

In the previous development, it has been assumed that the non-linear term $\epsilon(t)$ is known. This section will overcome this assumption and will describe how to estimate the non-linearity directly from the deramped data using a reference response at short distance, i.e. the response of a delay line. The starting point is (3.13), which is rewritten here:

$$\epsilon_{if}(t, \tau_{ref}) = (\epsilon(t) - \epsilon(t - \tau_{ref})) \approx \tau_{ref}\epsilon'(t) \tag{3.19}$$

In order to isolate the delay line response, windowing has to be applied in the range profile. Usually, the initial part of the beat signal is discarded, because of the presence of high frequency components, influencing the resulting estimated phase at the beginning of the signal. An example is shown in fig. 3.6(a), which plots the actual and estimated first derivative of the non-linear term $\epsilon(t)$. As can be noted, the estimation of $\epsilon'(t)$ differs considerably in the initial part of the sweep. Indicating the estimated term as $\tilde{\epsilon}$, the following expression correctly describes the estimation in the remaining part of sweep:

$$\tilde{\epsilon}'(t) = \epsilon'(t) + const \tag{3.20}$$

When estimating the non-linear term

$$\tilde{\epsilon}(t) = \int \tilde{\epsilon}'(t)\mathrm{d}t \tag{3.21}$$

the constant term in (3.20) will cause the presence of an unwanted linear phase term. The contribution of this term is the shift of the range profile, as shown in fig. 3.6(b), where the

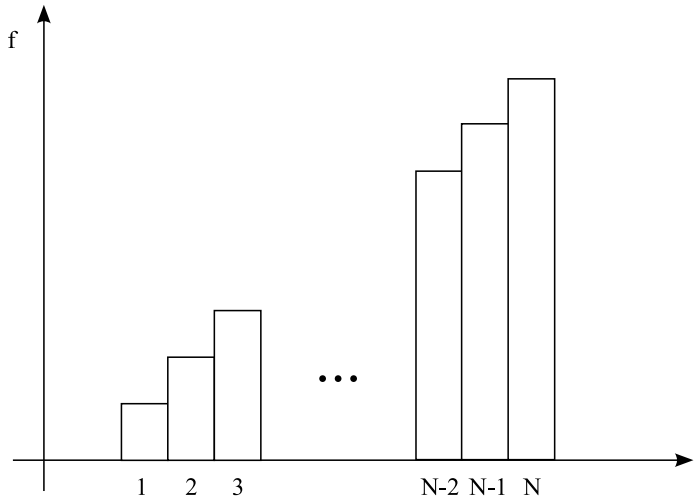


Figure 3.7: Linear stepped FMCW signal. The waveform is composed of N subpulses of duration T_s and constant frequency. The frequency is linearly increasing on a subpulse basis.

spectra of the actual and of the estimated non-linear term are plotted. The shift can be easily measured estimating the main peak position of the non-linearity spectrum and removed from the calculated non-linearity reference function.

3.5 Linear SFCW signal

Linear SFCW signals are a particular case of the linear FMCW modulation previously introduced. Theoretically, they can be thought as a discrete version of the linear FMCW: the frequency of the signal is increasing with time in a stepwise way, as depicted in fig. 3.7. The CW pulse is represented as a sequence of N shorter subpulses, each having a constant frequency and duration T_s. The range resolution is the same as for linear FMCW; for the determination of the maximum unambiguous range, the stepped modulation can be thought as a linear FMCW sampled with a frequency equal to $1/T_s$, leading to:

$$R_u = \frac{c}{2\alpha T_s} = \frac{c}{2\Delta f} = \frac{cN}{2B} \tag{3.22}$$

where Δf is the amount of frequency step and B the total bandwidth. A complex sampling has been assumed. The corresponding unambiguous frequency is $f_u = 1/T_s = N/PRI$.

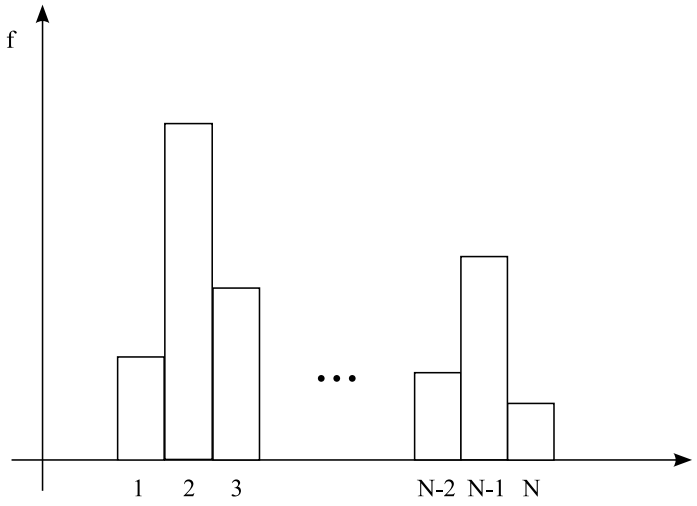


Figure 3.8: Randomized SFCW signal. The waveform is composed of N subpulses of duration T_s and constant frequency. The frequency order is non linear and it is randomly chanced from pulse to pulse.

3.6 Randomized non-linear SFCW

Randomized SFCW signals are waveforms composed of a number of subpulses with constant frequency. The frequency order is non-linear and it is randomly changed from pulse to pulse, giving this kind of modulation noise-like characteristics resulting in range ambiguities suppression and Doppler intolerant properties [11]. The range ambiguities suppression gives to a system using this kind of modulation the capability of looking at further range when compared with a system deploying linear FMCW and with the same resolution and sampling frequency. The noise-like behavior is also very important when low probability of interception (LPI) properties are required. The frequency change is, in fact, not linear anymore and therefore more difficult to estimate and reproduce for a third party system. Also, the system is less likely to interfere with other systems. In the following sections a novel deramping technique extended to non-linear modulation is presented; successively, randomized non-linear SFCW response when illuminating stationary and moving targets is analyzed.

3.6.1 Non linear deramping technique

This section derives an analytical model for the deramped non-linear SFCW signal. Based on such a description, an inversion scheme to reconstruct the range information is presented. As shown in fig. 3.8, the transmitted signal can be thought as a sequence of N subpulses of

duration T_s and constant frequency f_n:

$$s_t(t) = \sum_{n=1}^{N} u\left(\frac{t - nT_s}{T_s}\right) \exp\Big(j(2\pi f_n(t - nT_s) + \phi_n)\Big) \tag{3.23}$$

where $u(t)$ is the step function defined as 1 for $0 \leq t < 1$ and 0 otherwise, while the phase term is equal to:

$$\phi_n = \int_{T_s}^{nT_s} 2\pi f_n \mathrm{d}t \tag{3.24}$$

in order to guarantee the continuity of the signal phase. The received signal is a delayed version of the transmitted (any amplitude characteristic is discarded in the present derivation):

$$s_r(t) = \sum_{n=1}^{N} u\left(\frac{t - nT_s - \tau}{T_s}\right) \exp\Big(j(2\pi f_n(t - nT_s - \tau) + \phi_n)\Big) \tag{3.25}$$

In an homodyne receiver the received and transmitted signal are mixed, producing the intermediate frequency signal:

$$\begin{aligned} s_{if}(t,\tau) = s_t(t)s_r(t)^* = \\ \sum_{n=1}^{N}\sum_{k=1}^{N} u\left(\frac{t - nT_s}{T_s}\right) u\left(\frac{t - \tau - kT_s}{T_s}\right) \\ \exp\Big(j(2\pi(f_n(t - nT_s) - f_k(t - kT_s - \tau)) + \phi_n - \phi_k)\Big) \end{aligned} \tag{3.26}$$

If the sampling frequency is such that one sample is taken for every subpulse, the sampling time can be written as $t = mT_s + t_0$ with $0 \leq t_0 < T_s$ and $0 \leq m < N$ with $m \in \mathbb{N}$:

$$\begin{aligned} s_{if}(t = mT_s + t_0, \tau) = \\ \sum_{n=1}^{N}\sum_{k=1}^{N} u\left(\frac{(m-n)T_s + t_0}{T_s}\right) u\left(\frac{(m-k)T_s + t_0 - \tau}{T_s}\right) \\ \exp\Big(j(2\pi(f_n(mT_s + t_0 - nT_s) \\ -f_k(mT_s - kT_s + t_0 - \tau)) + \phi_n - \phi_k)\Big) \end{aligned} \tag{3.27}$$

Simplifying:

$$\begin{aligned} s_{if}(t = mT_s + t_0, \tau) = \sum_{k=1}^{N} u\left(\frac{(m-k)T_s + t_0 - \tau}{T_s}\right) \\ \exp\Big(j\left(2\pi\left(f_m t_0 - f_k(mT_s - kT_s + t_0 - \tau)\right) + \phi_n - \phi_k\right)\Big) \end{aligned} \tag{3.28}$$

Expressing τ as $lT_s + \tau_0$, with $l \in \mathbb{N}$ and $0 \leq \tau_0 < T_s$, the time delay is divided in parts, each one of duration equal to T_s. The intermediate frequency signal can be written in the

following way:

$$s_{if}(t = mT_s + t_0, \tau = lT_s + \tau_0) = \sum_{k=1}^{N} u\left(\frac{(m-k-l)T_s + t_0 - \tau_0}{T_s}\right) \exp\Big(j(2\pi (f_m t_0 - f_k((m-k-l)T_s + t_0 - \tau_0)) + \phi_n - \phi_k)\Big) = \exp\Big(j(2\pi((f_m - f_{m-l})t_0 + f_{m-l}\tau_0) + \phi_m - \phi_{m-l})\Big) \tag{3.29}$$

From the previous equation it is clear that all the terms which do not carry any information about the target range have to be removed, in order to reconstruct the range information when the time delay is larger than the subpulse duration. The phase correction is performed by a multiplication with the following reference function:

$$\exp\Big(-j(2\pi(f_m - f_{m-l})t_0 + \phi_m - \phi_{m-l})\Big) \tag{3.30}$$

The resulting signal is:

$$\exp(j2\pi f_{m-l}\tau_0) \tag{3.31}$$

Next, a reordering of the samples is performed, such that the corresponding subpulse frequency order is linear. This operation allows the use of an FFT to obtain the range profile. However, each of the reference function multiplication and reordering correctly reconstructs only one part of the time delay profile, depending on the value of l. Each value of l corresponds to a constant range interval R_{T_S}. To have the complete range profile, this operation has to be performed varying the parameter l.

At the cost of increased computation, the described extension of the deramping technique to the randomized SFCW allows the use of such a technique not only for linear modulated signals, but also for nonlinear ones. The deramping method leads to a lower sampling rate and to a simpler hardware in the radar system: the receiver sampling frequency does not need to be higher than the complete bandwidth (complex sampling) of the transmitted signal, but it has to be only enough to have one sample for every subpulse.

However, some comments on the sampling frequency are required. If a sample is taken during the transition of one frequency step in the received signal, the resulting phase could be not well determined. Having two complex samples per subpulse can solve the problem, at the cost of an increased processing load.

Nevertheless, the sampling constraints can be drastically reduced especially for high resolution systems.

3.6.2 Stationary targets

In order to validate the analytical development, a simulation analysis has been performed. A linear and randomized SFCW sequence have been generated with the parameters listed in tab. 3.1, in order to compare the two waveform responses.

Table 3.1: Waveform parameters and target distances for the non linear deramping simulations.

B	1 GHz	R_u	150 m
N	1000	R_{T_s}	150 m
T_s	1 μs	target 1	50 m
PRI	1 ms	target 2	225 m
PRF	1 kHz	target 3	400 m

A bandwidth of 1 GHz is transmitted using 1000 subpulses, leading to an unambiguous range (R_u) of 150 m for linear modulation. The subpulse duration is 1 μs, so the range profile is divided in parts (R_{T_s}) of 150 m extension. It is interesting to note that R_u and R_{T_s} coincide when $1/N = B/T_s$, as it is the case in the example used for the simulation.

Three stationary targets have been simulated with same power response at ranges such that their time delay is within one, larger than one and larger than two subpulse duration, respectively. Results are reported in fig. 3.9. It can be seen that only the first target distance is correctly measured using a linear SFCW signal (fig. 3.9(a)). In fact, the distance of the other two targets is larger than the maximum unambiguous range R_u and therefore folded back. However, using a randomized SFCW, the range ambiguity is suppressed; only the target that is in the range part correctly reconstructed by the particular phase correction and reordering is imaged (fig. 3.9(b), 3.9(c), 3.9(d)). Finally, combining the results of the range processing for different values of l, a complete range profile is obtained (fig. 3.9(e)).

When compared with the linear SFCW output, it is possible to observe the increase of the noise floor in the random modulation output, due to the presence of other targets. In fact, their energy is suppressed by spreading it over the range spectrum. Coherent averaging can reduce this noise floor, as it is illustrated in fig. 3.9(f) where 10 processed sweeps are averaged, because randomization destroys the sidelobe coherence from sweep to sweep [12], while preserving the target main lobe.

3.6.3 Moving targets

In this section, the response of a moving target illuminated by a randomized stepped frequency modulation is briefly mentioned. Opposite to linear modulations, non-linear signals have the characteristic of being Doppler intolerant, which means that a moving target response amplitude can be much lower than the corresponding stationary case. The concept is analytically described by the ambiguity function of the signal; for randomized non-linear stepped frequency it is expressed by:

$$|\chi(\tau, f_D)|^2 = |sinc(B\tau)sinc(f_D T_p)|^2 \tag{3.32}$$

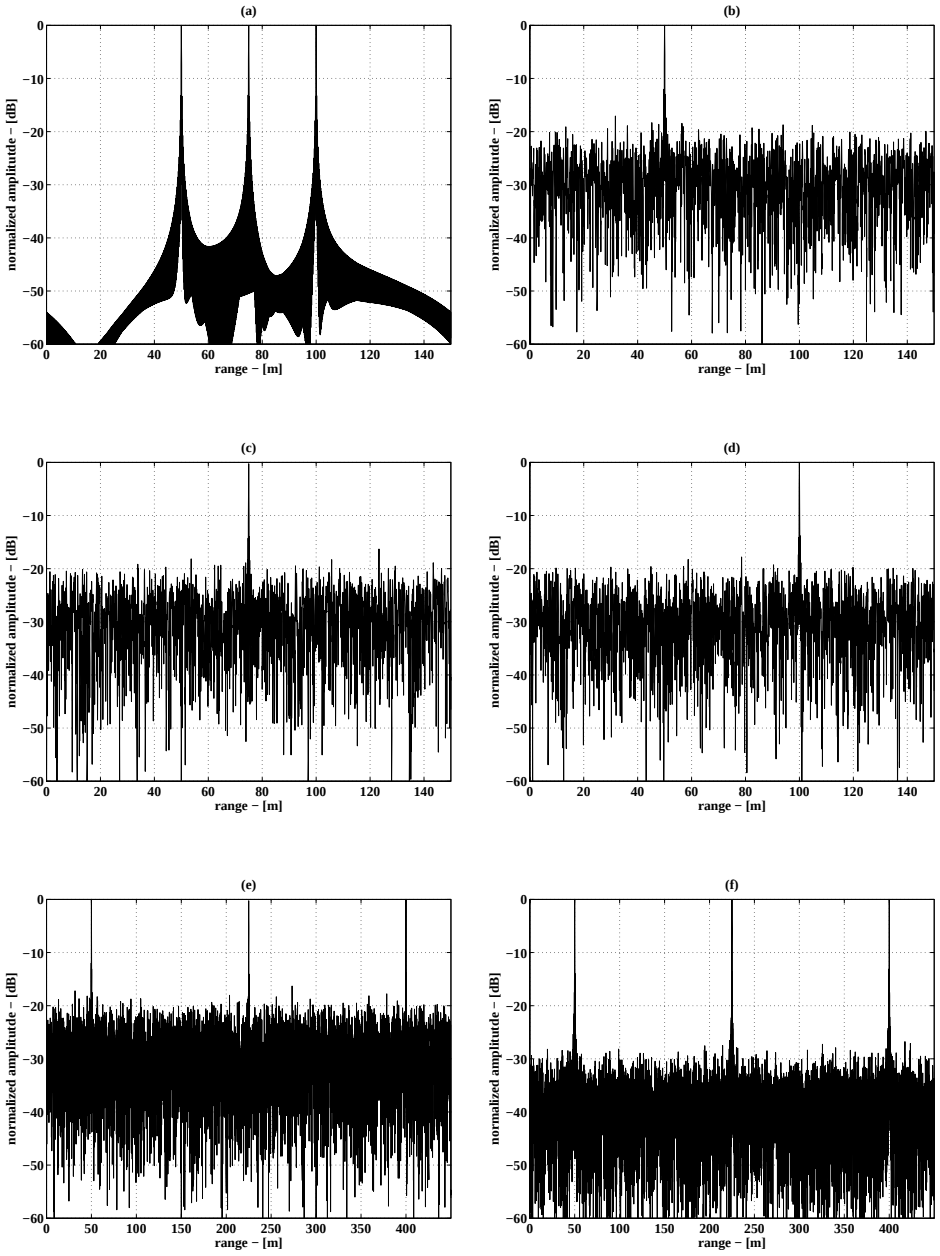


Figure 3.9: Range profile simulation results using linear FMCW (a); randomized SFCW with reference function and reordering corresponding to $l = 0, 1, 2$ (b, c, d) and their combination (e). In the last figure (f), the plot shows the coherent combination of 10 processed profiles. The range extension in the last row is three times larger than in the other rows.

showing that the Doppler response is a $sinc$ whose width depends on the pulse duration. In continuous wave systems, the pulse duration is equal to PRI , therefore the Doppler response will have nulls at multiples of PRF .

3.6.4 Influence of hardware non ideality

The previous section has developed an inversion scheme to reconstruct the range profile from deramped randomized SFCW signals. Basically, when the time delay is larger than the subpulse duration, the intermediate frequency signal is undersampled. It can be reconstructed because the sequence of the pulse is known. However, the reference function in (3.30) requires the value of t_0, that is the time instant the sample is taken.

When l is equal to zero (time delay shorter than the subpulse duration) the reference function is constant and in this case a simple reordering (and FFT) is enough for the range reconstruction, but for other values of l the knowledge of the exact value of t_0 is important.

By means of simulations, this section analyzes the effect of inaccurate knowledge of the sampling time, due to the jitter of the clock signal, for example. One target is simulated at a distance placed in the second part of the range profile ($l = 1$) and three range parts are reconstructed ($l = 0, 1, 2$), as shown in fig. 3.10; in this way the noise floor of the first and third range part is due to the spreading of the target energy, while the noise floor in the second range part is due to the sampling inaccuracy.

Since the spreading induced noise is dominant, the sampling induced noise has to be

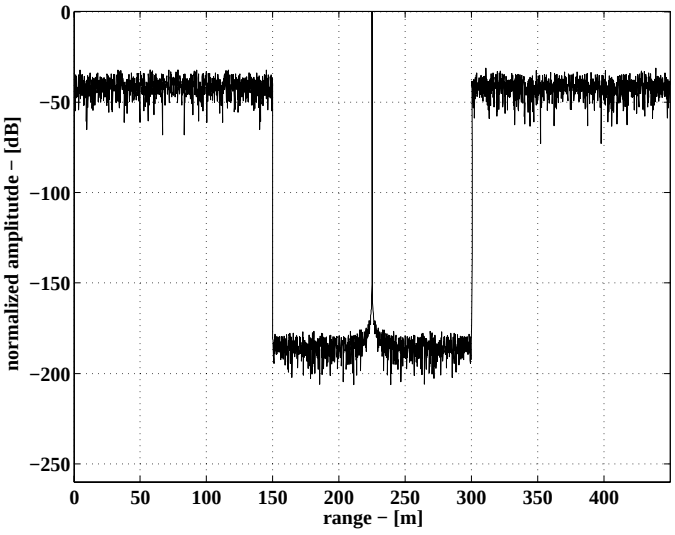


Figure 3.10: Simulation of only one target placed in the second part of the range profile. In the first and third part the noise floor is due to the target energy spreading when the deramping is performed for other value of the parameter l in the reference function multiplication and reordering. When jitter is present, the noise floor in the second part will rise.

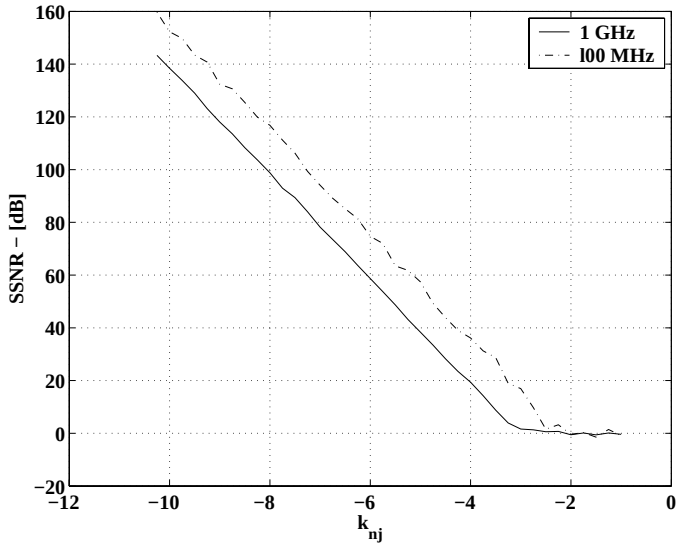


Figure 3.11: Spreading induced noise to jitter induced noise ratio plotted versus the k_{nj} value and for two different values of the transmitted bandwidth.

lower, and for this reason their ratio is used as description parameter. At least one sample per subpulse (complex sampling) has to be taken, therefore the following sampling frequency is used as reference:

$$f_s = \frac{N}{PRI} \tag{3.33}$$

The jitter is simulated as white noise with maximum amplitude equal to a fraction of the reference sampling frequency and added to the sampling time variable:

$$t_{0jitter} = t_0 + 10^{k_{nj}} f_s wgn(t) \tag{3.34}$$

where $wgn(t)$ a unitary white gaussian noise function. Simulation results are reported in fig. 3.11, where the spreading to sampling induced noise ratio (SSNR) is plotted versus the parameter k_{nj} of (3.34). Two curves are obtained, for a transmitted bandwidth of 100 MHz and 1 GHz, respectively, and with 1 MHz as reference sampling frequency (using a *PRI* of 1 ms and N equal to 1000). It is shown how the SSNR increases for lower value of k_{nj} and for lower transmitted bandwidth.

3.7 Summary

The chapter has described the range processing of FMCW data in a complete and detailed manner. It presented a novel processing solution, developed within the framework of this thesis, which completely removes the frequency non-linearity effects. It corrects for the non-linearity effects for the whole range profile at once, operates directly on the deramped data

and it is very computationally efficient. The removal of the defocusing is range and Doppler independent. The integration of the non-linearity correction in FMCW SAR algorithms is described in appendix A. Non linear SFCW modulation has also been treated in the chapter; a deramping technique extended to the case of non linear signals has been introduced. With the extended deramping technique proposed here, reduced sampling frequency as for the linear case can be used also for randomized SFCW signals, at the cost of increased computation.

References

[1] A. G. Stove, "Linear FM-CW Radar Techniques," *IEE Proc. Part F Radar Signal Process.*, vol. 139, no. 5, pp. 343–350, Oct. 1992.

[2] S. O. Piper, "Homodyne FM-CW Radar Resolution Effects with Sinusoidal Nonlinearities in the Frequency Sweep," in *Proc. IEEE Int. Radar Conf. '95*, Alexandria, USA, May 1995, pp. 563–567.

[3] D. E. Barrick, "FM-CW Radar Signals and Digital Processing," in *National Oceanic and Atmospheric Administration, Tech. Rep. AD-774-829*, July 1973.

[4] S. O. Piper, "FMCW Linearizer Bandwidth Requirements," in *Proc. IEEE Radar Conf. '91*, Mar. 1991, pp. 142–146.

[5] M. Vossiek, P. Heide, M. Nalezinski, and V. Magori, "Novel FMCW radar system concept with adaptive compensation of phase errors," in *Proc. European Microwave Conf. EuMC'96*, Prague, Czech Republic, Sept. 1996, pp. 135–139.

[6] Z. Zhu, W. Yu, X. Zhang, and X. Qiu, "A Correction Method to Distortion in FM-CW Imaging System," in *Proc. IEEE Aerospace Electronics Conf. NEACON'96*, Dayton, USA, May 1996, pp. 323–326.

[7] M. Edrich, "Design Overview and Flight Test Results of the Miniaturised SAR Sensor MISAR," in *Proc. EuRAD'04*, Amsterdam, The Netherlands, Oct. 2004, pp. 205–208.

[8] A. Meta, P. Hoogeboom, and L. P. Ligthart, "Range non-linearities correction in FMCW SAR," in *Proc. IEEE Int. Geoscience and Remote Sensing Symp. IGARSS'06*, Denver, CO, USA, July 2006.

[9] ——, "Range Frequency Non-linearity Correction for FMCW SAR," *European Patent Application*, no. 06076057.6, May 2006.

[10] W. G. Carrara, R. S. Goodman, and R. M. Majewski, *Spotlight Synthetic Aperture Radar*. Boston, Artech House Inc., 1995.

[11] J. E. Luminati, T. B. Hale, M. A. Temple, M. J. Havrilla, and M. E. Oxley, "Doppler Aliasing Artifacts Filtering in SAR Imagery using randomized Stepped-Frequency Waveforms," *IEE Electronic Letters*, vol. 40, no. 22, pp. 1447–1448, Oct. 2004.

[12] K. Morrison, "Increasing the Effective Bandwidth of an SF-CW SAR using Frequecy Agility," in *Proc. IEEE Int. Radar Conference*, Arlington, USA, May 2005, pp. 201–205.

Chapter 4

Cross-range imaging with FMCW SAR

The conventional stop-and-go approximation used in pulse radar algorithms can be not valid anymore in FMCW SAR applications, therefore the motion within the sweep needs to be taken into account. The chapter presents an analytical development of the FMCW SAR signal model, starting from the deramped signal and without using the stop-and-go approximation. The novel model is first validated with a stripmap simulation and then applied to spotlight and single transmitter/multiple receiver Digital Beam Forming (DBF) synthetic aperture operational modes. In the latter cases, the effect of the motion during the transmission and reception of the pulse, if not compensated for, can become seriously degrading for the SAR image quality.

4.1 Introduction

Synthetic Aperture Radar techniques allow a finer resolution in the cross-range direction by simulating a long antenna array using a single moving sensor. The antenna is usually mounted on an aircraft or satellite, which provide the moving platform. Three categories of motion can be distinguished during the SAR data collection [1]: motion occurring between successive transmitted pulses, between transmission and reception of a pulse, and during transmission and reception. Conventional monostatic SAR algorithms are based on the exploitation of the first kind of motion. The second category gives rise to bistatic effects while the motion during transmission and reception of the pulse is usually neglected. However, its effect becomes important when the pulse duration increases. This is the case when using FMCW radar sensors. They will play an important role in the airborne earth observation field where special attention is devoted to lightweight, cost-effective imaging sensors of high resolution.

The aim of this chapter is to develop a complete FMCW SAR signal model which takes into account also the effects of the motion during the sweep. Conventional SAR algorithms have been developed for pulse radars and are not optimal for the FMCW case. Therefore, when using FMCW sensors, proper algorithms have to be used to achieve the expected results with the maximum resolution. In [2], an algorithm processing FMCW SAR signals is presented; however, it requires the complete bandwidth of the transmitted signal to be sampled and a single long FFT to be performed over the whole collected data for the processing.

In contrast, an algorithm which uses the inherent FMCW deramp-on-receive operation [3] [4] [5] is proposed here; in this way, the raw data bandwidth can be drastically reduced, specially for high resolution systems.

The remainder of the chapter is divided into six sections. In section 4.2, a brief heuristic overview of the FMCW SAR signal is described, indicating when conventional SAR algorithms cannot be used, while section 4.3 derives an analytical description of the FMCW SAR signal without any approximation. A stripmap FMCW SAR simulation is reported in section 4.4. Successively, in section 4.5 and 4.6 the model is applied to spotlight and single transmitter/multiple receiver operational modes, respectively, where the effect of the motion during the transmission and reception of the pulse can become seriously degrading for the SAR image quality if not compensated for. The chapter is finalized by section 4.7 where conclusions are stated.

4.2 Signal processing aspects

For typical pulse SAR systems, the pulse length T_p is sufficiently short for the radar to be assumed stationary during the transmission and the reception of the signal. This is called the stop-and-go approximation: while the aircraft is flying it is as if it stops, sends a pulse, receives it and then moves to the next position. Conventional SAR algorithms use this assumption and the azimuth compression is achieved by using the geometry of the imaging scenario; the Doppler effect within the sweep is not important because the aircraft is assumed stationary. If the Pulse Repetition Interval is varied, while still properly sampling the instantaneous Doppler bandwidth, nothing changes for the SAR processing algorithm [6]. In fig. 4.1 a stripmap SAR geometry is illustrated: θ_{az} is the antenna beamwidth, (x_1, y_1) are the coordinates of the scene center, h is the flight altitude and $R = \sqrt{h^2 + y_1^2}$ is the distance between the aircraft trajectory and a parallel line passing through the scene center. If a scatterer is seen by the radar under a look angle γ, the Doppler frequency can be expressed as

$$f_D = \frac{2v}{c} f_r \sin\gamma \tag{4.1}$$

where c is the speed of light, f_r is the transmitted frequency. Indicating with γ_{min} and γ_{max} the minimum and maximum angle under which a scatterer is illuminated, we can introduce the instantaneous B_{Di} and entire Doppler bandwidth B_D, respectively defined as:

$$B_{Di} \approx \frac{2v}{c} f_c \sin\theta_{az} \tag{4.2}$$

$$B_D = \frac{2v}{c} f_c (\sin\gamma_{max} - \sin\gamma_{min}) \tag{4.3}$$

where f_c is the center frequency. In order to analyze the effects of the motion within the sweep in FMWC SAR configurations, it is convenient to define the following parameters, the duty cycle η, the oversampling factor μ and the instantaneous to entire Doppler bandwidth

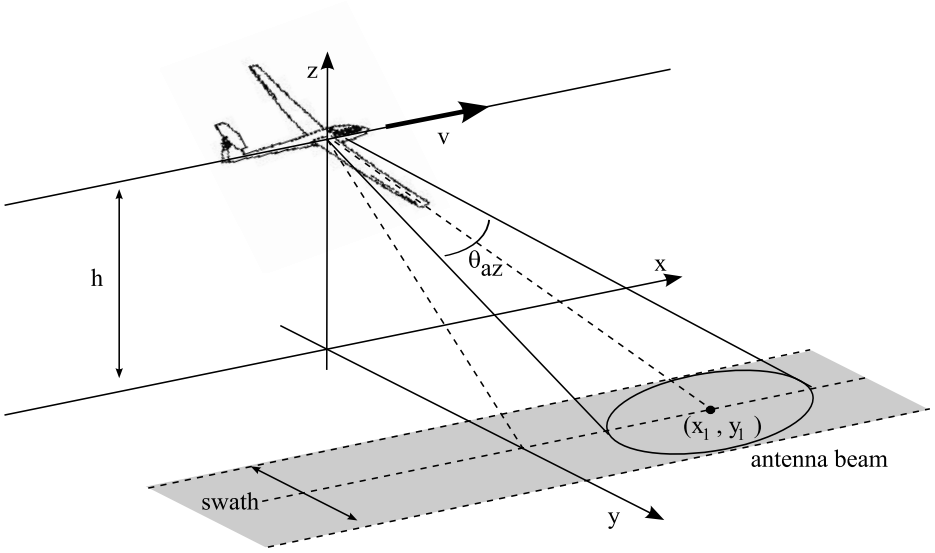


Figure 4.1: SAR system geometry.

ratio ξ, respectively, as:

$$\eta = T_p/PRI \tag{4.4}$$

$$\mu = PRF\,/B_{Di} \tag{4.5}$$

$$\xi = B_{Di}/B_D \tag{4.6}$$

where PRF is the Pulse Repetition Frequency. Finally, we define:

$$K = \frac{B_D}{\delta f_r} \tag{4.7}$$

as the ratio between the entire Doppler bandwidth and the range frequency resolution δf_r, equal to $1/T_p$. The parameter K indicates how much the Doppler frequency due to the motion within the pulse transmission is comparable to the frequency resolution, and therefore how good it can be measured. Rearranging the expression in (4.7) in terms of the parameters introduced above yields:

$$K = \frac{\eta}{\mu\xi} \tag{4.8}$$

Equation (4.8) directly relates K to the radar configuration (η) and SAR operational mode (μ, ξ). For typical pulsed SAR systems $K \ll 1$, but when K becomes closer to unity the stop-and-go approximation cannot be considered valid anymore. As we will see in section 4.5 and 4.6, in spotlight and multiple tranmitter/receivers SAR modes, ξ and μ, respectively,

can be smaller than unity and, combined with the use of CW sensors (η equal to one), that means the value of K can become even larger than one.

When the stop-and-go approximation is not valid, the frequency of the received signal is better described as shifted with respect to the transmitted by an amount equal to the Doppler frequency. Figure 4.2 shows qualitatively the signal support band in the two-dimensional range spatial frequency K_r and azimuth spatial frequency K_x domain for a wideband FMCW SAR. The support band will differ from the usual representation because it is squinted; however, the most important aspect is that the "frequency of the signal" in the two-dimensional frequency domain will also be shifted by the appropriate Doppler component.

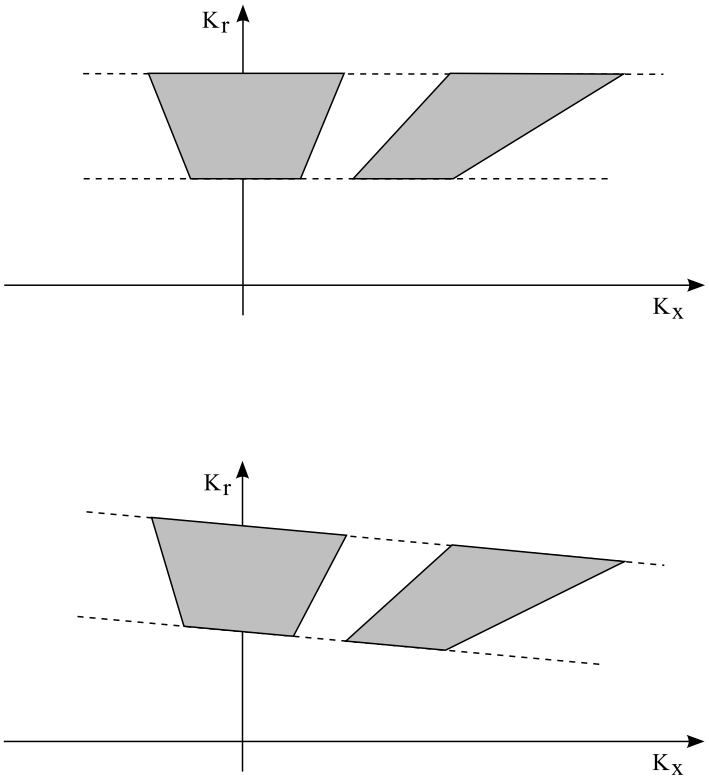


Figure 4.2: Pulse SAR and FMCW SAR support band in the two-dimensional spatial frequency domain. The squinting is exaggerated for purposes of clarity.

4.3 Analytical development

This section derives an analytical development for the description of the FMCW SAR signal in the two-dimensional frequency domain. The radar continuously transmits linear FM chirps having duration T_p equal to the *PRI* , chirp rate $\alpha = B/PRI$, where B is the transmitted bandwidth and center frequency f_c, see fig. 4.3. The transmitted frequency is expressed as:

$$f_r = f_c + \alpha t \tag{4.9}$$

where $-PRI/2 \leq t < PRI/2$. In dechirp-on-receive systems, the received and transmitted signal are mixed in order to reduce the required system sampling rate. The intermediate frequency signal S_{IF} output of the mixer is:

$$S_{IF} = \exp\left(j2\pi\left(f_c\tau + \alpha\tau t - \frac{1}{2}\alpha\tau^2\right)\right) \tag{4.10}$$

The last term is an unwanted phase term known as Residual Video Phase (RVP) [1]; it is usually negligible, or otherwise can be corrected. In the rest of the analysis, it is assumed removed. A more general model including frequency non-linearities and RVP is derived in appendix A, where also a novel and efficient processing algorithm for FMCW SAR data is introduced. The time delay τ due to a point target located in the center of the scene is:

$$\begin{aligned} \tau &= \frac{2r\left(R, x_1, t'\right)}{c} = \frac{2\sqrt{R^2 + (vt' - x_1)^2}}{c} \\ &= \frac{2\sqrt{R^2 + (x_n + vt - x_1)^2}}{c} \end{aligned} \tag{4.11}$$

where $t' = T_n + t$ is the continuous time variable and $T_n = nPRI$, with n integer, is what is usually referred to as slow time variable; $x_n = vT_n$ is the position of the aircraft along its

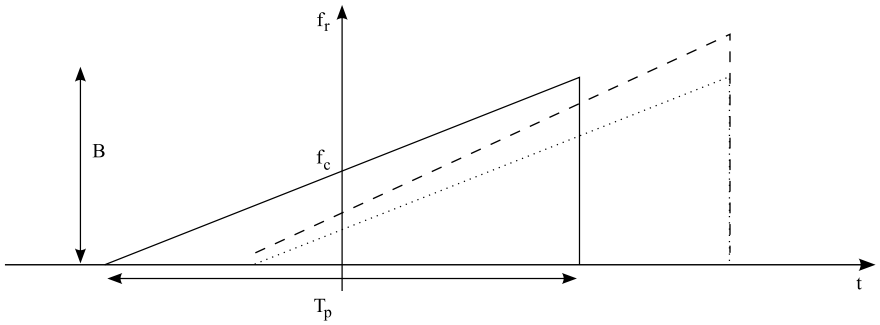


Figure 4.3: Chirp pulse in the frequency-time domain. The received signal (dotted) is a delayed version of the transmitted one (solid). If a Doppler effect is present, the received signal will be shifted in frequency of an amount proportional to the instantaneous frequency (dashed).

ideal straight line path, at regular time intervals.

The intermediate frequency signal (without the RVP term) is written as:

$$\begin{aligned} S_{IF}(K_r, x_n) &= \exp(j2\pi(f_c\tau + \alpha\tau t)) = exp(jK_r r) \\ &= \exp\left(jK_r\sqrt{R^2 + (x_n + vt - x_1)^2}\right) \end{aligned} \tag{4.12}$$

where the spatial range frequency is equal to:

$$K_r = \frac{4\pi}{c} f_r = \frac{4\pi}{c}\alpha\left(\frac{f_c}{\alpha} + t\right) = K_{rc} + \Delta K_r \tag{4.13}$$

where K_{rc} is the central range spatial frequency and ΔK_r is its variation around K_{rc}. In order to obtain an expression for the FMCW SAR signal in the two-dimensional frequency domain, a Fourier transform with respect to the variable x_n is performed on (4.12) (from now on we suppress the subscript n in the variable x_n, and we refer to it simply as x):

$$\mathcal{F}_x(S_{IF}) = \int \exp\left(jK_r\sqrt{R^2 + (x + vt - x_1)^2} - jK_x x\right) \mathrm{d}x \tag{4.14}$$

Using the substitution $x' = x + vt$, the integral in (4.14) can be rewritten as:

$$\int \exp\left(jK_r\sqrt{R^2 + (x' - x_1)^2}\right) \exp(-jK_x(x' - vt))\, \mathrm{d}x' \tag{4.15}$$

Bringing the exponential term $\exp(jK_x vt)$ out of the integral and solving it by means of the principle of the stationary phase yields:

$$S_{IF}(K_r, K_x) = \exp(jK_x vt) \exp\left(jR\sqrt{K_r^2 - K_x^2} - jK_x x_1\right) \tag{4.16}$$

Equation (4.16) describes the FMCW SAR signal in the two-dimensional spatial frequency domain. It differs from the conventional description in the presence of the first exponential term. This is a space-invariant term that takes into account the motion within the sweep, leading to a more general solution.

The stop-and-go approximation assumes the radar stationary while transmitting and receiving the pulse, so v is equal to zero; in (4.16) the first exponential term would disappear reverting to the conventional pulse SAR equation [1][2]. However, since the derived expression is a more general description of the SAR signal, it has to hold also when the true velocity value is inserted. In fact, the variation of t is very small compared with the product $K_x v$ in pulse radar cases and therefore the phase of the first exponential is practically constant.

4.4 Stripmap FMCW SAR simulation

For a first validation of the derivation, a stripmap FMCW SAR simulation of one target has been carried out with the following parameters: carrier frequency $f_c = 10$ GHz, transmitted bandwidth 500 MHz, $PRI = 1$ ms, antenna beamwidth 10^o, squint angle 20^o, target

range distance $R = 403$ m and aircraft velocity $v = 50$ m/s, leading to a value of K equal to 0.46. After the raw data are generated according to (4.10), a range deskew operation is performed to remove the RVP and then an FFT in the azimuth direction makes the signal in the two-dimensional frequency domain available. In order to compare the conventional and the described SAR model, the signal in the two-dimensional frequency domain is matched filtered with the conventional and proposed reference function for the range of the simulated target. Figure 4.4(a) shows the real part after matched filtering with a reference function that does not take into account the motion within the sweep (stop-and-go approximation) while fig. 4.4(b) has been produced by filtering the signal with our proposed model expressed in (4.16). Only in the last picture the phase is practically constant, indicating that the reference function really matches the scatterer signal.

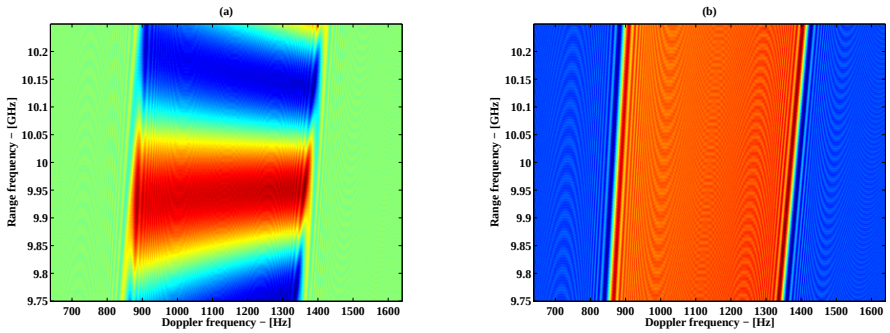


Figure 4.4: Stripmap simulation results: real part of the two-dimensional domain for a target in the scene center after conventional (a) and proposed (b) matched filtering.

4.5 Spotlight FMCW SAR

In spotlight mode SAR, the antenna beamwidth is not constrained to a fixed direction, but it can be steered in order to illuminate a certain area for a longer period. In this way, the angle under which a target can be observed is not limited by the antenna beamwidth and therefore a larger Doppler bandwidth is available, leading to a better achievable azimuth resolution. For a larger Doppler bandwidth, a larger PRF should be used in order to correctly sample the SAR signal. However, it is important to note that at every instant a sample is taken, the actual Doppler bandwidth observed by the SAR system is limited by the antenna beamwidth. The PRF has to be high enough to sample this instantaneous bandwidth, therefore the bandwidth to take into account for the Nyquist theorem formulation is the instantaneous bandwidth and not the complete Doppler bandwidth. In order to correctly reconstruct the Doppler bandwidth, the azimuth data are processed in a similar way to the ramping of the deramped range signal [7]. The technique is briefly reviewed. The SAR raw data are modulated in cross-range

direction by an hyperbolic function that depends on the range frequency K_r and target range history:

$$s(K_r, x) = exp(jK_r\sqrt{R^2 + (x + vt - x_1)^2}) \tag{4.17}$$

In order to compress the signal bandwidth, the raw data are multiplied with the reference function:

$$s_{ref}(K_r, x) = exp(-jK_r\sqrt{R_0^2 + x^2}) \tag{4.18}$$

where R_0 is a reference range, i.e. the range at the center of the scene. This reference function is sampled at the same frequency as the raw data, that is at PRF . The compressed signal

$$s_{comp}(K_r, x) = s \cdot s_{ref} \tag{4.19}$$

has a reduced bandwidth and it can be used to reconstruct the original bandwidth. In fact, it is not aliased anymore and can be upsampled (using zero padding and FFT) at a frequency $mPRF$, with m large enough such that $mPRF > B_D$. Finally, multiplying the upsampled compressed signal with the reference function (also sampled now at $mPRF$), the original signal is reconstructed without aliasing.

In such a scenario, the image degradation can be quite high if the effects of the motion within the sweep are not corrected for because the Doppler bandwidth can be larger than the PRF ($\xi < 1, \mu > 1$), differently from the stripmap case. In fact, every time the Doppler bandwidth extends of a PRF value, the response in range direction migrates of one resolution cell. This is demonstrated in fig. 4.5 by means of simulated data, where the following parameters are used: carrier frequency $f_c = 10$ GHz, transmitted bandwidth 500 MHz, $PRI = 4$ ms, illumination angle 20^o, squint angle 10^o, target range distance $R = 120$ m and aircraft velocity $v = 40$ m/s. The choice of these parameters results in a value of K equal to 3.64. The parameter K does not depend on the target range value. Therefore, the low range value was chosen for the simulation only for computational reasons. Similar to the stripmap example, the raw data are first generated according to (4.10), processed in order to reconstruct the unaliased signal with the technique previously described, Fourier transformed with respect to the cross-range direction and finally matched filtered with both the conventional SAR reference signal and the proposed one, expressed by (4.16). The results are shown in fig. 4.5, where the improvements due to the proposed correction are clearly visible.

4.6 Digital beam forming FMCW SAR

Spotlight mode gives the advantage of higher cross range resolution compared to stripmap mode, at the expense of a reduced imaged area. In both the operational modes, the image swath is limited by the PRF in conventional radars; its value is determined by the maximum allowable distance travelled by the radar platform between successive transmitted pulses and by the fact that the PRF has to be high enough to sample the instantaneous clutter Doppler bandwidth.

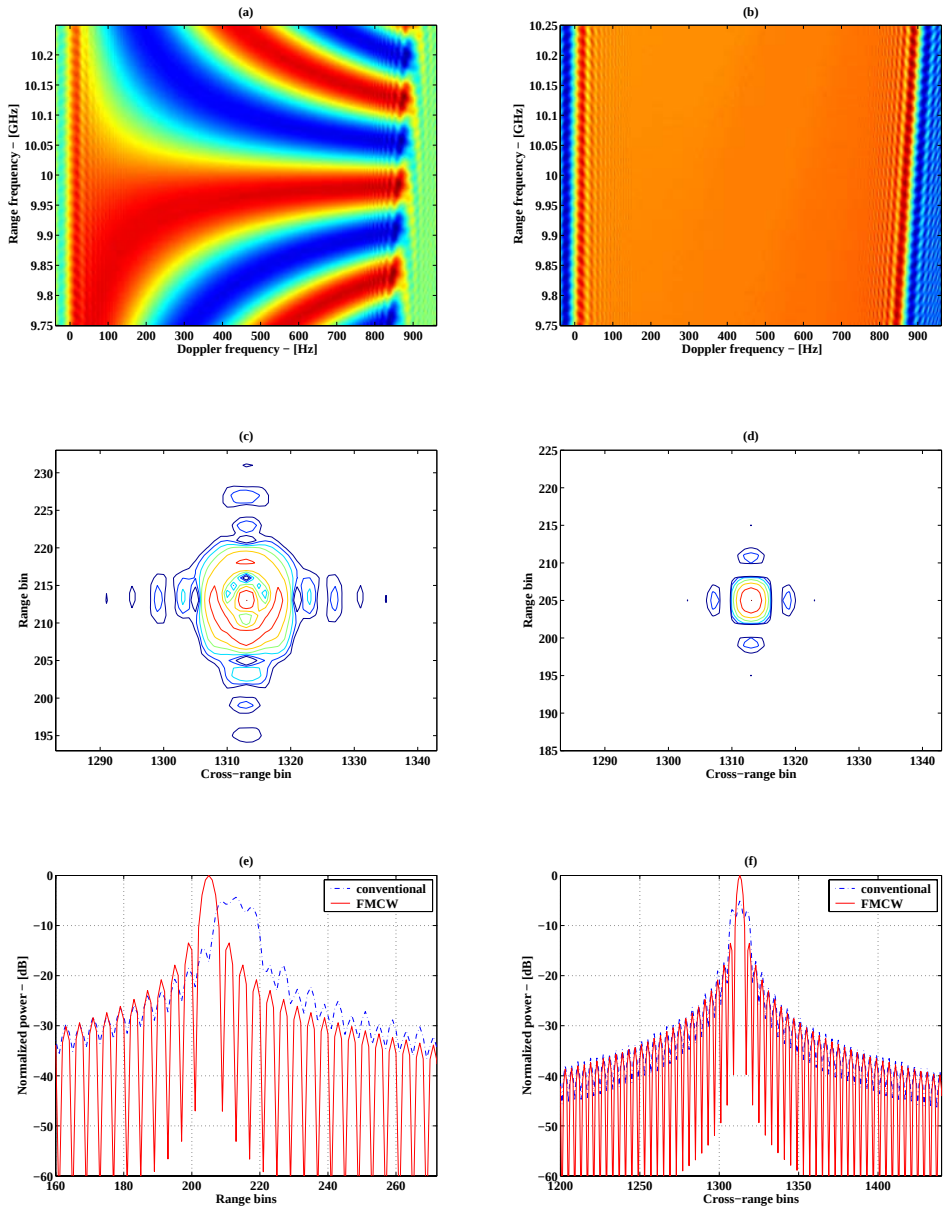


Figure 4.5: Spotlight simulation results for K equal to 3.64; real part of the two-dimensional domain for a target in the scene center after conventional (a) and proposed (b) matched filtering; contour plots of the resulting point response (c, d) and range and cross-range profile comparison (e, f).

These limitations are overcome by using multiple channels in Digital Beam Forming SAR configuration. In general, a DBF SAR consists of an array of transmitters and receivers. If N is the number of receivers, at every instant, N data streams are recorded and from every channel a SAR image can be produced. Proper processing of the N channels allows a lowering of the *PRF* [8]. This means that a larger swath can be imaged, still correctly sampling the clutter Doppler bandwidth. In fact, the signal from a single channel will be undersampled in the cross-track direction; however the complete Doppler spectrum can be reconstructed by combining the information of the whole receive subarrays. Every transmitter/receiver bistatic configuration can be thought as a monostatic sensor placed in between them [9], and therefore N samples are available at the same time in the spatial domain, allowing a *PRF* reduction of the same factor N. As shown in fig. 4.6 for a single transmitter/ multiple receivers case, the spatial sampling is reduced from d_i, the space one single antenna has moved during one sweep, to d_N, the distance of two adjacent subarray phase center, after DBF processing.

In the present discussion, we will assume the aircraft velocity such that the resulting samples are equally spaced in the azimuth direction. The removal of this limitation is treated in literature [10], and is not relevant for the topic discussed in this section. The focus here is the fact that the *PRF* of the single channel is lower than the instantaneous clutter Doppler bandwidth ($\mu < 1$). As described in the previous sections, this results in performance degradations when conventional SAR processing algorithms are used, neglecting therefore the effects of the motion during the sweep.

A simulation with the following parameters has been performed: single transmitter, 5 receivers, carrier frequency $f_c = 40$ GHz, transmitted bandwidth 500 MHz, $PRI = 1$ ms,

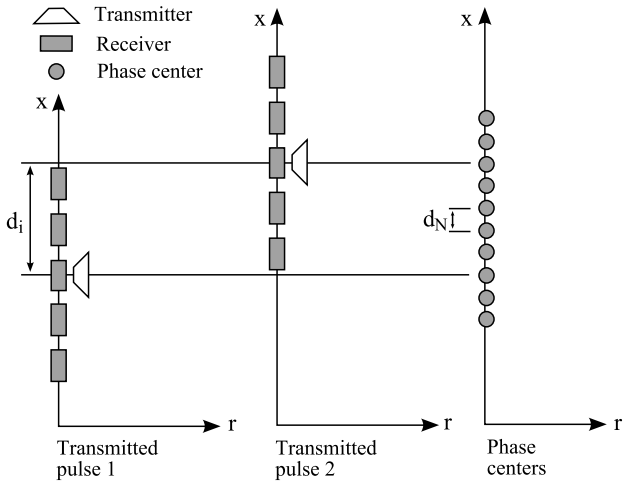


Figure 4.6: Digital beam forming principle.

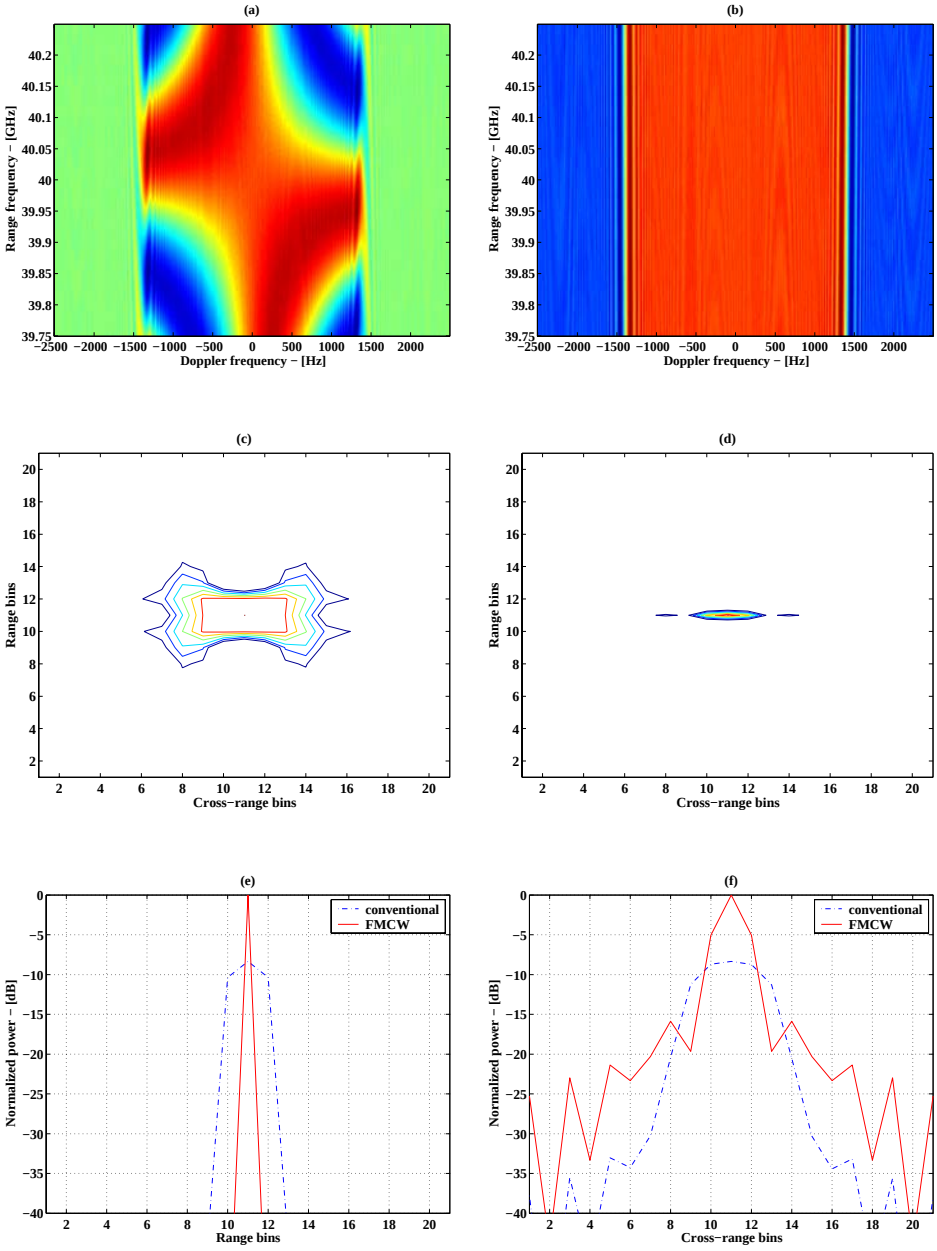


Figure 4.7: Digital Beam Forming simulation results for K equal to 2.8; real part of the two-dimensional domain for a target in the scene center after conventional (a) and proposed (b) matched filtering; contour plots of the resulting point response (c, d) and range and cross-range profile comparison (e, f).

illumination angle 6^o, range distance $R = 300$ m and aircraft velocity $v = 100$ m/s. The resulting K is 2.8. Simulation outcomes are shown in fig. 4.7. The response behavior is similar to the spotlight example of the previous section, but less accentuated due to a lower value of K.

4.7 Summary

In this chapter, the FMCW SAR signal description in the two-dimensional frequency domain has been derived without any approximation. From this model an algorithm that corrects for the motion within the sweep has been proposed. If conventional algorithms are used, the motion within the sweep is not taken into account and this results in resolution degradation. In FMCW SAR systems, the proposed correction leads to a better image quality. The effects of the motion during transmission and reception of the pulse become noticeable when the maximum Doppler frequency is comparable to or larger than the range frequency resolution, equal to the PRF in CW systems. Therefore, in operational mode where the PRF can be lower than the entire Doppler bandwidth, as can be the case for spotlight and multiple receiver systems, the degradation induced by the motion within the sweep can seriously decrease the quality of the image. Applying the model developed in the chapter, deramped linear FMCW SAR data can be correctly processed and theoretical results are obtained. The integration of the non-linearity correction in FMCW SAR algorithms is described in appendix A, leading to a more general and efficient processing algorithm for FMCW SAR data.

References

[1] W. G. Carrara, R. S. Goodman, and R. M. Majewski, *Spotlight Synthetic Aperture Radar*. Boston, Artech House Inc., 1995.

[2] M. Soumekh, *Fourier Array Imaging*. Prentice Hall Inc., 1994.

[3] J. J. M. de Wit, A. Meta, and P. Hoogeboom, "Modified range-Doppler processing for fm-cw synthetic aperture radar," *IEEE Geosci. Remote Sensing Letters*, vol. 3, no. 1, pp. 83–87, Jan. 2006.

[4] A. Meta and P. Hoogeboom, "Signal Processing Algorithms for FMCW Moving Target Indicator Synthetic Aperture Radar," in *Proc. IEEE Int. Geoscience and Remote Sensing Symp. IGARSS'05*, Seoul, Korea, July 2005, pp. 316–319.

[5] A. Meta, P. Hoogebbom, and L. P. Ligthart, "Correction of the effects induced by the continuous motion in FMCW SAR," in *Proc. IEEE Radar Conf. '06*, Verona, NY, USA, Apr. 2006, pp. 358–365.

[6] D. C. Munson and R. L. Visentin, "A Signal Processing View of Strip-Mapping Synthetic Aperture Radar," *IEEE Trans. on Acoustic Speech and Signal Processing*, vol. 37, no. 12, pp. 2131–2147, Dec. 1989.

[7] M. Soumekh, D. A. Nobles, M. C. Wicks, and G. R. J. Genello, "Signal Processing of Wide Bandwidth and Wide Beamwidth P-3 SAR Data," *IEEE Transactions on Aerospace and Electronic Systems*, vol. 37, no. 4, pp. 1122–1141, Oct. 2001.

[8] P. Barton, "Digital beam forming for radar," *IEE Proceedings*, vol. 127, no. 4, Aug. 1980.

[9] M. Soumekh, "Bistatic synthetic aperture radar inversion with application in dynamic object imaging," *IEEE Transactions on Signal Processing*, vol. 39, no. 9, pp. 2044–2055, Sept. 1991.

[10] M. Youwn, *Digital Beam-Forming for High Resolution Wide Swath Real and Synthetic Aperture Radar*. Karlsruhe University, Ph. D. thesis, 2004.

Chapter 5

Moving Targets and FMCW SAR

The chapter exploits the peculiar characteristics of the complex FMCW SAR image for Moving Target Indication (MTI) purposes. Two SAR MTI methods are proposed. The first is based on the frequency slope diversity in the transmitted modulation by using linear triangular FMCW SAR. The second makes use of the Doppler filtering properties of randomized SFCW modulations.

5.1 Introduction

There is a need in several applications for the detection of ground moving targets and the estimation of their velocity. The motion of ground-based moving target such as car, truck or military vehicle, causes the radar signature of the moving target to shift outside of the normal ground return of a imaging radar. The problem of detecting slow moving vehicles in a land clutter environment is compounded by the fact that a significant portion of the useful signal bandwidth from the antenna's main lobe and sidelobe is often occupied by the ground return. When a single channel radar is used, the minimum detectable velocity of the target must be high enough to be clear of the main lobe and sidelobe clutter for robust target detection. The moving target Doppler shift from the clutter region is caused by the radial velocity component. Since the Doppler domain is sampled at the pulse repetition frequency, the available region extension is limited; moving targets with radial velocity high enough can have their Doppler spectrum folded back in the clutter region, and therefore they cannot be discriminated from stationary returns by frequency detection. Usually, in pulse SAR radars, the PRF can be chosen high enough for the unambiguous velocity to be less unlikely to occur; however, a large pulse duration, and therefore a low PRF , is desirable in FMCW SAR because this relaxes the sampling requirements and the circuitry complexity for a given range resolution and maximum range.

The chapter proposes two novel methods to discriminate moving targets which have their Doppler spectrum folded back in the clutter region. The first is based on the frequency slope diversity in the transmitted modulation by using linear triangular FMCW SAR while the second makes use of the Doppler filtering properties of randomized SFCW modulations.

5.2 Moving target Doppler spectrum

This section reviews the effects induced by the radial velocity component of a moving target on its Doppler spectrum. A stripmap mode case is analyzed and the scenario is illustrated in fig 5.1. Clutter spectrum response is approximately a chirp-like spectrum, whose band-

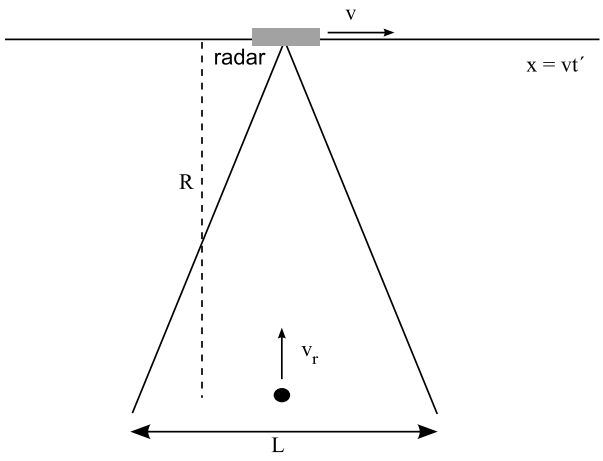


Figure 5.1: Moving target with radial velocity component in a stripmap scenario.

width is proportional to the antenna beamwidth, centered around the Doppler centroid, equal to zero for broadside SAR mode. The movement of a target induces a Doppler frequency proportional to the radial velocity, causing a shift of the target response. Figure 5.2(a) qualitatively represents the Doppler spectrum of a scenario where clutter, a slow and a fast moving target are present. The bandwidth of the slow moving target is almost completely covered by the clutter spectrum, while the fast moving target spectrum is in a clutter free region.

One simple MTI method makes use of the Doppler shift induced by the radial velocity of the moving target [1]. When the Doppler shift is high enough to have the moving target spectrum outside the clutter region, the latter can be filtered out and only signatures of moving objects remain in the SAR data. However, this technique has two limitations:

1. slow moving targets can be suppressed as well, since their spectrum can still be in the clutter region. This limitation is due to the fact that only one antenna is used. With more antennas, a spatial dimension is added to the range and Doppler information of usual SAR images, allowing the discrimination between angle of arrival and Doppler frequency, therefore enhancing the separation between clutter and slow moving targets [2][3];

2. moving targets with Doppler shift multiple of PRF will have their spectrum folded back into the clutter region. In fact, SAR data are sampled in the along track direction

with a sampling frequency equal to PRF. That means, the accessible Doppler information is between $\pm PRF/2$ and all the Doppler spectrum is mapped in this region, see fig. 5.2(b).

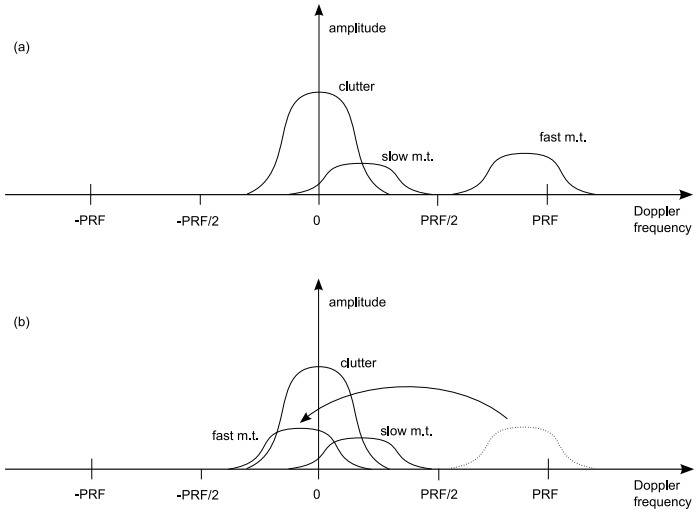


Figure 5.2: Doppler spectrum of clutter, a slow and a fast moving target.

Using a linear FMCW modulation, the Doppler region available for moving targets can be increased by having a larger PRF. However, transmitting the same bandwidth and using the same sampling frequency, also the frequency rate of the chirp is increased of the same factor therefore limiting the maximum range.

5.3 MTI with linear triangular FMCW SAR

This section provides a description of the effects of a moving target as they appear in an FMCW SAR image [4]; the results can be used to assist MTI capabilities. In conventional SAR systems, it is known from literature [1], that a moving target, when compared to a stationary target, is imaged smeared in range and shifted in azimuth because of its radial velocity and defocused as a consequence of its cross-range velocity and radial acceleration. The main aspect of this section is to emphasize the effect of the target radial velocity v_r on the FMCW SAR image. A broadside stripmap narrow-bandwidth and narrow-beamwidth case is

analyzed. The distance between the radar and the moving target is for a broadside mode:

$$\begin{aligned} r\left(R,x,t\right) &= \sqrt{(R-v_r t')^2+(vt'-x_1)^2} \\ &\approx \quad R-ax-v_r t+\frac{x^2}{2R}=r_{st}-ax-v_r t \end{aligned} \tag{5.1}$$

where $a=v_r/v$, $r_{st}=R+x^2/2R$ is the equivalent range distance if the target is stationary and the remaining variables are as defined in chapter 4. By using (5.1) in the equation for S_{IF}, expressed in (4.12), yields:

$$\begin{aligned} S_{IF} &= \exp\left(jK_r r\right) \approx \exp\left(jK_r\left(r_{st}-ax-v_r t\right)\right) \\ &\approx \exp\left(jK_{rc}\left(r_{st}-ax\right)+j\Delta K_r\left(r_{st}-ax-\frac{f_c v_r}{\alpha}\right)\right) \end{aligned} \tag{5.2}$$

After range compression, Fourier transforming the data with respect to the variable ΔK_r, the following is obtained:

$$\begin{aligned} s\left(r',x\right) \quad = \quad & \operatorname{sinc}\left(\frac{1}{\rho_r}\left(r'-\left(R-ax+\frac{x^2}{2R}-\frac{f_c v_r}{\alpha}\right)\right)\right) \\ & \exp\left(jK_{rc}\left(R-ax+\frac{x^2}{2R}\right)\right) \end{aligned} \tag{5.3}$$

where $\rho_r=c/2B$ is the image range resolution. In the exponential in (5.3), the linear term in x causes the Doppler spectrum of the moving target to be shifted with respect to the stationary case by an amount of $f_D=2v_r/\lambda_c$, where λ_c is the wavelength at the carrier frequency. This leads to the well known displacement in azimuth Δx of the moving target when displayed in a SAR image:

$$\Delta x = R\frac{v_r}{v}=\frac{R\lambda_c}{2v}f_D=\frac{L}{v}\frac{d}{2}f_D=\rho_{az}\frac{f_D}{\delta f_D} \tag{5.4}$$

where L is the SAR observation length for a distance R, d is the antenna length, ρ_{az} is the azimuth resolution and δf_D is the frequency resolution for the observation length L in the Doppler domain. If Δx is larger than L, the response in the image is shifted by [1]:

$$\Delta x_{imag}=\left(\left(\Delta x+\frac{L}{2}\right)\ \text{modulo}\ L\right)-\frac{L}{2} \tag{5.5}$$

and this is due to the ambiguity of PRF in the measurement of the Doppler frequency. From the $sinc$ function in (5.3) it is possible to see that the term ax causes the range smearing of the moving target image, and that the term $f_c v_r/\alpha$ shifts the response in the range direction of:

$$\Delta R=\frac{f_c v_r}{\alpha}=\frac{c}{2B}\frac{f_c}{c}2v_r PRI=\rho_r\frac{f_D}{PRF}=\rho_r\frac{f_D}{\delta f_r} \tag{5.6}$$

where δf_r is the range frequency resolution equal to the PRF (twice the PRF for symmetric triangular modulations). The range shift is a typical characteristic of FMCW radars [5] and it

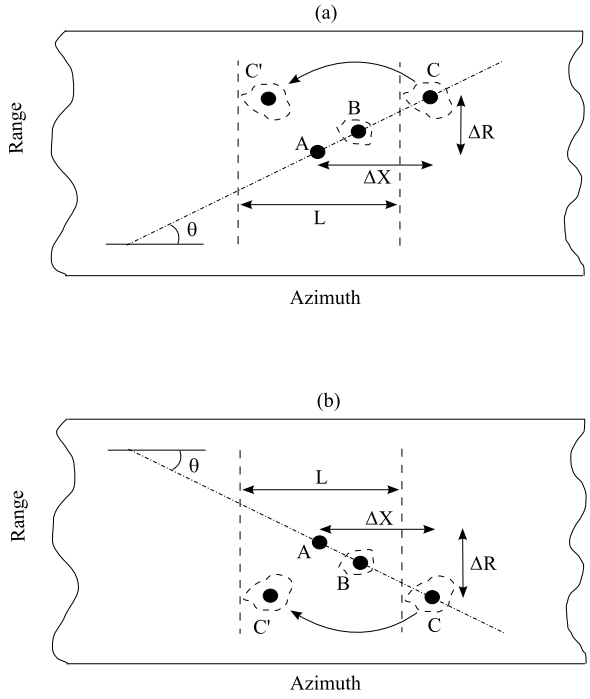


Figure 5.3: Effects induced by moving targets in FMCW SAR images. When compared to a stationary case (A), the moving target responses are shifted in range and azimuth (dots), smeared (dashed contours) and imaged within the dashed lines (B, C'). FMCW SAR images produced with the upslope part of the modulation (a) show opposite range shift compared to downslope image (b).

is not present in conventional pulse SAR systems because of their very poor frequency range resolution. The sign of ΔR depends on the sign of v_r (approaching or receding target) and of α (upslope or downslope modulation). The relation between ΔR and Δx is expressed as (see fig.5.3):

$$\tan(\theta) = \frac{\Delta R}{\Delta x} = \frac{\rho_r \frac{f_D}{\delta f_r}}{\rho_{az} \frac{f_D}{\delta f_D}} = \frac{\rho_r}{\rho_{az}} \frac{\delta f_D}{\delta f_r} \tag{5.7}$$

and, if the image pixel is symmetric (i.e. the azimuth and range resolution are equal) (5.7) reduces to $\tan(\theta) = \delta f_D / \delta f_r$.

When the target position is known, one simple technique to estimate the radial velocity, used with single antenna pulse SAR, consists of measuring the azimuth shift and so the Doppler frequency and the radial velocity. Since the measurable shift is not Δx but actually Δx_{image}, the velocity estimation can be ambiguous. In FMCW SAR systems using triangular modulation, two images of the same scene can be produced: one processing the upslope

part of the received signal and another one using the downslope. After correction of the motion within the sweep described in chapter 4, stationary targets are imaged in the same way in the two pictures, while the moving target has the same shift in the azimuth direction but opposite shift in the range direction. Once ΔR is estimated, Δx is derived from (5.7) and so the radial velocity estimated without ambiguity. This technique, like the previous one described for the pulse SAR system, works properly if the range shift can be observed, i.e. if the moving target is visible in both the images. In order to detect changes induced by the motion of the targets in the two images, standard interferometric deformation techniques can be used [6]. The processing block diagram is shown in fig. 5.4. An example of the application of the method on real data is reported in section 7.8.

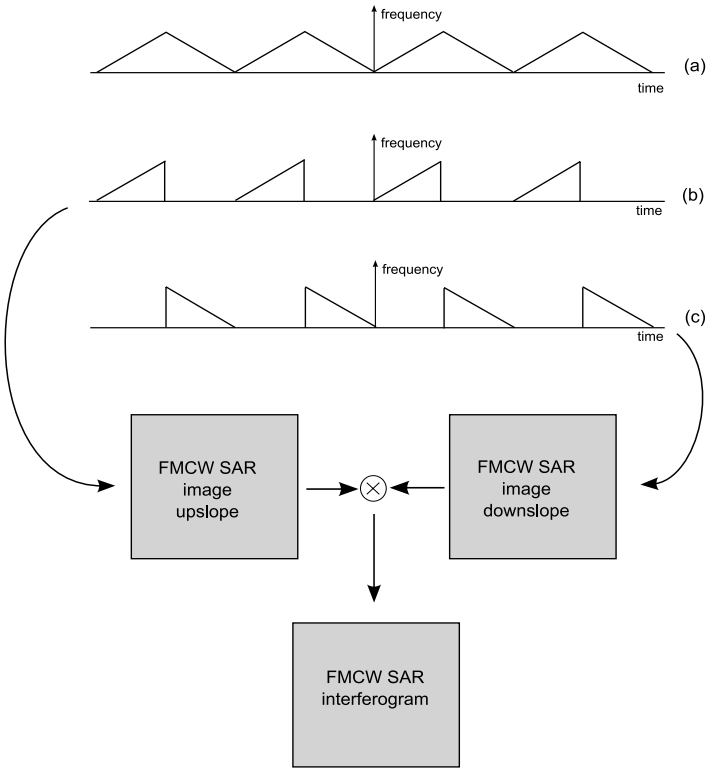


Figure 5.4: MTI with triangular FMCW modulation. The original raw data (a) is divided in two sequences containing the upslope (b) and downslope (c) part, respectively. From each of them, one FMCW SAR image is produced and successively the two are processed using interferometric deformation techniques in order to detect changes induced by moving targets.

5.4 MTI with randomized non-linear SFCW SAR

Randomized non-linear SFCW signals have been introduced in section 3.6. This class of modulation can be described as noise like signals, which have the property of suppressing range ambiguities and being Doppler intolerant. In [7], a randomized SFCW modulation has been used in SAR imaging to mitigate the effects of Doppler aliasing due to the undersampling of the Doppler bandwidth, especially if the PRF is limited and the antenna beamwidth large. This technique is based on the fact that the stepped frequency order inside the pulse is randomly changed from pulse to pulse. After collection of an adequate number of pulses, signal compression leads to a composite ambiguity function equal to:

$$|\chi(\tau, f_D)|^2 = |sinc(B\tau)sinc(f_D T_p)|^2 \tag{5.8}$$

where B is the transmitted bandwidth, τ is the range time delay, f_D the Doppler frequency and T_p is the time duration of the complete stepped frequency waveform. In most of the usual applications, SAR Doppler aliasing artifacts occur at multiples of the PRF; choosing T_p equal to Pulse Repetition Interval (PRI = 1/PRF), that means Continuous Wave (CW) operation mode, the artifacts will be removed by the range compression operation.

In the present section, the technique is extended to the case of moving targets [8]. It is known from SAR literature [9] that imaging a moving target is equivalent to squint mode SAR processing of a stationary target. The equivalent squint angle depends on the target velocity; therefore, there are certain velocities that induce a squint angle such that the moving target Doppler bandwidth falls over (due to the undersampling) in the clutter region. It is not possible to discriminate these moving targets using solely the Doppler information. However, with the randomized technique it is possible to produce an ambiguity function that minimize the clutter return and enhance MTI capabilities.

The aim of this section is to describe how to use non-linear SFCW signals to enhance the indication of a certain category of moving targets in SAR images using systems with a single antenna. Using randomized SFCW signals, the composite ambiguity function is well approximated by (5.8), indicating that the nulls of the $sinc$ function in the Doppler direction are placed at multiples of $1/T_p$. In CW signals, the pulse duration is equal to the PRI and therefore the nulls are at multiples of the PRF. In this way, range compressing the raw SAR signal (with matched filtering or with deramping technique described in section 3.6) with the proper Doppler frequency, it is possible to suppress the clutter return and to have only the Doppler region of interest. This is obtained multiplying the raw SAR data with the following function:

$$\exp(j2\pi f_D t) \tag{5.9}$$

where f_D is the Doppler of interest and $-PRI/2 < t < PRI/2$. Successively, range and azimuth processing is performed.

In order to validate the concept, simulations have been performed. Ten stationary and moving targets have been simulated with the parameters listed in tab. 5.1 and represented in

Table 5.1: Target scenario for the moving target simulations

Scatterer Number	Range (m)	Azimuth (m)	Doppler (PRF)
1	350	-3	0
2	340	3	0
3	300	-3	0
4	290	3	0
5	250	-3	0
6	240	3	0
7	270	-1	-0.5
8	310	-1	-1
9	305	2	0.5
10	260	2	1

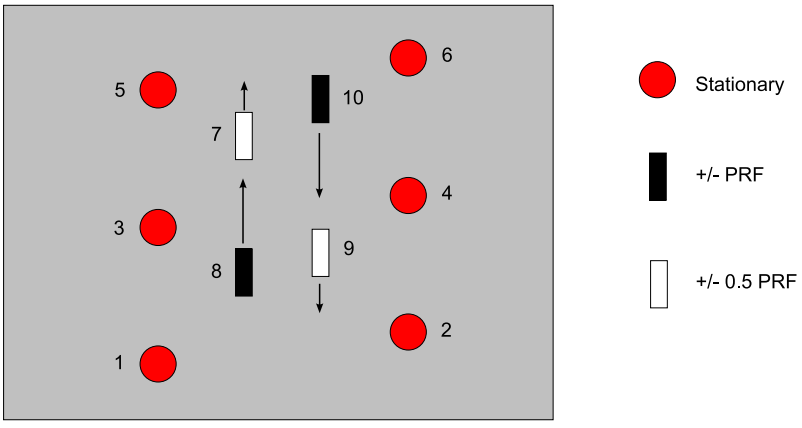


Figure 5.5: Moving and stationary target scenario for the randomized SFCW SAR MTI simulation.

fig. 5.5, while the radar parameters are the same as reported in tab. 3.1, except the transmitted bandwidth, reduced to 100 MHz in this simulation. The radar platform velocity and the antenna beamwidth values have been set to 50 m/s and 8^o, respectively. A broadside case has been analyzed, and using a 10 GHz carrier frequency results in a clutter Doppler extension of 500 Hz centered around zero Doppler. The moving targets travel along the radial direction with velocities such that their spectrum is shifted by the amount reported in the last column of tab. 5.1. Both linear and randomized SFCW signals have been generated; the azimuth compression processes a bandwidth of 250 Hz centered around zero Doppler. Resulting SAR images are shown in fig. 5.6. In fig. 5.6(a), the image obtained using linear SFCW modulation is reproduced; it can be noticed that stationary targets are correctly imaged, as well as target 8 and 10 (only some range blurring is observable, due to the range migration). In fact, the Doppler spectrum of target 8 and 10 is folded back in the clutter region and therefore their phase history matches the SAR reference compression function. This also means that filtering out the clutter region will suppress these two moving targets. Obviously, target 7 and 9 are not imaged because their spectrum is outside the processed bandwidth; they can be detected processing the remaining part of the Doppler spectrum.

Using randomized SFCW modulation, the Doppler filtering is performed directly during the range compression, reducing in this way aliasing problems. Results are reported in fig. 5.6(b), 5.6(c) and 5.6(d): the three images have been produced centering the Doppler region of interest to zero, -PRF and +PRF, respectively. It is evident how the three different Doppler regions can be suppressed separately, enhancing in this way the moving target indication capability.

A close up view of the normalized amplitude cross-range profile of the corresponding SAR images of fig. 5.6 is shown in fig. 5.7. The two curves are the responses of the stationary target 5 (solid line) and of the moving target 10 (dot-dashed line). By comparing fig. 5.7(b) with fig. 5.7(c) and fig. 5.7(d), clutter suppression can be quantified to be approximately 25 dB.

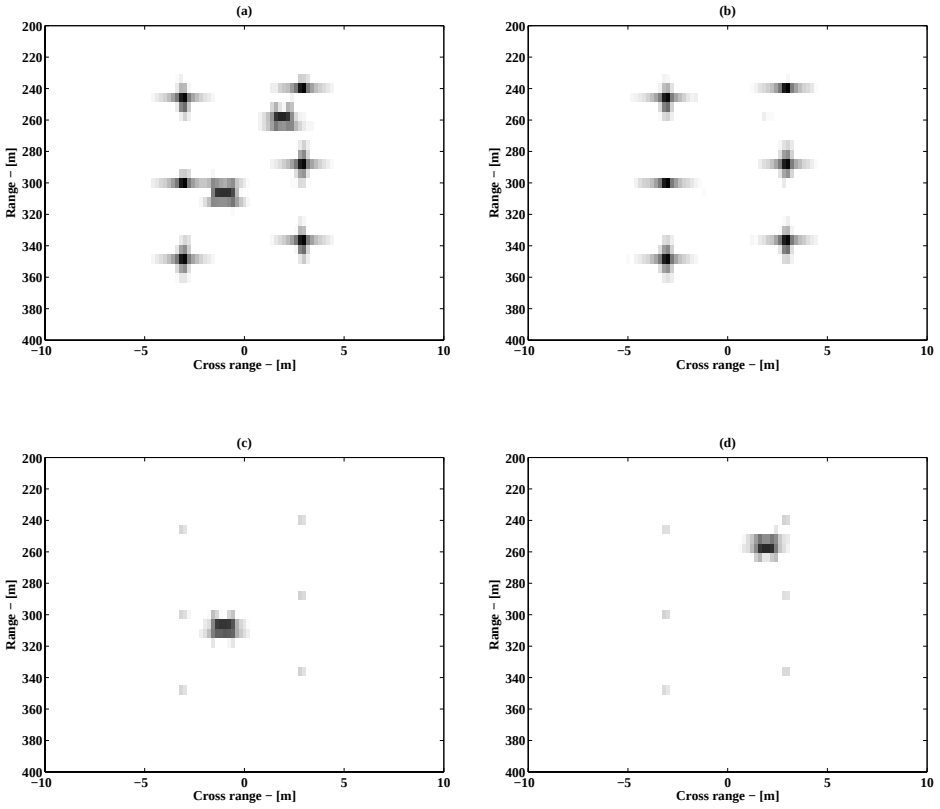


Figure 5.6: Moving target simulations. SAR images produced when transmitting linear SFCW (a) and when using randomized SFCW with range compression relative to zero, minus one and plus one time the PRF, (b), (c), (d) respectively. In the latter cases, it is possible to discriminate moving and stationary targets.

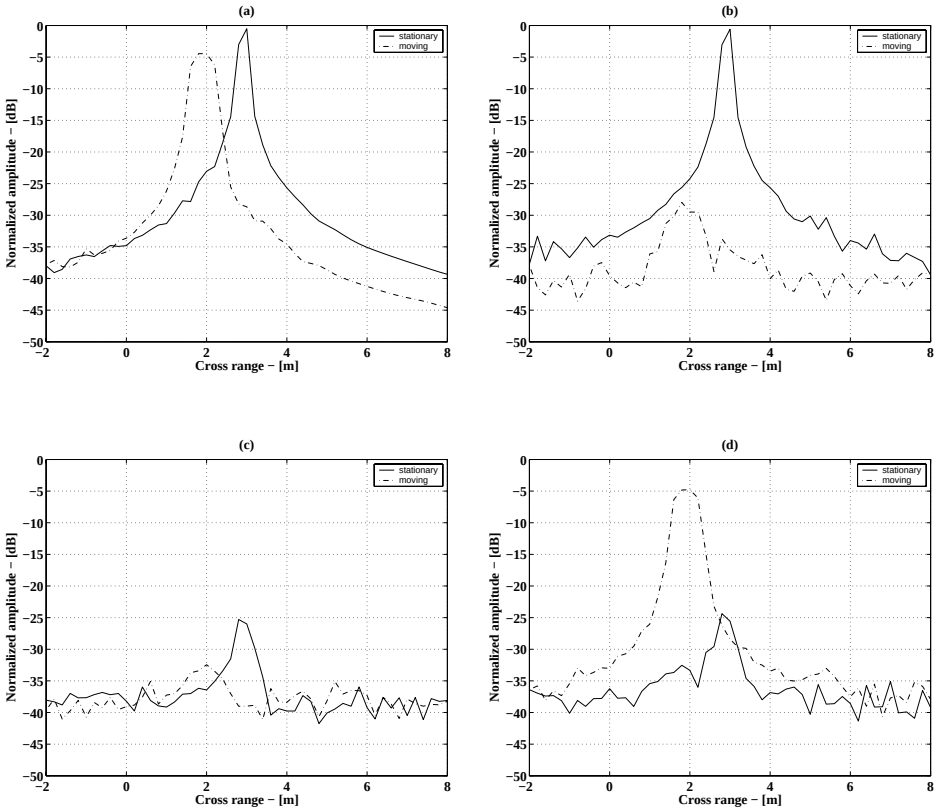


Figure 5.7: Moving target simulations. Close up view of the normalized amplitude cross-range profile of the corresponding SAR images of fig. 5.6. The two curves are the responses of the stationary target at 250 m (solid line) and of the moving target at 260 m (dot-dashed line), target 5 and 10 in fig. 5.5 respectively. In (a) the response of the SAR image obtained with linear SFCW is shown, while (b), (c), (d) report the response of the SAR images obtained with randomized SFCW with range compression relative to zero, minus one and plus one time the PRF, respectively.

5.5 Summary

The chapter has described some peculiar characteristics of the complex FMCW SAR image for Moving Target Indication (MTI) purposes. Two SAR MTI methods have been proposed. The first is based on the frequency slope diversity in the transmitted modulation by using linear triangular FMCW SAR. Two images are produced by separately processing the upslope and downslope part of the received signal. Successively, deformation interferometric techniques are applied to the pair of images, discriminating moving targets from the stationary clutter and solving the velocity ambiguity estimation.

The use of randomized SFCW signals, where the frequency order is randomly changed from pulse to pulse, has been proposed for enhancing the indication of moving target with Doppler shift multiples of the PRF and when single antenna systems are used. Clutter suppression of 25 dB has been shown, while still preserving the moving target response. The suppression is performed directly during the range compression, avoiding in this way spectrum aliasing problems in the Doppler domain. Because SFCW signals are uncorrelated from pulse to pulse, the use of this kind of modulations also gives the capability to look at further range, because the range ambiguities are suppressed as well.

References

[1] R. K. Raney, "Synthetic Aperture Imaging Radar and Moving Targets," *IEEE Transactions on Aerospace and Electronic Systems*, vol. 7, no. 3, pp. 499–504, May 1971.

[2] R. Klemm, *Principles of Space-Time Adaptive Processing*. IEE-UK, 2002.

[3] J. R. Guerci, *Space-Time Adaptive Processing for Radar*. Artech House, 2003.

[4] A. Meta and P. Hoogeboom, "Signal Processing Algorithms for FMCW Moving Target Indicator Synthetic Aperture Radar," in *Proc. IEEE Int. Geoscience and Remote Sensing Symp. IGARSS'05*, Seoul, Korea, July 2005, pp. 316–319.

[5] M. I. Skolnik, *Introduction to Radar Systems*. McGraw-Hill, Inc., 1980.

[6] R. F. Hanssen, *Radar Interferometry*. Kluwer Academic Publishers, 2001.

[7] J. E. Luminati, T. B. Hale, M. A. Temple, M. J. Havrilla, and M. E. Oxley, "Doppler Aliasing Artifacts Filtering in SAR Imagery using randomized Stepped-Frequency Waveforms," *IEE Electronic Letters*, vol. 40, no. 22, pp. 1447–1448, Oct. 2004.

[8] A. Meta, P. Hoogeboom, and L. P. Ligthart, "Moving Target Indication enhancement in FMCW SAR using deramped randomized stepped-frequency signals," in *Proc. Waveform Diversity and Design Conf. WDDC'06*, Lihue, HI, USA, Jan. 2006.

[9] M. Soumekh, *Synthetic Aperture Radar Signal Processing with MATLAB Algorithms*. John Wiley & Sons, Inc., 1999.

Chapter 6

FMCW SAR demonstrator system

The chapter describes the FMCW SAR demonstrator system, including a detailed analysis of the X-band radar front-end, developed at the Delft University of Technology. A complete system model is provided in order to estimate and analyze the performances of the FMCW SAR demonstrator. Laboratory measurements show very good consistency with the calculated values, validating therefore the model description.

6.1 Introduction

One of the main objectives of the project was to show the feasibility of an FMCW SAR operated under practical conditions and that this aim could be reached with a cost effective, yet efficient, approach. Therefore, concurrently with the studies on the FMCW SAR digital signal processing algorithms described in the previous chapters, a complete SAR system has been developed at the IRCTR, Delft University of Technology. The work for the initial requirements to the FMCW SAR system, the acquisition design and the development of the controlling software has been done by dr.ir. J.J.M. de Wit within the framework of the project, and the reader is referred to [1] [2] [3] for further details. The system overview is briefly reviewed in this section in order to have a complete picture of the SAR demonstrator. Next, a detailed analysis of the 10 GHz radar front-end, developed within the framework of this thesis, will be given in the remaining of the chapter.

In designing a SAR system, the operational modes in which the sensor operates and the characteristics of the aircraft which carries the sensor have to be taken into account. The FMCW SAR demonstrator was meant to fly in a stripmap configuration and to be able to operate in different resolution modes, up to 45 cm resolution in range as well in azimuth. A small aircraft was chosen as platform in order to show the feasibility of an FMCW SAR with such a kind of carrier. The Stemme S10 light motor glider, manufactured by Stemme GmbH, fulfills this requirement and provides a relatively cheap test aircraft. The S10 is a twin seat, light surveillance glider, with a maximum altitude of 7 km and a velocity which can vary between 30 m/s and 60 m/s. The maximum payload is 50 kg and the complete demonstrator system had to be tailored to this constraint.

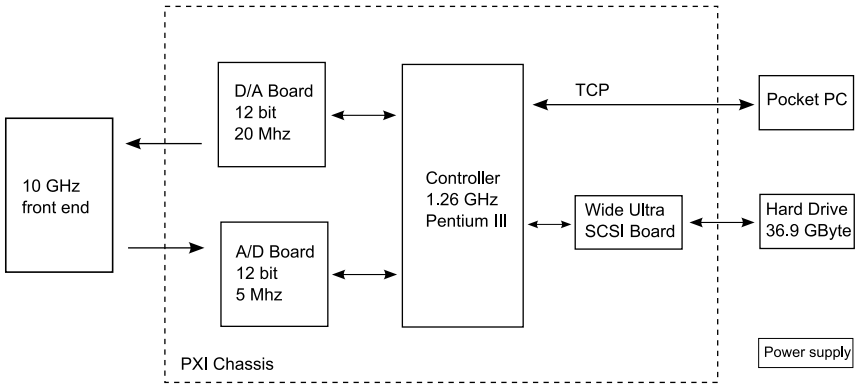


Figure 6.1: Block diagram of the FMCW SAR demonstrator system.

The core of the demonstrator system is a PXI chassis manufactured by National Instruments. This chassis includes an embedded controller, a waveform generator to control the FMCW front-end and a fast Analog to Digital Converter (ADC) board to sample the radar data. During the flights, the system can be monitored and controlled from the cockpit with a pocket PC [4]. The radar data are sampled at 5 MHz. The samples are stored as 16 bits leading to a continuous data rate of 9.5 Mbytes/s [2]. Of the 16 bits, only 12 carry information and this number can be further reduced in a following improvement of the system. A block diagram of the complete FMCW SAR demonstrator system is shown in fig. 6.1. For the motor glider, standard under wing pods are available. The pods have a useful length of 80 cm and a diameter of 35 cm. The FMCW SAR demonstrator has been fitted in such a pod. However almost all the payload is constituted by the PXI chassis and the battery. With a dedicated design, outside the scope of this thesis, the size and weight of the whole system can be drastically reduced.

6.2 Front-end

A diagram of the radar front-end is shown in fig. 6.2. The core of the device is an X-band VCO; a voltage signal, generated by the Digital to Analog Converter (DAC), is used to steer the VCO which produces the signal bandwidth directly in the RF frequency band. Before entering the VCO, the steering signal is filtered with a Low Pass Filter (LPF) in order to eliminate the peaks due to the quantized nature of waveform generator output and attenuated to not damage the VCO. The output of the VCO feeds directly the transmitting antenna; a small fraction of the transmitted signal is attenuated and sent through the delay line, a Sur-

face Acoustic Wave (SAW) embedded in the front-end, which produces a delay of 0.5 μs, equivalent to a distance of 75 m. The SAW output is then connected to the receiver chain. The delay line response is used for internal calibration and for linearization purposes. The received signal intercepted by the antenna beam is amplified with a low noise amplifier (LNA) and mixed with part of the transmitted signal. The output of this process, the Intermediate Frequency (IF) signal, is successively high pass filtered in order to remove the strong direct coupled signal, which could saturate the sampling card, and amplified. Before being sampled by the acquisition card, which use a real sampling frequency of 5 MHz, the IF signal is low pass filtered in order to meet the Nyquist sampling requirements. The sampled IF signal is then processed via the algorithms described in chapter 3 in order to obtain the range information. An optimal design would have included also a pass band filter before the LNA, and a image rejection filter at the mixer stage. However, these components were not available at the time of the assembling, and the obtainable improvement (noise level decreased of about 5 db) was not crucial for proving the feasibility of an FMCW SAR.

6.2.1 Steering signal

In order to avoid problems related with the discrete nature of the steering signal, an external voltage offset has been provided implementing an operational amplifier. In this way the voltage excursion can be centered around the mean value required by the VCO. In the demonstrator system, the maximum measurable frequency is 2.5 MHz; the discrete steering signal leads to a stepped frequency modulation whose unambiguous beat frequency is equal to $f_u = N/PRI$, where N is the number of steps (see section 3.5). By using 12 bits for the steering signal and a PRI of 1.024 ms (the longest used by the FMCW SAR demonstrator), the unambiguous beat frequency is equal to 4 MHz and therefore out of the frequency range of interest. Furthermore, the operational amplifier has a slew rate characteristic such that it is insensitive to frequencies higher than 1 MHz; therefore the high frequency part of the steering signal is filtered and any residual effect of the quantization is eliminated.

6.2.2 Predistorted linearization

In the system, a digital to analog converter reads a digital table whose values range from -1 to 1, and produces an analog signal which, after being combined with an external offset, is used to steer the VCO. If $s(t)$ is the signal table stored in the DAC memory, the frequency at the output of the VCO can be expressed as:

$$f_{VCO}(t) = f_c + \alpha t + e(t) = f_c + \alpha \frac{PRI}{2} s(t) + h_{nl}(t) \tag{6.1}$$

where $e(t)$ is a zero mean function describing the frequency non-linearity at the VCO output, $h_{nl}(t)$ is a function accounting for the VCO non-linearity and t is varying within the period time interval.

If a reference signal is available, e.g. from a delay line, the range response of such a signal can be used to estimate the non-linearities, and to produce a new steering signal for the

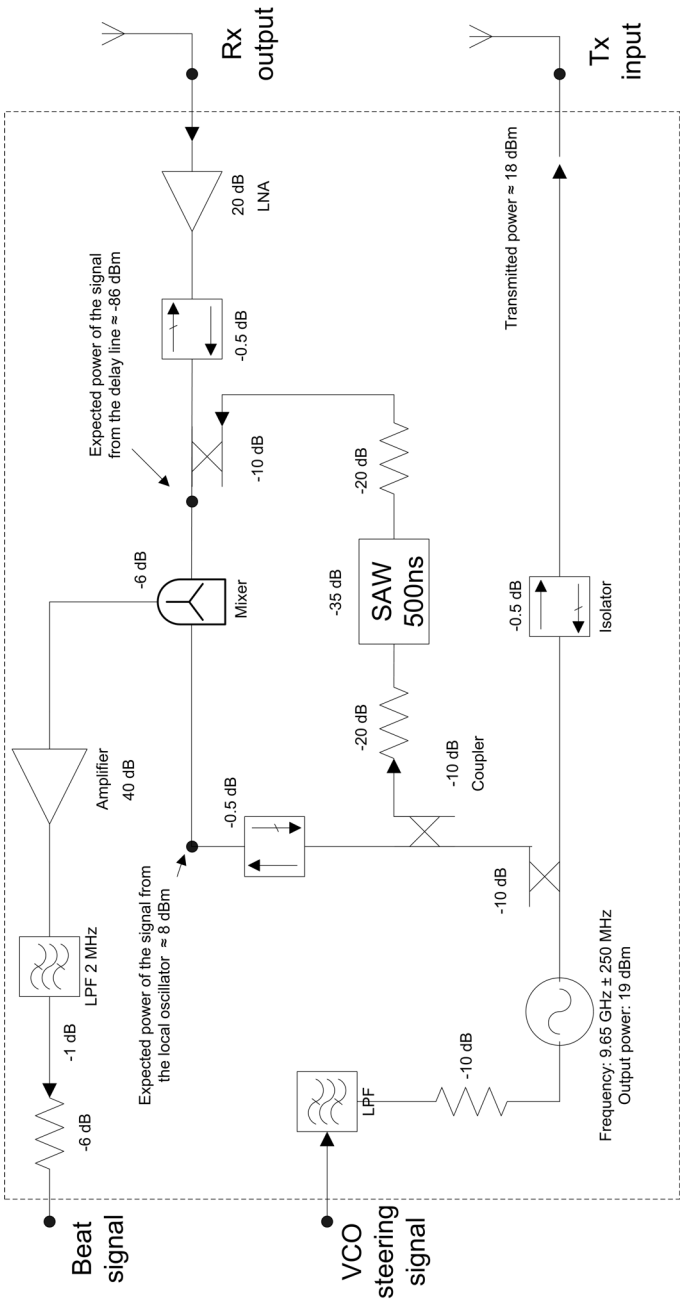


Figure 6.2: Radar front-end diagram.

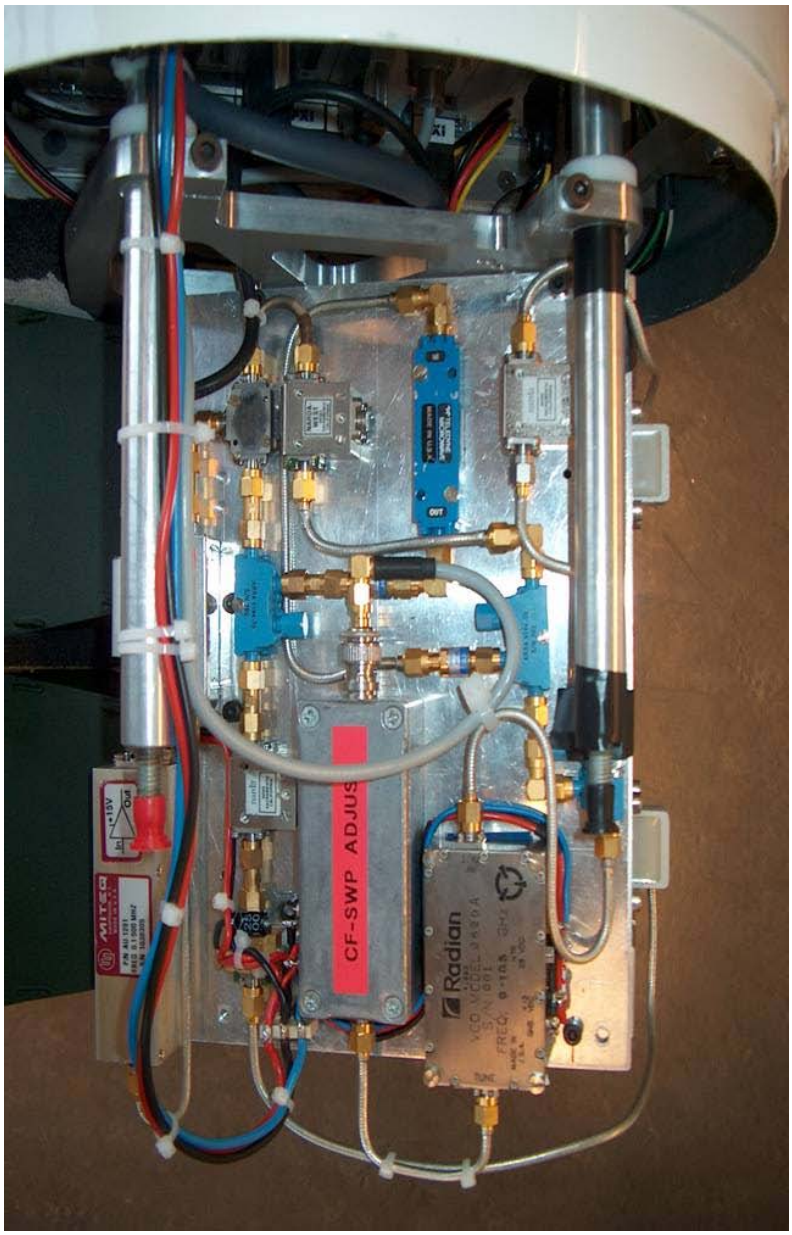


Figure 6.3: The X-band radar front-end.

VCO which compensates for for the non-linearities. Writing the transmitted signal as:

$$s_T(t) = \exp\left(j2\pi \int f_{VCO}(t)\,\mathrm{d}t\right) = \exp\left(j2\pi \int (f_c + \alpha t + e(t))\,\mathrm{d}t\right) \tag{6.2}$$

and the reference as:

$$s_{ref}(t) = \exp\left(j2\pi \int (f_c + \alpha(t-\tau_{ref}) + e(t-\tau_{ref}))\,\mathrm{d}t\right) \tag{6.3}$$

the intermediate frequency signal can be expressed as:

$$s_{IF}(t) = \exp\left(j2\pi\left(\alpha\tau t + \int (e(t) - e(t-\tau_{ref}))\,\mathrm{d}t\right)\right) \tag{6.4}$$

$$\approx \exp\left(j2\pi\left(\alpha\tau_{ref} t + \int (\tau_{ref} e'(t))\,\mathrm{d}t\right)\right) \tag{6.5}$$

$$= \exp\left(j2\pi(\alpha\tau_{ref} t + \tau_{ref} e(t))\right) = \exp(j2\pi\varphi(t)) \tag{6.6}$$

After the division of the sweep time in short intervals, the beat frequency of the reference signal as function of time can be estimated using a spectrogram, i.e. short time FFT. If the intervals are short enough, $e(t)$ can be considered linear, and, in this case, a Fourier transform will estimate the derivative of the function $\varphi(t)$:

$$f_b(t) = \frac{\mathrm{d}\varphi(t)}{2\pi \mathrm{d}t} = \alpha\tau + \tau e'(t) \tag{6.7}$$

Noting that the mean value of (6.7) is $\alpha\tau_{ref}$ and that τ_{ref} is known, α and $e'(t)$, and therefore also $e(t)$, can be estimated. From (6.1) $e(t)$ can be expressed as:

$$\begin{aligned} e(t) &= \alpha\frac{PRI}{2} s(t) - \alpha t + h_{nl}(t) \\ &= \alpha\frac{PRI}{2} s(t) - \left(\alpha\frac{PRI}{2} s_{lin}(t) + h_{nl}(t)\right) + h_{nl}(t) \\ &= \alpha\frac{PRI}{2}(s(t) - s_{lin}(t)) = \alpha\frac{PRI}{2} s_e(t) \end{aligned} \tag{6.8}$$

where $s_{lin}(t)$ is the predistorted signal which, when applied to the VCO input, produces a linear frequency sweep (equal to αt) at its output, and $s_e(t)$ is the correction to be applied to the signal stored in the DAC memory.

The algorithm can be iteratively repeated in order to achieve a better performance. It has been applied to real data collected with the radar front-end, where the reference signal was the delay line signal, and the results are shown in fig. 6.4. The reproduced range profiles have been obtained without applying any windowing. A 120 m cable was also connected from the transmitter output to the receiver input. After 5 iterations, the predistorted steering signal removes the frequency non-linearities effects almost completely. If not performed before every measurement, a drawback of this method (as well as of any other solution based on the

use of a predistorted signal for the non-linearity correction) is that the linearization degrades quite drastically as soon as the external conditions, e.g. temperature, change. If this is the case, the post processing non-linearity correction algorithm, developed within the framework of this thesis and described in chapter 3, can be applied on the collected data.

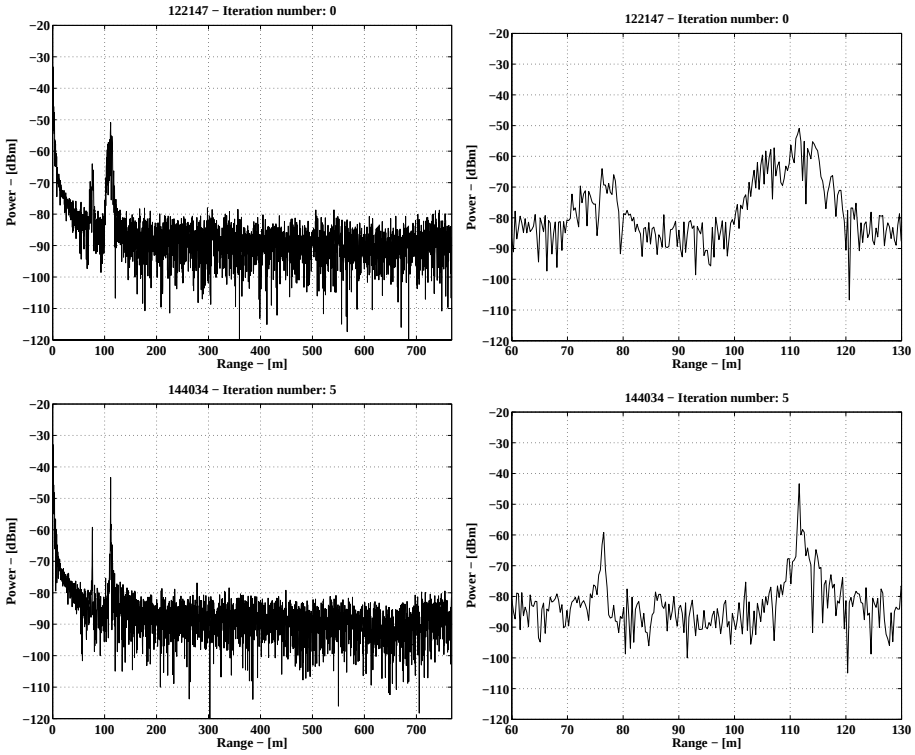


Figure 6.4: Linearization results. Range profiles of a reference delay line and a cable, which reproduce point target responses placed at a distance of 75 m and 120 m, respectively. No windowing has been applied in order to reduce the sidelobes. After 5 iterations, the predistorted steering signal removes the frequency non-linearities effects almost completely.

6.3 Noise power calculation

In this section, a complete and detailed noise power calculation for the X-band FMCW radar front-end is derived analyzing the contribution of the thermal noise, phase noise and quantization noise. Using the schematic receiver chain of fig. 6.5, the total gain and the total noise figure of the whole receiver part is G = 47 dB and $F \approx 3.7$ dB.

6.3.1 Thermal noise

The thermal noise power at the input of the ADC is expressed as [5]:

$$N_t = kT_0BFG \tag{6.9}$$

where $k = -228.6$ dBW/K/Hz is Boltzmann's constant, $T_0 = 290$ K is the standard temperature and B,F and G are the bandwidth, the noise figure and the gain of the complete receiver part, respectively. After range compression, the noise power is spread over all the available range cells, therefore the signal to noise ratio is increased by a factor equal to the time-bandwidth product of the frequency modulated signal, that is $B \cdot PRI$ or, equivalently, B/PRF . The thermal noise power in one resolution cell is:

$$N_t = \frac{kT_0BFG}{BPRI} = kT_0PRF\,FG \tag{6.10}$$

Using a PRF equal to 1 kHz, the value of the theoretical thermal noise power is:

$$N_t = -228.6\text{dBW/K/Hz} + 24.6\text{dBK} + 30\text{dBHz} + 4\text{dB} + 47\text{dB} = -123 \quad \text{dBW} \tag{6.11}$$

However, since the 10 GHz radar front-end developed at the Delft University of Technology does not have an image filter rejection, the actual measured noise $N_{t_{DSB}}$ is the Double Side

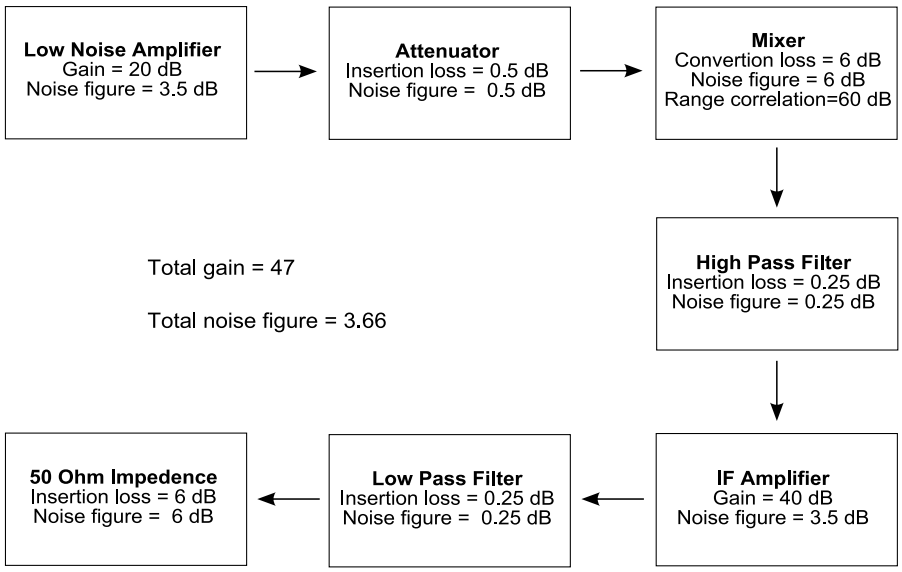


Figure 6.5: Schematic description of the complete receiver chain

Band (DSB), therefore 3 dB have to be added to the previous calculated value:

$$N_{t_{DSB}} = -120 \quad \text{dBW} \tag{6.12}$$

6.3.2 Phase noise

Because the front-end has two different antennas for the transmitting and the receiving part, the major contribution of the phase noise is determined by the coupling of the mixer. The phase noise power related to the coupling of the mixer is [6]:

$$N_{p1} = \frac{P_{LO} Nosc(f_{ofs})}{\chi} \tag{6.13}$$

where P_{LO} is the Local Oscillator (LO) signal power, N_{osc} is the oscillator phase noise at a frequency offset f_{ofs} relative to the carrier frequency and χ is the mixer isolation between the RF and LO input signal. The phase noise is reduced due to the range correlation effect if a fraction of the transmitted signal is used as LO signal [7]. The range correlation factor is equal to:

$$K^2 = 4\sin(\pi f_{ofs} \Delta t_{pn}) = 4\sin(\pi f_{ofs} \frac{2\Delta R_{pn}}{c}) \tag{6.14}$$

in which Δt_{pn} and ΔR_{pn} are the time delay and the path of the mixer coupling. In fig. 6.6 the range correlation factor is plotted as function of the coupling path (for constant frequency offset) and of the offset frequency (for constant coupling path).

After amplification, sampling and range compression, assuming the oscillator phase noise constant in a frequency bandwidth equal to the PRF , the phase noise power in one resolution cell is:

$$N_p = N_{p1} PRF\, K^2 G_m \tag{6.15}$$

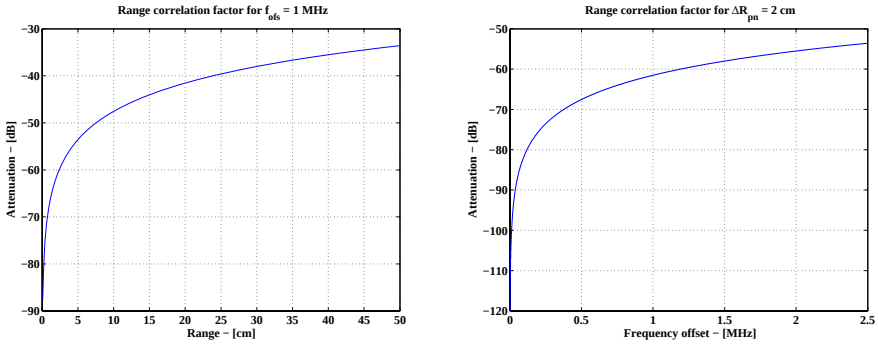


Figure 6.6: Range correlation factor for the phase noise power as function of the path length (for a constant frequency offset of 1 MHz) and of the frequency offset (for a constant path length of 2 cm).

where G_m is the gain of the receiver chain without the LNA, that is starting from the mixer. For the 10 GHz radar front-end, the following parameters hold for the calculation of the phase noise: P_{LO} = -21 dBW, N_{osc}(1 MHz) = -113dBc/Hz, χ = -40dB, $K^2 \approx$ -60dB (at 1 MHz and assuming for the mixer a coupling path of 2 cm) and G_m = 27. Using (6.13) and (6.15) yields to:

$$\begin{aligned} N_p &= -21\text{dBW} - 113\text{dBc/Hz} - 40\text{dB} + 30\text{dBHz} - 60\text{dB} + 27\text{dB} \\ &= -177\ \text{dBW} \end{aligned} \tag{6.16}$$

For the final calculation, the same discussion done for the thermal noise holds for the phase noise. The Double Side Band phase noise $N_{p_{DSB}}$ is 3 dB higher than the previously calculated:

$$N_{p_{DSB}} = -174 \quad \text{dBW} \tag{6.17}$$

6.3.3 Quantization noise

The quantization noise can be expressed as:

$$N_q = \frac{q^2}{12} \tag{6.18}$$

where q is the quantization interval, and after range compression:

$$N_q = \frac{q^2}{12}\frac{PRF}{B} \tag{6.19}$$

The dynamic range of the system ADC is 0.4 Vpp and 12 bits are used ($q = 0.4\text{V}/2^{12}$), so from (6.19) the following value for the quantization noise in one resolution cell is obtained:

$$N_q = 2(-3.97 - 36.12) - 10.79 + 30 - 86.9 = -147.87 \quad \text{dBW} \tag{6.20}$$

6.3.4 Total noise

Combining (6.11), (6.16) and (6.20), the total noise power in one resolution cell, after sampling of the IF signal and range compression, equals to:

$$N_{tot} = N_{p_{DSB}} + N_{p_{DSB}} + N_q \approx -120\text{dBW} = -90 \quad \text{dBmW} \tag{6.21}$$

6.4 Experimental tests

Several tests and measurements have been carried out in order to verify the consistency of the front-end model previously developed. In the following subsections, laboratory measurements of the noise level and phase stability are reported.

6.4.1 Noise laboratory measurements

A measurement of the total system noise power N_{tot} with the transmitting antenna switched off has been performed. In this configuration only the noise and the delay line response contribute to the range profile. The results are presented in fig. 6.7; no windowing has been applied. The measurements show a noise level around -87.5 dB, a value very close to the expected for the total noise power. The measured difference is around 2.5 dB. Also the delay line peak response, around -59 dB, matches very well the predicted power.

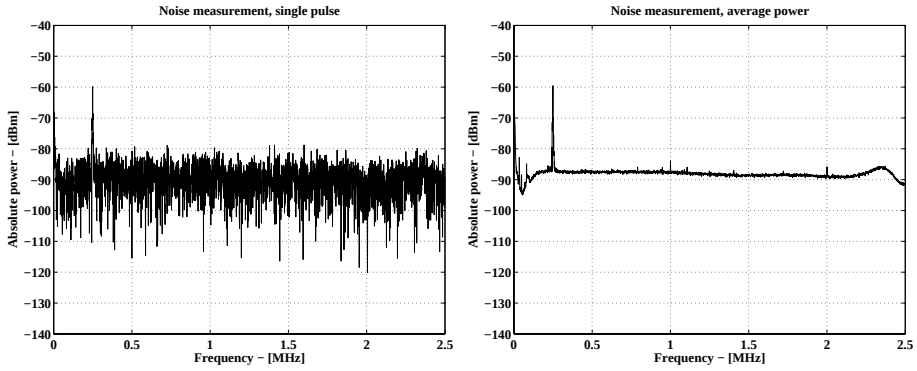


Figure 6.7: Noise power measurement results, with the delay line response present. In (a) a single processed sweep is shown, while (b) presents the response after incoherent averaging of 1024 sweeps, corresponding to 1 second of data acquisition.

6.4.2 Phase measurements

A phase stability analysis has been performed on the collected data observing the behavior of the phase of the delay line response from sweep to sweep. Results are shown in fig. 6.8. The standard deviation of the phase has been calculated and corresponds to 0.119 radians. Additionally, measurements with the 1 MHz filtering removed have been performed and reported in the figure, where a slight phase degradation is noticeable.

6.5 Summary

The chapter has described the complete FMCW SAR system developed at the IRCTR, Delft University of Technology. Particularly, a detailed analysis of the 10 GHz radar front-end, developed within the work of this thesis, has been provided. Noise power calculations, based on the schematic chain of the front-end, correspond very well with the laboratory measurements.

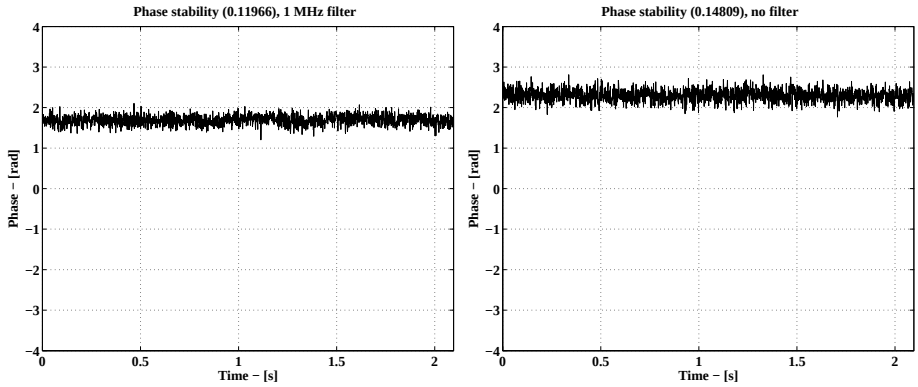


Figure 6.8: Filter effects on the phase stability.

References

[1] J. J. M. de Wit, *Development of an Airborne Ka-Band FM-CW Synthetic Aperture Radar*. Delft University of Technology, Ph. D. thesis, 2005.

[2] J. J. M. de Wit and P. Hoogeboom, "High-Rresolution Airborne FM-CW SAR: Design and Processing Aspects," in *Proc. European Conf. Synthetic Aperture Radar EUSAR'02*, Cologne, Germany, June 2002, pp. 163–166.

[3] J. F. M. Lorga, A. Meta, J. J. M. de Wit, P. Hoogeboom, and J. A. Mulder, "Airborne FM-CW SAR and Integrated Navigation System Data Fusion," in *Proc. AIAA Guidance, Navigation, Control Conf. GNC'05*, San Francisco, USA, Aug. 2005, pp. 201–205.

[4] D. Kalloemisier, *Remote Control Software voor de FM-CW SAR Demonstrator*. TU Delft - IRCTR, Tech. Rep. IRCTR-SH-013-03, 2003.

[5] M. I. Skolnik, *Introduction to Radar Systems*. McGraw-Hill, Inc., 1980.

[6] W. P. Robins, *Phase Noise in Signal Sources*. Peter Peregrinus, London, 1982.

[7] M. C. Budge and M. P. Burt, "Range Correlation Effects in Radar," in *Proc. IEEE Nat. Radar Conf. '93*, Lynnfield, USA, Apr. 1993, pp. 212–216.

Chapter 7

Flight test campaign results

The chapter presents an overview of the FMCW SAR flight test campaign organized during the last part of 2005 and the results obtained. Thanks to the special algorithms which have been developed during the research project and described in the previous chapters, FMCW SAR images with a measured resolution up to 45 cm times 25 cm (including Hamming windowing) were produced. Several tests performed during the flight campaign (imaging at different resolutions, varying the incident angle, MTI experiment) are reported and discussed. For the first time, high resolution SAR images have been produced with an FMCW radar based on a simple VCO technology and the outstanding improvements achievable with the invented frequency non-linearity correction algorithm have been demonstrated with real data.

7.1 Introduction

An airborne flight test campaign has been organized and carried out in October 2005, at the Strausberg airport, east of Berlin. The aim of the campaign was to show the practicability of an FMCW SAR and provide images of high resolution. The data acquired are of very high interest: they represent one of the very first FMCW SAR data collection and have been used to verify the developed algorithms on real data.

The 10 GHz FMCW SAR demonstrator system developed and built at the IRCTR, Delft University of Technology, and described in the previous chapter, was brought to Strausberg where Stemme GmbH is located. The company was asked to provided the S10 light motor glider used for the flight test campaign. The particular aircraft was chosen because it could provide the means to prove that an airborne FMCW SAR can be operated with such a kind of carrier and because it was a very relatively cheap test aircraft.

Several runs were flown over the Strausberg urban area and rural fields. Different incident angles, resolution and altitude configuration were tried; some tests illuminating a highway were performed in order to validate MTI algorithms and the FMCW SAR model. The flight campaign was very successful [1]. The following sections report FMCW SAR images obtained processing the data collected during the campaign, resolution performance and comparison with optical pictures. The algorithms described in the previous chapters have

been applied to the data, particularly the range non-linearity correction, the removal of the effects induced by the continuous motion and MTI techniques using triangular modulations. Comments follow on the obtained improvements. For the first time, SAR images have been produced with an FMCW radar based on a simple VCO technology.

7.2 Overview of the flight campaign

On addition to provide one of the first FMCW SAR data collection, the flight test campaign was a very good example of how interesting such imaging sensors can be for civil applications, where low cost requirements are called for. In fact, the total cost of the campaign, consisting of 10 flight hours, was only few thousands of euro. It was very easy to transport the system from Delft to Strausberg and attach it under the wing of the glider. Figure 7.1 illustrates an impression of the system assembling while fig. 7.2 shows one of the last checking of the radar before the beginning of the flight campaign.

The demonstrator system is completely independent from the carrier aircraft and has an autonomy of two hours. Most of the battery power is used by the PXI chassis. The S10 aircraft, the carrier used for the airborne experiments, is a twin seat glider (fig. 7.3) and there is no space in cockpit to operate large hardware; therefore, during the flights, the system was monitored and controlled from the cockpit with a pocket PC, as shown in fig. 7.4; in the figure,



Figure 7.1: Assembling of FMCW SAR demonstrator system built at the IRCTR, Delft University of Technology, under the glider wing.

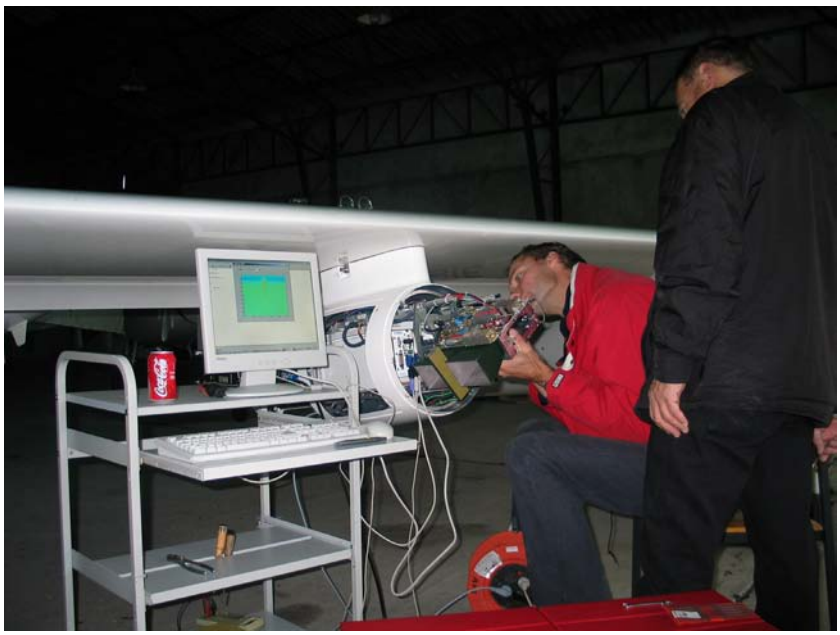


Figure 7.2: Checking FMCW SAR demonstrator system.

the main power switch, used to turn the system and the radar front-end on and off, is also visible. Figure 7.5 shows a picture of the FMCW SAR pod taken from the cockpit during an operational flight. During the flight stops, the system battery could be recharged; furthermore, additional checking and changing, i.e. varying the configuration antenna incident angle, could be performed very easily, see fig. 7.6.

In the flight test campaign, no motion sensors were installed in the demonstrator system, therefore the SAR images reported in this chapter have been obtained applying autofocusing techniques. Hamming windowing is used both in range and in azimuth in order to reduce the sidelobe levels, at the cost of a coarser resolution.



Figure 7.3: Preparation for one flight with the twin seat S10 motor glider.

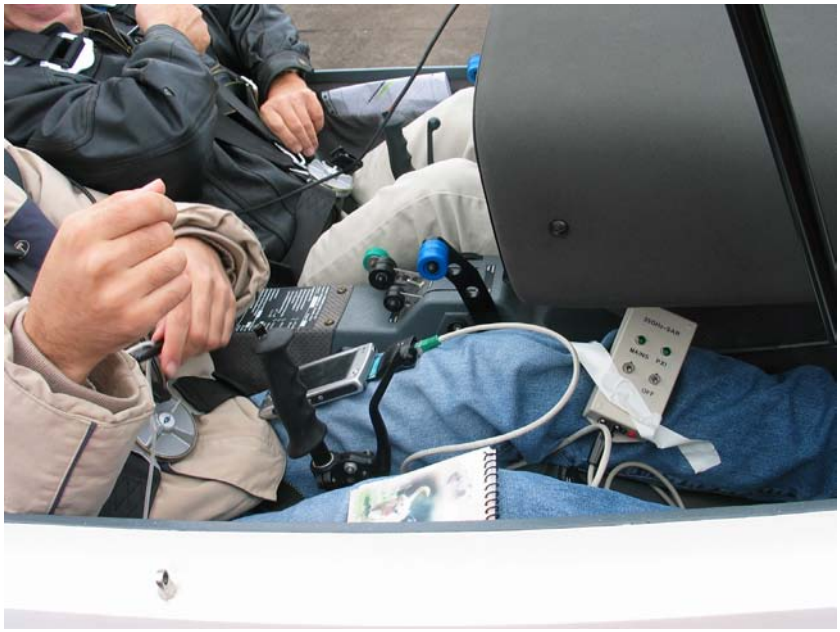


Figure 7.4: The Pocket PC used to control the FMCW SAR demonstrator system and the main switch are visible.



Figure 7.5: FMCW SAR demonstrator system during one operational flight.



Figure 7.6: FMCW SAR demonstrator system during one flight stop. Battery charging and additional checking or changing could be easily performed.

7.3 Non-linearities correction

A novel and efficient processing technique for the frequency non-linearity correction has been introduced in chapter 3. It has been applied to the real data collected during the flight test campaign resulting in outstanding improvements in the FMCW SAR images, both in terms of resolution and signal to noise ratio. Three representative examples are reported here.

7.3.1 First example

The first example is about results obtained with data collected during a flight with a medium resolution configuration, transmitting a bandwidth of 260 MHz. The phase non-linearity estimation and the corresponding spectrum are shown in fig. 7.7, while fig. 7.8 illustrates the SAR images produced with and without frequency non-linearity correction. The improvements are clearly visible. In the lower-right part of the SAR images a bright scatterer response is visible. The response of this point of opportunity is used to quantify the improvement achieved with the non-linearity correction. Figure 7.9(a) shows the range profile obtained without the non-linearity correction, while results obtained with the correction applied are reported in fig. 7.9(b). The peak level increases of almost 7 dB while the integrated sidelobe level (ISL) improves of approximately 9.2 dB. The ISL shall here mean the square root of the ratio of the integrated sidelobe power (ISP) of the response to the power in the main lobe of the response. Since the analyzed response is the echo of a point of opportunity, the integrated power contained in an area of three resolution cells around the maximum peak has been used as main lobe power. The results of the analysis are summarized in tab. 7.1.

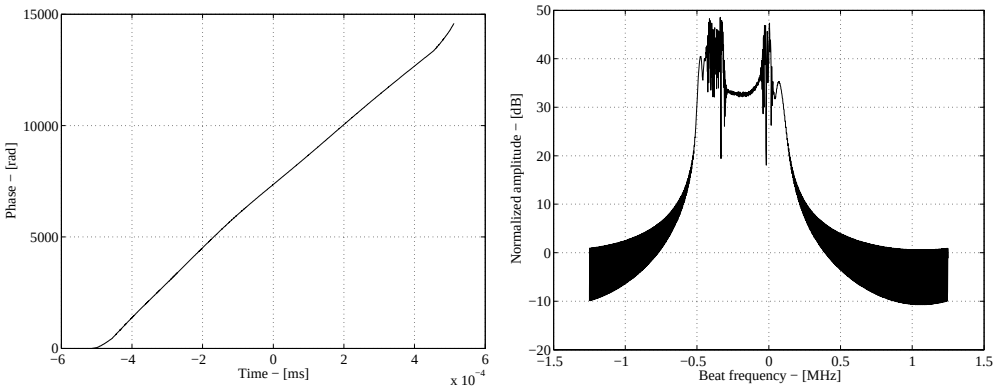


Figure 7.7: First example. Phase of the estimated non-linearity and corresponding spectrum.

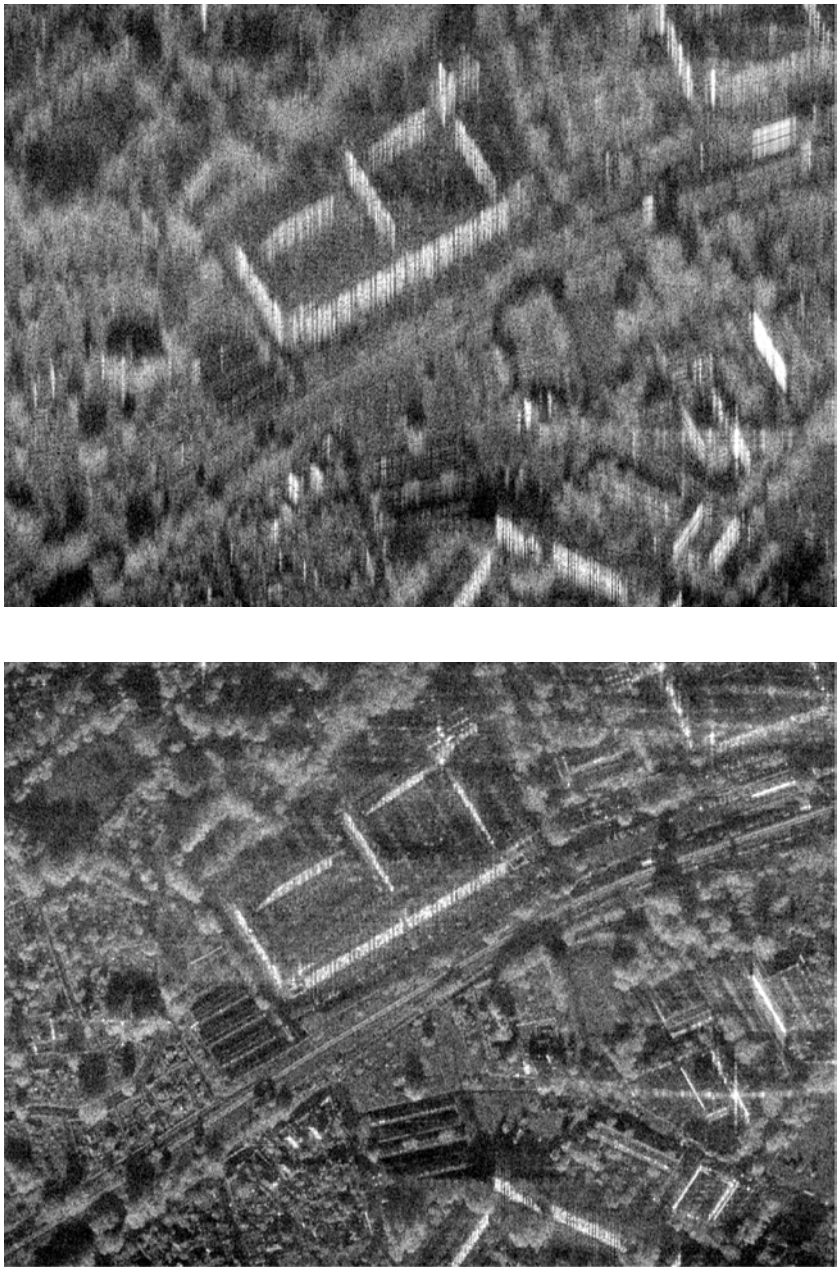


Figure 7.8: First example. Results of the non-linearity correction algorithm applied to FMCW SAR data collected with the medium resolution configuration. Slant range is on the vertical axis.

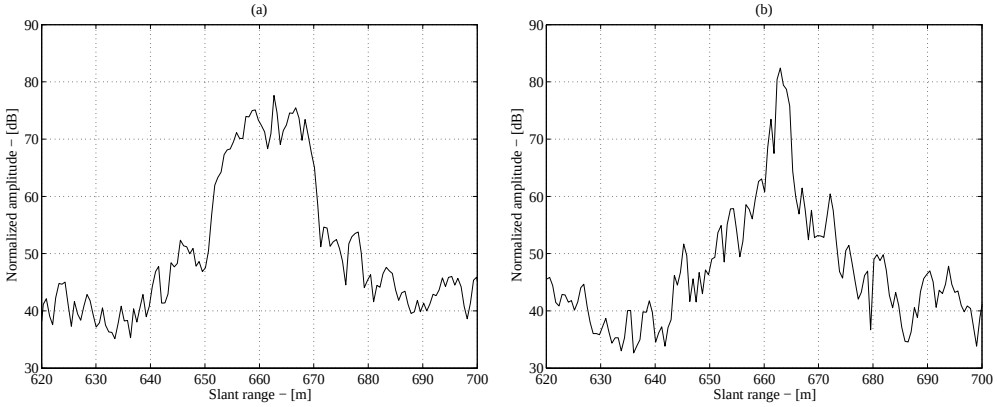


Figure 7.9: First example. Range profiles of a point of opportunity visible in the lower-right part of the SAR image shown in fig. 7.8: in (a) without the non-linearity correction and in (b) with the correction. An increased peak level and an improved integrated sidelobe level can be noticed.

Table 7.1: Results for the point of opportunity analysis.

	without correction	with correction
Peak level [dB]	77.62	84.40
ISP [dB]	86.95	71.90
ISL [dB]	2.72	-6.40
Range resolution at -3 dB [m]	1.2	1.2
Range resolution at - 10 db [m]	17	3.7

7.3.2 Second example

The second example is about data collected one hour later than the case described in the previous example, with exactly the same configuration. However, from fig. 7.10, it is possible to see that the estimated non-linearity spectrum is different from the one reported in fig. 7.7. The external conditions changed within one hour. Figure 7.11 shows the improvements on the SAR image due to the frequency non-linearity correction.

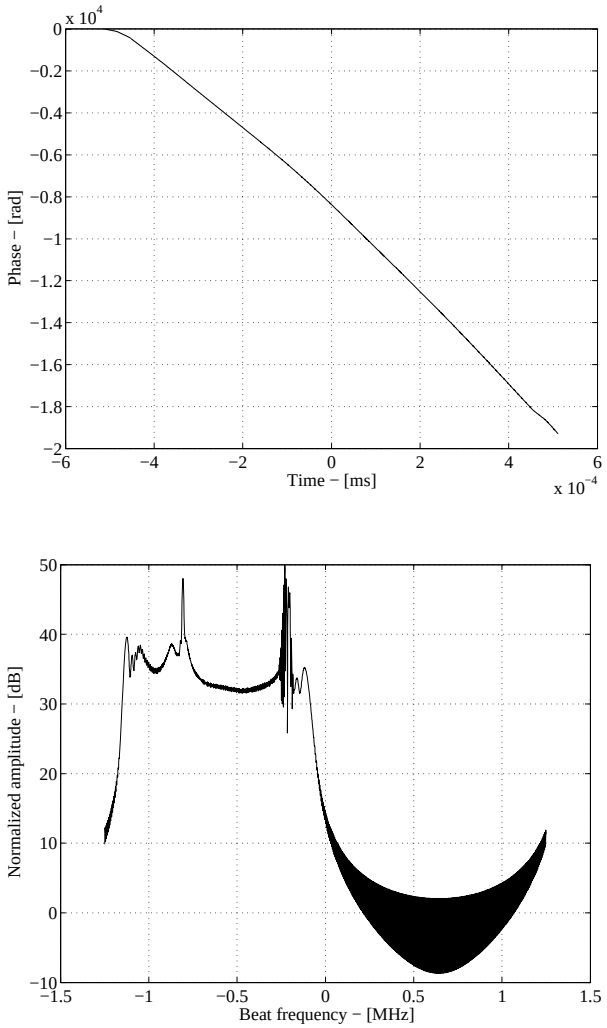


Figure 7.10: Second example. Phase of the estimated non-linearity and corresponding spectrum.

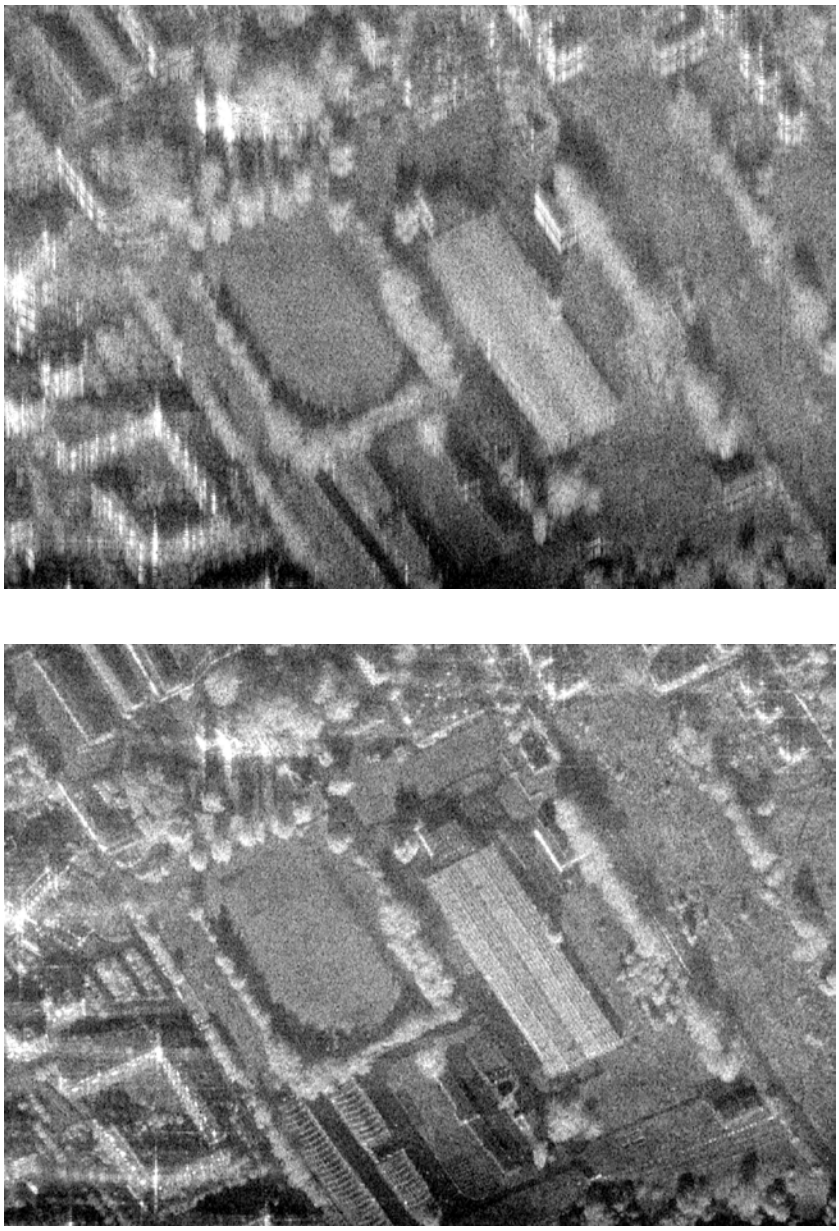


Figure 7.11: Second example. Results of the non-linearity correction algorithm applied to FMCW SAR data collected with the medium resolution configuration. Slant range is on the vertical axis.

7.3.3 Third example

The last example reports the non-linearity estimation (fig. 7.7) and the effects of its correction on the SAR image (fig. 7.11) collected over a forest area with a low resolution configuration with a transmitted bandwidth of 130 MHz and *PRI* of 0.5 ms. Since the non-linearities are estimated from a delay line embedded in the front-end, it is not necessary to have point target responses in the SAR image.

The three examples demonstrate that the non-linearity has to be estimated for every data file, because even small changes in external conditions can drastically affect the behavior of the VCO.

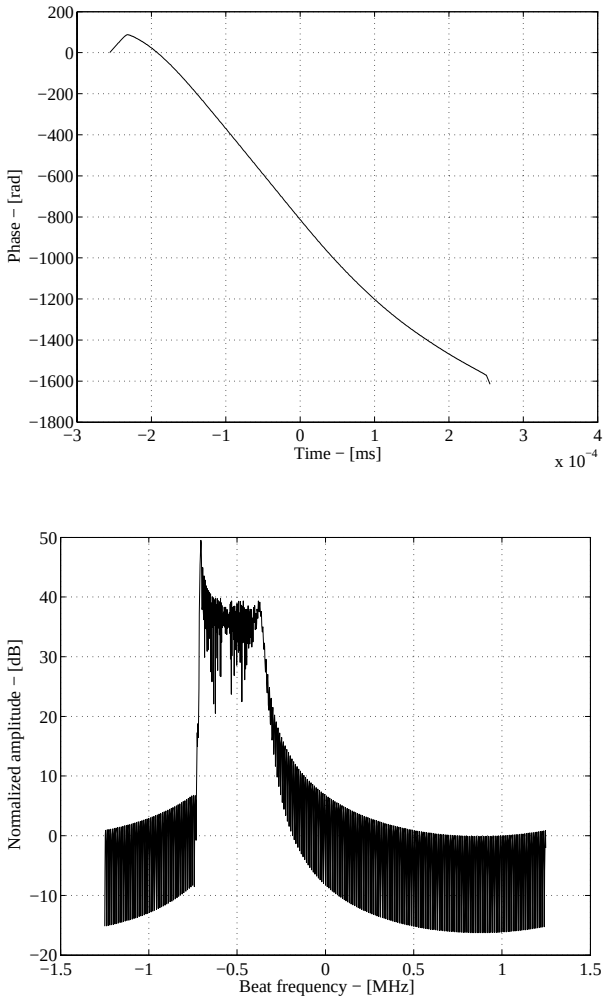


Figure 7.12: Third example. Phase of the estimated non-linearity and corresponding spectrum.

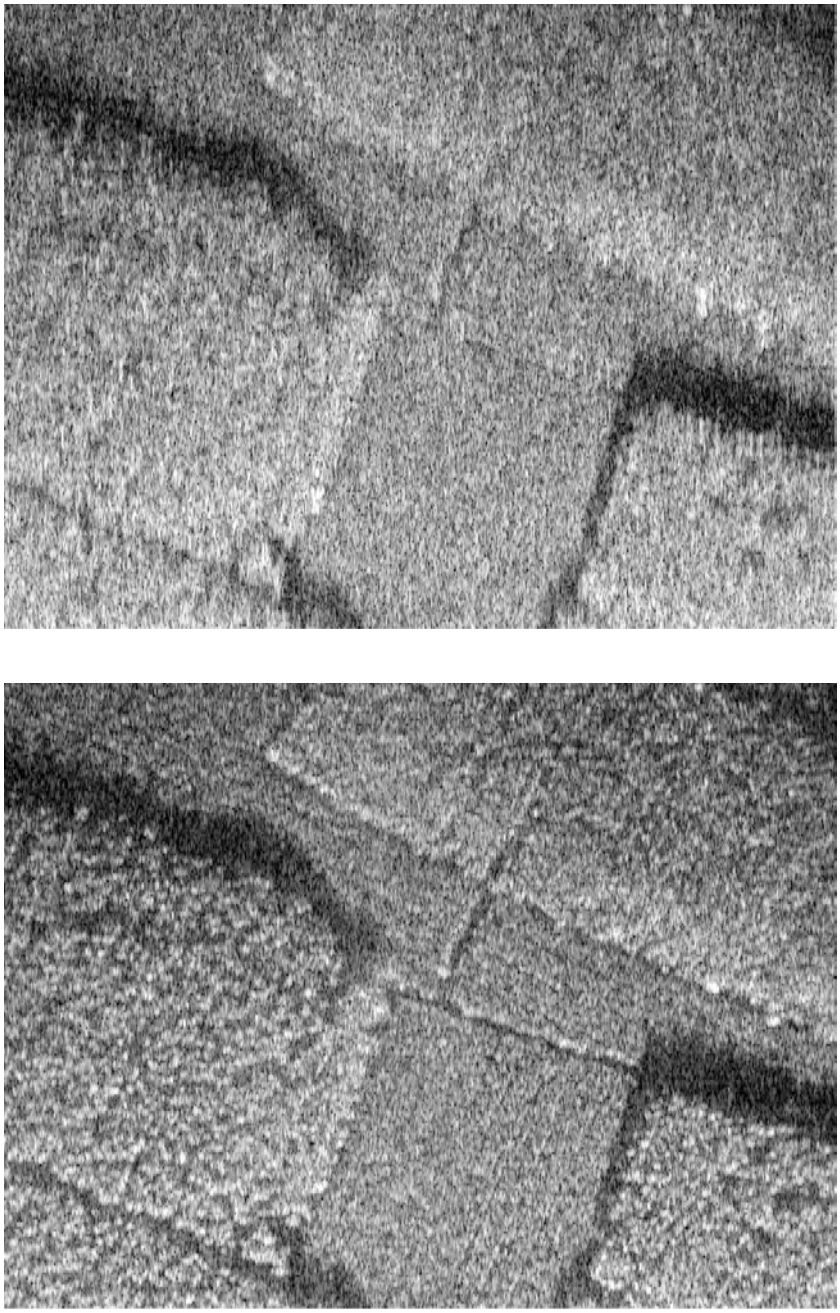


Figure 7.13: Third example. Results of the non-linearity correction algorithm applied to FMCW SAR data collected with the low resolution configuration. Slant range is on the vertical axis.

7.4 High resolution images

Some data at high resolution have been collected during a flight over the area near the Strausberg airport with the following flight and radar configuration:

altitude	240 m;
incident angle	55^o;
Range bandwidth	520 MHz;
Pulse duration	1 ms;
Maximum range	721 m.

Two images are reproduced in fig. 7.14 and fig. 7.15. After non-linearity correction, the processed SAR bandwidth has been set to 200 Hz, and an averaging of 16 cells in the cross direction has been performed in order to reduce the speckle. In fig. 7.15, the response of a corner reflector is visible belove the crossing-roads. The resolution profiles are reported in fig. 7.16, which show an obtained resolution of 45 cm in slant range times 25 cm in cross-range. The slant range resolution is slightly poorer than the theoretical 30 cm mainly because of Hamming windowing which reduces the sidelobe level to -40 dB but also introduces a resolution degradation of approximately a factor of 1.5.



Figure 7.14: High resolution image.



Figure 7.15: High resolution image.

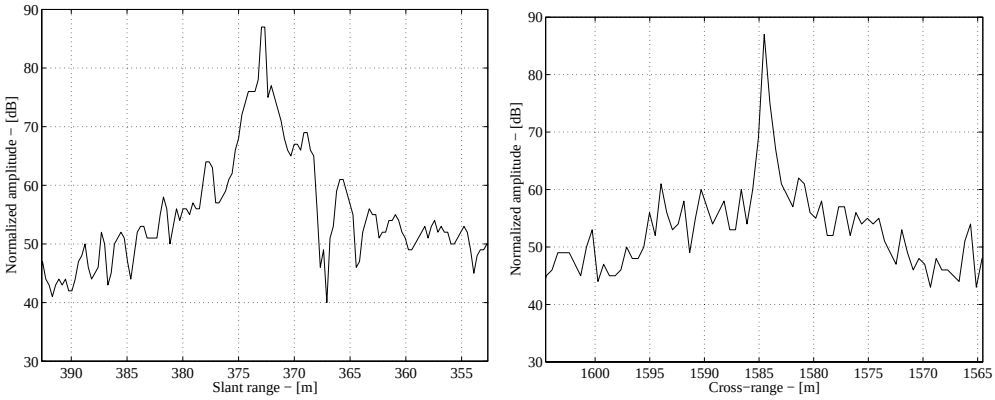


Figure 7.16: Range and cross-range profile of the corner reflector response in the high resolution image.

7.5 Medium resolution images

In this section some examples of medium resolution images produced with the 10 GHz FMCW SAR system are reported. In all the flights the aircraft and radar configuration parameters were:

altitude	310 m;
incident angle	65^o;
Range bandwidth	260 MHz;
Pulse duration	1 ms;
Maximum range	1442 m.

Also these images have been obtained processing 200 Hz of Doppler bandwidth, and averaging 16 cells in the cross-range direction. Figure 7.17 shows an image of an urban area in the city of Strausberg; fig. 7.18 is a picture of the area around the airport and can be compared with an optical image of the same area, in fig. 7.19, obtained from the Google Earth software (http://earth.google.com). Figure 7.20, compared with fig. 7.21, is a SAR image of the same area used as an example for the high resolution mode and reported in the previous section. The response of the corner reflector has been used for resolution analysis and the profiles are reported in fig. 7.22, which shows an obtained resolution of 120 cm in slant range times 30 cm in cross-range.



Figure 7.17: Medium resolution image.



Figure 7.18: Medium resolution image.



Figure 7.19: Google image.

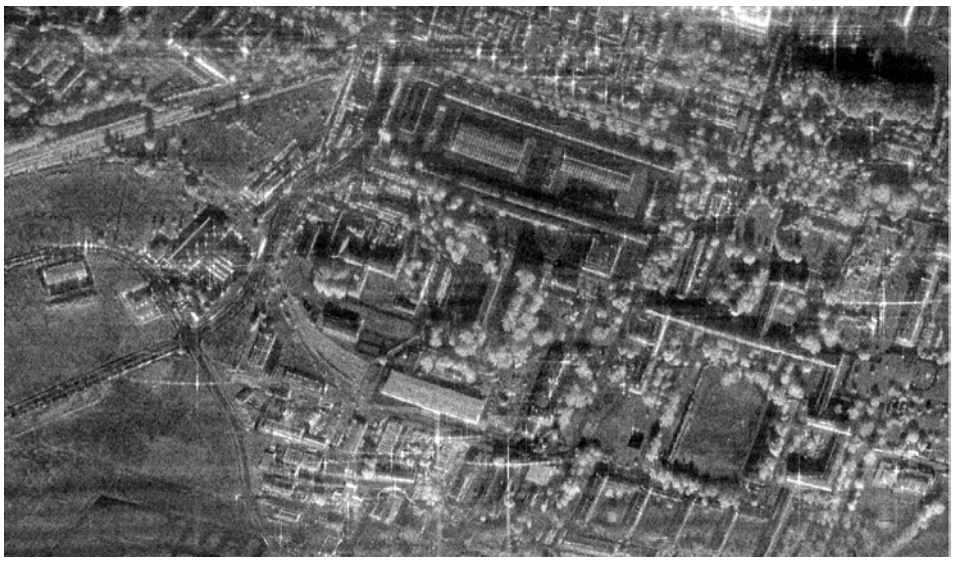


Figure 7.20: Medium resolution image.



Figure 7.21: Google image.

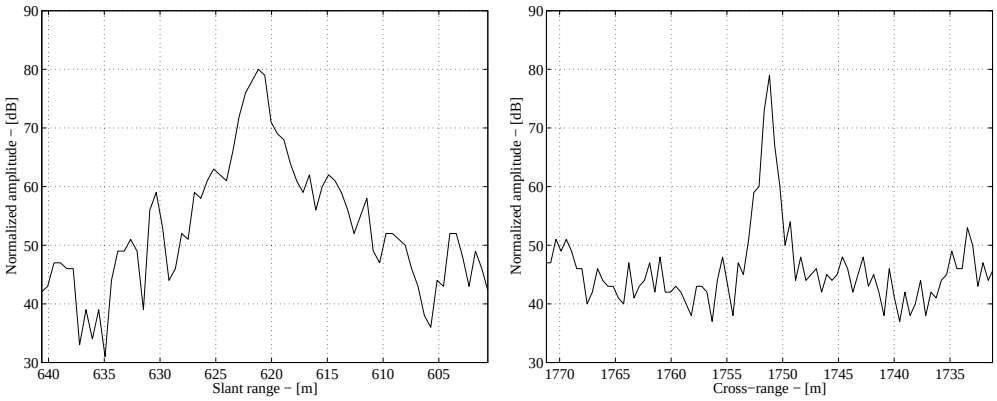


Figure 7.22: Range and cross-range profile of the corner reflector response in the medium resolution image.

7.6 Low resolution image

An example of low resolution image over a vegetation area with a road crossing a highway is shown in fig. 7.23, which can be compared with a Google image of the same area, in fig. 7.24. Grass and tree leaves are imaged in different ways in radar and optical images. Also the different shadow directions of the isolated trees, in the grass field in the middle-right part of the images, can be seen. The SAR data were collected with the following configuration:

altitude	380 m;
incident angle	65^o;
Range bandwidth	130 MHz;
Pulse duration	0.5 ms;
Maximum range	1442 m.



Figure 7.23: Low resolution image.



Figure 7.24: Google image.

7.7 Resolution comparison

Several flights with different resolution configurations were flown over the same region around the airport area. A close view of the SAR images on the same building area at low, medium and high resolution is reported in fig. 7.25, fig. 7.26, fig. 7.27, respectively.



Figure 7.25: Low resolution image.

It can be seen how the details become clearer and sharper with increasing resolution. Finally, a corresponding optical image, taken from the glider cockpit with an optical camera during one of the flights, is shown in fig. 7.28. In the upper right corner of the image, parked cars are visible. In the high resolution FMCW SAR image they are clearly detected and discriminated.



Figure 7.26: Medium resolution image.



Figure 7.27: High resolution image.



Figure 7.28: Optical camera image.

7.8 Triangular FMCW SAR test

Data acquired transmitting a triangular modulation were used to verify the FMCW SAR model developed in chapter 4 and the MTI algorithm using frequency slope diversity described in chapter 5. In triangular modulation, the frequency rate α of the upslope part is the opposite of the downslope. If not corrected for, the motion within the sweep will have opposite effects in the SAR images produced with the two different parts of the modulation, as described in (4.16), reformulated here exploiting the term α:

$$\begin{aligned} S_{IF}(K_r, K_x) &= \exp(jK_x vt) \exp j\left(R\sqrt{K_r^2 - K_x^2} - K_x x_1\right) \\ &= \exp\left(jK_x v \frac{K_r - K_{rc}}{4\pi\alpha}\right) \exp j\left(R\sqrt{K_r^2 - K_x^2} - K_x x_1\right) \end{aligned} \quad (7.1)$$

After correction of the effects induced by the continuous motion within the sweep, the stationary clutter in the two images has to be imaged exactly in the same way if flying along to a straight line. During this test, the radar was moving at around 33 m/s, the antenna aperture beamwidth was 20^o, and the duration of the transmitted 130 MHz triangular modulation period 1 ms (half for the upslope and half for the downslope). Therefore, for each image, the value of K (introduced in chapter 4, (4.7)) is approximately equal to 0.4. The amplitude image obtained with the upslope part is illustrated in fig. 7.29.

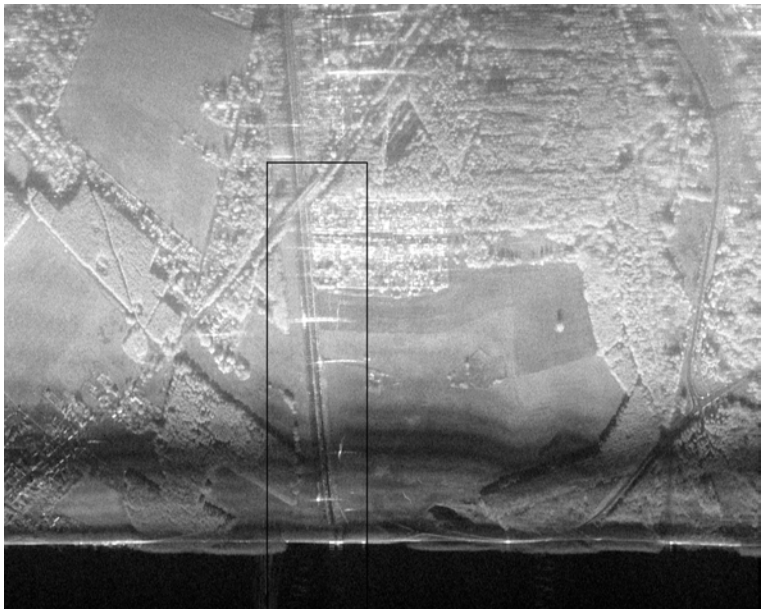


Figure 7.29: Results of the flight test transmitting 130 MHz triangular modulation showing the upslope image amplitude where the part within the rectangular frame has been used for the subsequent interferogram comparison.

In order to validate the proposed FMCW SAR signal model, the upslope and downslope images are compared by using their interferogram. For small values of K, the resolution degradation is not severe in the amplitude image. However, it can be noticed from the phase degradation.

A first interferogram can be obtained with the images produced applying conventional SAR algorithms, and a second using the images generated with the proposed FMCW SAR signal model. The two interferogram are shown in fig. 7.30. It can be seen that the phase of the second interferogram (fig. 7.30(b)) is flatter when compared to the first one (fig. 7.30(a)), indicating that the two images are much more similar after the FMCW correction than before, validating the proposed model. For instance, the highway is clearly distinguishable in fig. 7.30(a) while it can be hardly seen after the correction. Strong differences in the phase can reveal the presence of a moving target, see section 5.3, and some examples are indicated with arrows in the last interferogram of fig. 7.30. The responses in the circle could also be interpreted as moving targets; however, no difference is noticed comparing the range position of the responses in the upslope and downslope images, therefore they are stationary

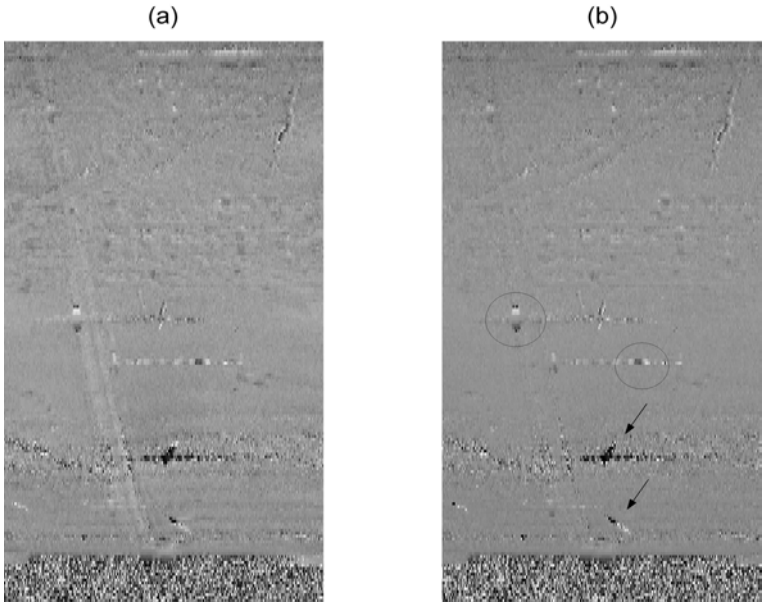


Figure 7.30: Results of the flight test transmitting 130 MHz triangular modulation: the interferogram obtained using the upslope and downslope image produced with conventional SAR algorithm (a) and with the proposed signal model (b). In the last picture, the phase of the interferogram is flatter revealing that the clutter is imaged in a more similar way in the two images after the FMCW correction. The arrows indicate moving targets.

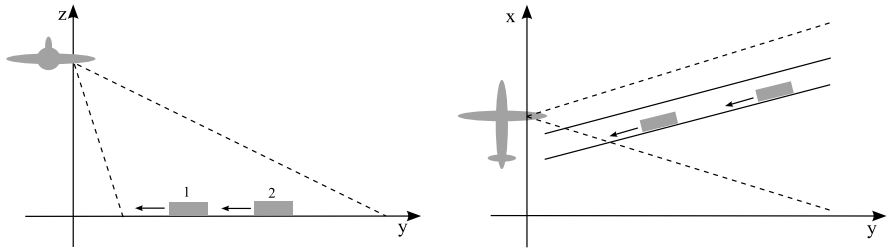


Figure 7.31: Schematic representation of the moving target experiment. The two cars are driving on the highway.

targets. Additionally, this was confirmed by ground truth. The particular response of these strong stationary targets in the interferogram, similar to a moving target response, is due to the fact that part of the processed target energy is coming from the antenna sidelobes. Therefore, the Doppler response of these stationary targets contains also energy folded back in the clutter bandwidth, which disturbs the phase response in the final SAR image. Remaining phase discrepancies could be due to a not completely exact motion compensation; in fact, the demonstrator system was not provided with motion sensors and therefore the SAR processing relays entirely on autofocusing techniques, which can assure a good image focusing but cannot guarantee an accurate flight geometry reconstruction.

A quantitative analysis has been performed for the responses of the two moving targets indicated with an arrow in fig. 7.30 in order to calculate their velocity. The PRF ambiguity has been resolved measuring the range displacement n_v, in terms of resolution cells, of the response in the upslope and downslope FMCW SAR images. The Doppler frequency of the target is finally obtained using also the ambiguous Doppler information estimated from the

Table 7.2: Results for the moving target analysis.

	target 1	target 2
Slant range [m]	450	540
Ground range [m]	241	383
Elevation angle [^{o}]	32.4	45.3
n_v	1	1
Measured Doppler [Hz]	-200	100
Target Doppler [Hz]	800	1100
Ground velocity [km/h]	82.4	85.4

spectrum response. An inclination of 12^o between the highway and the cross track direction has been assumed, as shown in fig. 7.8, for the calculation of the target ground velocity. The results of the analysis are consistent with the illuminated scenario and are reported in tab. 7.2.

7.9 Summary

The chapter has presented an overview of the FMCW SAR flight test campaign organized during the last part of 2005 and the results obtained. Thanks to the special algorithms which have been developed during the research project and described in the previous chapters, FMCW SAR images with a measured resolution up to 45 cm times 25 cm (including Hamming windowing) were obtained. During the campaign, the system was not provided with motion sensors therefore a complete motion compensation has not be performed. The SAR processing relied on autofocusing techniques which can achieve a good cross-range focusing.

Several tests performed during the flight campaign (imaging at different resolutions, varying the incident angle, triangular modulation experiment for MTI and validation of the FMCW SAR model) are reported and discussed. For the first time, SAR images have been produced with an FMCW radar based on a simple VCO technology and the outstanding improvements achievable with the invented frequency non-linearities correction algorithm have been demonstrated with real data.

References

[1] A. Meta, P. Hakkaart, F. V. der Zwan, P. Hoogeboom, and L. P. Ligthart, "First demonstration of an X-band airborne FMCW SAR," in *Proc. European Conf. on Synthetic Aperture Radar EUSAR'06*, Dresden, Germany, May 2006.

Chapter 8

Conclusions and discussion

Synthetic Aperture Radar is very successfully used in many earth observation applications. Operating existing SAR systems, however, are quite costly, which makes them an unlikely choice for extensive applications requiring frequent revisits. Additionally, their use is problematic in many military tasks where very compact and lightweight high-resolution imaging systems are required, which can operate independently of the weather conditions and sun illumination.

The combination of FMCW technology and SAR techniques offers a solution to the increasing request for low cost, compact imaging sensors with high resolution. FMCW radars operate with a low transmission power and their raw data bandwidth is drastically reduced as compared to conventional SAR systems.

With the work described in the thesis, the practical feasibility of an airborne FMCW SAR has been demonstrated. Algorithms for the proper processing of FMCW SAR data, which result in outstanding improvements when compared with conventional methods, allowed the use of very simple and cheap technology. The contents of this thesis represent an important contribution to the development of compact, low cost imaging sensors with high resolution. The author aimed to provide the scientific community with a complete and detailed analysis of the FMCW SAR signal and the proper tools to process it.

8.1 Contributions of this research

Within the framework of the project, the following novelties and main results have been reached and have been presented in the thesis:

Non-linearity correction. A novel processing solution, which completely solves the problem of the presence of frequency non-linearities in FMCW SAR, has been invented. It corrects the non-linearity effects for the whole range profile at once, and it allows a perfect range focussing. The proposed method operates directly on the deramped data and it is very computationally efficient [1].

A complete FMCW SAR signal model. A detailed analytical description for the FMCW SAR signal in the two-dimensional frequency domain has been presented. Based on this

model, proper algorithms have been developed which guarantee the best performance when processing FMCW SAR data. The results of their use on real data proved their validity [2].

MTI with frequency modulated CW SAR. Two SAR MTI methods are proposed. The first is based on the frequency slope diversity in the transmitted modulation by using linear triangular FMCW SAR [3]. The second makes use of the Doppler filtering properties of randomized SFCW modulations [4].

First demonstration of an X-band FMCW SAR. A flight campaign has been organized during the last part of 2005 to test the 10 GHz FMCW radar front-end developed at the IRCTR. The feasibility of an operational FMCW SAR under practical circumstances has been demonstrated and one of the very first FMCW SAR data collection has been acquired. The results were very successful. Thanks to the special algorithms developed, high resolution FMCW SAR images have been obtained for the first time using a simple front-end based on cheap FMCW technology [5].

8.2 Recommendations

The development of new algorithms for the proper processing of FMCW SAR data and a practical implementation of an FMCW SAR system have been presented in the thesis. During the research stage, a number of new problems have been identified, which require further studies. A list of new directions to be investigated include:

- evaluation of the robustness of the SAR MTI algorithm based on triangular FMCW presented in section 5.3.

- validation with real data of the proposed deramping technique described in section 3.6.1 and of the MTI applications of the randomized SFCW signals proposed in section 5.4.

- investigation of the use of DDS technology for randomized SFCW signals and, in general, for CW noise radars. DDS can offer a great versatility for many signal processing techniques which require high precise deterministic waveforms.

- study of a bistatic dechirp-on-receive FMCW SAR configuration. Having a receiving antenna on a separate carrier can eliminate the constraint of limited maximum range in conventional monostatic FMCW radar, imposed by the coupling of transmitting and receiving chain.

- analysis of adaptive FMCW waveforms for in-flight autofocusing. For instance, the commonly used adaptation of the PRF to account for along track velocity errors in conventional SAR involves a change of the frequency rate in FMCW sensors, if a constant transmitted bandwidth is wanted. An adapted version of the non-linearity correction algorithm described in chapter 3 could be used.

8.3 Related works at other institutes

That FMCW SAR will play an in increasing important role in future small, low-cost imaging radar applications is additionally demonstrated by the fact that, very recently, other institutes have developed systems or started concept studies on SAR based on FMCW technology. A brief description of them follows.

MISAR system [6]; it is a miniaturized FMCW SAR designed by EADS (European Aeronautic Defence System) in Ulm, Germany. It can be carried by a small UAV. Raw data are transmitted to the ground, with standard video links, where they are successively processed. The system operates at 35 GHz and produces images with a resolution up to 0.5 m x 0.5 m.

3D imaging radar ARTINO [7]; at FGAN (Forschungsgesellschaft für Angewandte Naturwissenschaften) in Wachtberg, Germany, a 3D FMCW radar concept is being developed under the name ARTINO. The main idea of the system is the use of a linear array of nadir pointing antennas for across-track imaging. It operates at Ka band and it is designed for UAV applications.

BYU microSAR [8]; developed by Brigham Young University, USA, it is a low cost FMCW SAR system intended for operations on a small UAV. Raw data are stored on a compact flash disk and processed off-line. The front-end operates at 5.4 GHz transmitting a bandwidth of 80 MHz and it irradiates 1 W power through a patch antenna.

ONERA 3D FMCW SAR [9]; similar to the ARTINO project, it is a 3D SAR for radar imagery being developed by ONERA, France. It also works at Ka band and is foreseen to be deployed on a similar Stemme motor glider as the one used for the TU Delft FMCW SAR flight test campaign.

References

[1] A. Meta, P. Hoogeboom, and L. P. Ligthart, "Range non-linearities correction in FMCW SAR," in *Proc. IEEE Int. Geoscience and Remote Sensing Symp. IGARSS'06*, Denver, CO, USA, July 2006.

[2] A. Meta, P. Hoogebbom, and L. P. Ligthart, "Correction of the effects induced by the continuous motion in FMCW SAR," in *Proc. IEEE Radar Conf. '06*, Verona, NY, USA, Apr. 2006, pp. 358–365.

[3] A. Meta and P. Hoogeboom, "Signal Processing Algorithms for FMCW Moving Target Indicator Synthetic Aperture Radar," in *Proc. IEEE Int. Geoscience and Remote Sensing Symp. IGARSS'05*, Seoul, Korea, July 2005, pp. 316–319.

[4] A. Meta, P. Hoogeboom, and L. P. Ligthart, "Moving Target Indication enhancement in FMCW SAR using deramped randomized stepped-frequency signals," in *Proc. Waveform Diversity and Design Conf. WDDC'06*, Lihue, HI, USA, Jan. 2006.

[5] A. Meta, P. Hakkaart, F. V. der Zwan, P. Hoogeboom, and L. P. Ligthart, "First demonstration of an X-band airborne FMCW SAR," in *Proc. European Conf. on Synthetic Aperture Radar EUSAR'06*, Dresden, Germany, May 2006.

[6] M. Edrich, "Design Overview and Flight Test Results of the Miniaturised SAR Sensor MISAR," in *Proc. EuRAD'04*, Amsterdam, The Netherlands, Oct. 2004, pp. 205–208.

[7] M. Weiss and J. Ender, "A 3d imaging radar for small unmanned airplanes - ARTINO," in *Proc. EuRAD'05*, Paris, France, Oct. 2005, pp. 229–232.

[8] E. Zaugg, D. Hudson, and D. Long, "The BYU mSAR: a small, student-built for UAV operation," in *Proc. IEEE Int. Geoscience and Remote Sensing Symp. IGARSS'06*, Denver, USA, July 2006.

[9] R. Giret, H. Jeuland, and P. Enert, "A study ofa 3D-SAR concept for a millimiter-wave imaging radar onboard an UAV," in *Proc. EuRAD'04*, Amsterdam, The Netherlands, Oct. 2004, pp. 201–204.

Appendix A

Non-linear Frequency Scaling Algorithm for FMCW SAR data

This appendix presents a novel approach for processing data acquired with FMCW dechirp-on-receive systems by using a non-linear frequency scaling algorithm. The presented material is taken from [1]. The range frequency non-linearity correction, the Doppler shift induced by the continuous motion and the range migration removal are performed in the same step in the wavenumber domain with an efficient solution. The cross-range focusing is then achieved with conventional matched filtering.

A.1 Introduction

FMCW sensors can continuously transmit linear chirps, and the use of dechirp-on-receive configurations allows an high reduction of the sampling frequency. As described in chapter 3 non-linearities deteriorate the range resolution when deramping techniques are used because they spread the target energy through different frequencies.

For the processing of SAR data, several algorithms have been developed and each of them has different characteristics which make them appropriate for different applications. Particularly, the frequency scaling algorithm (FSA) can process deramped data [2] and it is able to correct the range migration without using interpolations.

The novel approach presented in the appendix aims to combine the non-linearity correction, developed by the author within the framework of the thesis, the FSA and the removal of the FMCW Doppler shift. Both non-linearity correction and FSA are based on residual video phase removal, therefore this property can be exploited to integrate the algorithms and decrease the, already low, computational load. The result is the non-linear frequency scaling algorithm, which is presented in this appendix. It has a computational load nearly equal to the conventional method, with the advantage of additionally correcting the Doppler shift effect induced by the continuous motion and the frequency non-linearity degradation. Therefore, the proposed algorithm is very suitable for the processing of FMCW SAR data.

The remaining of the appendix is structured in three sections. Section A.2 derives the wavenumber domain deramped FMCW signal taking into account the range frequency non-

linearities and without using the stop-and-go approximation. Next, the combination of the FMCW Doppler shift, frequency non-linearity and range migration correction is described in section A.3. Finally, conclusions are stated in section A.4.

A.2 Deramped non-linear FMCW SAR signal

This section derives an analytical description of the deramped FMCW SAR signal in the two-dimensional frequency domain including the range frequency non-linearities and without using the stop-and-go approximation. The radar continuously transmits linear FM chirps having duration T_p equal to the pulse repetition interval PRI , chirp rate $\alpha = B/PRI$, where B is the transmitted bandwidth and center frequency f_c. The transmitted frequency is expressed as:

$$f_r = f_c + \alpha t + e(t) \tag{A.1}$$

where $-PRI/2 \leq t < PRI/2$ and $e(t)$ is the frequency non-linearity term, which is unwanted. In dechirp-on-receive systems, the received and transmitted signal are mixed in order to reduce the required system sampling rate. In a stripmap configuration with the radar flying along a straight path, the target time delay is:

$$\tau = \frac{2}{c}\sqrt{R^2 + v^2(t+T)^2} \tag{A.2}$$

where R is the distance of closest approach, v is the aircraft velocity and T is the slow time variable. The deramped FMCW SAR signal can be described by:

$$s(t,T) = \exp(-j2\pi(f_c\tau + \alpha\tau t - \frac{1}{2}\alpha\tau^2 + e(t) - e(t-\tau))) \tag{A.3}$$

The first exponential term is the azimuth phase history; the second term is the range signal while the third term is the residual video phase. The last two terms of (A.3) represent the unwanted contribution of the frequency non-linearities; $e(t)$ can be directly measured or estimated from the raw data [3] and is assumed known in the rest of the analysis. Frequency non-linearities seriously degrade the system performances if not corrected for. Applying a Fourier transform with respect to the variable T to (A.3), and after developing the calculations, the signal in the range-Doppler domain can be expressed as:

$$\begin{aligned} s(t,f_D) \quad \approx \quad & \Big(\exp\left[-j\frac{4\pi R\beta(f_D)}{\lambda}\right]\exp\left[-j\frac{4\pi\alpha R}{c\beta(f_D)}t\right] \\ & \exp(j2\pi f_D t)\exp\left[j\left(e(t) - e\left(t - \frac{2R}{c\beta(f_D)}\right)\right)\right] \\ & src(t,f_D;R)\Big) * \exp(-j\pi\alpha t^2) \end{aligned} \tag{A.4}$$

where $*$ represents the convolution operation. Differently from [2], the expression in (A.4) includes the non-linearity and the Doppler shift terms The Doppler frequency f_D varies within:

$$\frac{-PRF}{2} + f_{Dc} \leq f_D \leq \frac{PRF}{2} + f_{Dc} \tag{A.5}$$

where PRF is the pulse repetition frequency and f_{Dc} is the Doppler centroid. The first two terms of (A.4) represent the azimuth phase history and the range modulation. The factor $\beta(f_D)$ describes the range cell migration as a function of the Doppler frequency:

$$\beta(f_D) = \sqrt{1 - \frac{f_D^2 \lambda^2}{4v^2}} \tag{A.6}$$

The third and fourth terms are the consequences of the continuous motion within the sweep, which introduces a Doppler shift, and of the presence of range frequency non-linearities. The modified non-linear frequency scaling algorithm differs from its conventional method for the ability to remove the effects of the aforementioned two terms.

The $src(t, f_D; R)$ term in (A.4) is the secondary range compression and its expression can be found in [2], for instance.

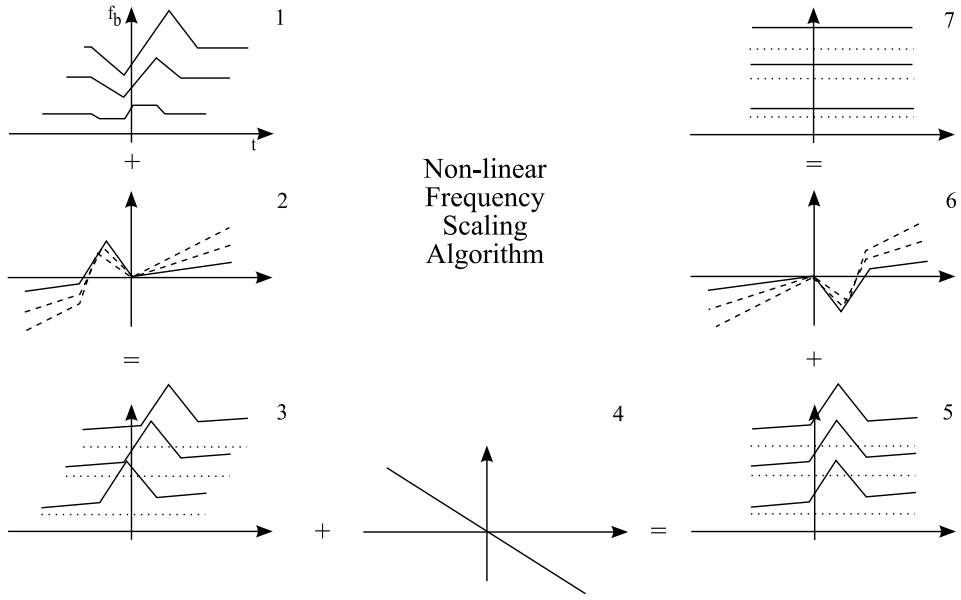


Figure A.1: Schematic representation of the non-linear frequency scaling algorithm. 1) raw data of three point scatterers. 2) Frequency scaling, Doppler shift, and transmitted non-linearity reference function. 3) Signal data after the multiply with the first reference function. 4) Residual video phase correction function. 5) Signal data after residual video phase correction. 6) Removal of the spreading induced by the frequency scaling and by the received non-linearity. 7) Signal after complete non-linear frequency scaling. Range time is on the horizontal axis whereas vertical axes represent range frequency. In 2) and 6) dashed curves indicate the dependency on the Doppler frequency.

A.3 Frequency non-linearity, Doppler shift and range cell migration correction

The non-linearity and RCM removal are obtained through the exploitation of the residual video phase. The two corrections are achieved at the same step. In fact, the frequency scaling can be thought as a special case of frequency non-linearity correction, namely a linear case. Additionally, also the Doppler shift effects, induced by the continuous motion within the sweep, can be corrected at this stage.

The first step is a multiply of (A.4) with the following reference function:

$$H_1(t, f_D) = \exp\left[-j(2\pi f_D t + e(t) - \pi\alpha t^2(1 - \beta(f_D)))\right] \tag{A.7}$$

which removes the Doppler shift, the transmitted non-linearity and scales the frequency. Successively, the signal is Fourier transformed with respect to t and multiplied with the RVP correction term:

$$H_2(f, f_D) = \exp\left[-j\frac{\pi f^2}{\alpha\beta(f_D)}\right] \tag{A.8}$$

An inverse Fourier transform brings the signal back to the time domain:

$$\begin{aligned} s(t, f_D) \quad = \quad & \exp\left[-j\frac{4\pi R\beta(f_D)}{\lambda}\right]\exp\left[-j\frac{4\pi\alpha R}{c}t\right] \\ & \exp\left[-j\pi\alpha t^2(\beta(f_D)^2 - \beta(f_D))\right] \\ & \exp\left[-je_{RVP}(t)\right] src(t, f_D; R) \end{aligned} \tag{A.9}$$

where e_{RVP} represents the non-linearity after it passed through the RVP filter. Finally, a last reference function

$$H_3(t, f_D) = \exp\left[j\pi\alpha t^2(\beta(f_D)^2 - \beta(f_D))\right]\exp\left[je_{RVP}(t)\right] \tag{A.10}$$

multiplies (A.9) removing the, now equalized, spreading of the peak response induced by the frequency scaling and by the non-linearities. After this last step, the following expression describes the resulting signal:

$$s(t, f_D) = \exp\left[-j\frac{4\pi R\beta(f_D)}{\lambda}\right]\exp\left[-j\frac{4\pi\alpha R}{c}t\right] src(t, f_D; R) \tag{A.11}$$

At this point, conventional steps can be performed to achieve secondary range compression and successively azimuth focusing. In the derivation, a reference range equal to zero has been used; when needed, expressions with a different value of the reference range can be easily derived. The proposed modified non-linear frequency scaling algorithm is very suitable for the processing of FMCW SAR data. In fact, it corrects, with practically no additional computational cost when compared with the conventional frequency scaling algorithm, the Doppler shift induced by the continuous motion in FMCW SAR and, particularly important,

the degradation caused by the frequency non-linearities. This last characteristic, in fact, allows the use of very simple and cheap sensors which can generate the transmitted modulation directly in the radio frequency band. A schematic representation of the algorithm is illustrated in fig A.1. When applied to real data, the algorithm has produced similar images to those presented in chapter 7 but with less computations.

A.4 Summary

This appendix has presented a modified non-linear frequency scaling algorithm for processing FMCW SAR data acquired with dechirp-on-receive systems. The range frequency non-linearity correction, the Doppler shift induced by the continuous motion and the range migration removal are performed at the same step in the wavenumber domain with a very efficient solution. The computational load of the described non-linear frequency scaling algorithm is practically the same as the conventional one. Therefore, the proposed method is very suitable for the processing of FMCW SAR data. The cross-range focusing is then performed with conventional matched filtering.

References

[1] A. Meta, P. Hoogeboom, and L. P. Ligthart, "Non-linear Frequency Scaling Algorithm for FMCW SAR Data," in *Proc. EuRAD'06*, Manchester, UK, Sep. 2006.

[2] J. Mittermayer, A. Moreira, and O. Loffeld, "Spotlight SAR Data Processing Using the Frequency Scaling Algorithm," *IEEE Trans. on Geoscience and Remote Sensing*, vol. 37, no. 5, pp. 2198–2214, Sep. 1999.

[3] A. Meta, P. Hoogeboom, and L. P. Ligthart, "Range non-linearities correction in FMCW SAR," in *Proc. IEEE Int. Geoscience and Remote Sensing Symp. IGARSS'06*, Denver, CO, USA, July 2006.

List of acronyms

ADC	Analog to Digital Converter
DBF	Digital Beam Forming
CW	Continuous Wave
DAC	Digital to Analog Converter
DDS	Direct Digital Synthesizer
DLR	Deutsches Zentrum für Luft-und Raumfahrt (German Aerospace Center)
EADS	European Aeronautic Defence and Space company
FFT	Fast Fourier Transform
FGAN	Forschungsgesellschaft für Angewandte Naturwissenschaften (Research Establishment for Applied Science)
FM	Frequency Modulated
FMCW	Frequency Modulated Continuous Wave
FSA	Frequency Scaling Algorithm
IF	Intermediate Frequency
IRCTR	International Research Centre for Telecommunications and Radar
ISL	Integrated Sidelobe Level
ISP	Integrated Sidelobe Power
LNA	Low Noise Amplifier
LO	Local Oscillator
LPF	Low Pass Filter
LPI	Low Probability of Interception
MTI	Moving Target Indicator
PRF	Pulse Repetition Frequency
PRI	Pulse Repetition Interval
RF	Radio Frequency
RVP	Residual Video Phase
SAR	Synthetic Aperture Radar
SAW	Surface Acoustic Wave
SFCW	Stepped Frequency Continuous Wave
SSNR	Spreading to Sampling induced Noise Ratio
UAV	Unmanned Aerial Vehicle
VCO	Voltage Controlled Oscillator

List of symbols

B	transmitted bandwidth
B_D	entire Doppler bandwidth
B_{Di}	instantaneous Doppler bandwidth
c	speed of light
d_i	space one single antenna has moved during one sweep
d_N	space between two adjacent subarray phase center
e	frequency non-linearity
f	frequency
f_b	beat frequency
$f_{b_{max}}$	maximum beat frequency
$f_{b_{min}}$	minimum beat frequency
f_c	carrier frequency
f_D	Doppler frequency
$f_{D_{max}}$	maximum Doppler frequency
$f_{D_{min}}$	minimum Doppler frequency
f_n	subpulse constant frequency
f_r	transmitted frequency
f_s	sampling frequency
f_u	unambiguous frequency
$\mathcal{F}.$	Fourier transform operator
$\mathcal{F}^{-1}.$	Inverse Fourier transform operator
h_{nl}	VCO frequency non-linearity function
k_{nj}	jitter noise factor
K	FMCW SAR parameter
K_c	carrier range spatial frequency
K_r	range spatial frequency
K_x	cross-range spatial frequency
h	flight height
l_{az}	antenna length in the azimuth direction
L	SAR observation length
n_v	number of range cell difference in triangular modulation MTI
N	subpulse number or number of antennas

r	slant range
R	slant range of closest approach
R_u	unambiguous range
s	steering signal
s_e	steering correction signal
s_{if}	intermediate frequency signal
$s_{if\ lin}$	linear intermediate frequency signal
s_{lin}	steering signal producing a VCO linear output
s_t	transmitted signal
s_ϵ	frequency non-linearity signal
$s_{\epsilon\ RVP}$	frequency non-linearity signal after RVP
t	time within the pulse
T_p	pulse duration
T_s	subpulse duration
x	radar cross-range position
x_1	cross-range coordinate of the scene center
y_1	range coordinate of the scene center
v	aircraft velocity
v_r	radial velocity
α	frequency sweep rate
β	range migration factor
γ	look angle
γ_{max}	maximum look angle
γ_{min}	minimum look angle
δaz	azimuth resolution
δf_b	beat frequency resolution
δf_r	range frequency resolution
δr	slant range resolution
δT	slow time resolution
Δf	frequency step
ΔX	azimuth displacement for moving target
ΔX_{imag}	azimuth displacement for moving target in the SAR images
ΔR	range displacement for moving target in the SAR images
ϵ	non-linear error function
ϵ_{if}	intermediate frequency non-linear error function
ϵ_{RVP}	non-linear error function after RVP correction
$\tilde{\epsilon}$	estimated non-linear error function
η	duty cycle
θ	displacement slope of moving target in FMCW SAR images
θ_{az}	azimuth 3-dB antenna beamwidth
λ	wavelength
λ_c	carrier wavelength

μ	oversampling factor
ξ	instantaneous to entire Doppler bandwidth ratio
ρ_r	range SAR resolution
ρ_{az}	azimuth SAR resolution
τ	time delay
τ_{ref}	reference time delay
τ_{max}	maximum time delay
τ_{min}	minimum time delay
τ_0	constant time delay
ϕ_n	initial subpulse phase
$\chi(\tau, f_D)$	square root of the ambiguity function

Summary

In the field of airborne earth observation there is special attention to compact, cost effective, high resolution imaging sensors. Such sensors are foreseen to play an important role in small-scale remote sensing applications, such as the monitoring of dikes, watercourses, or highways. Furthermore, such sensors are of military interest; reconnaissance tasks could be performed with small unmanned aerial vehicles (UAVs), reducing in this way the risk for one's own troops.

In order to be operated from small, even unmanned, aircrafts, such systems must consume little power and be small enough to fulfill the usually strict payload requirements. Moreover, to be of interest for the civil market, cost effectiveness is mandatory.

Frequency Modulated Continuous Wave (FMCW) radar systems are generally compact and relatively cheap to purchase and to exploit. They consume little power and, due to the fact that they are continuously operating, they can transmit a modest power, which makes them very interesting for military operations. Consequently, FMCW radar technology is of interest for civil and military airborne earth observation applications, specially in combination with high resolution *Synthetic Aperture Radar* (SAR) techniques. The novel combination of FMCW technology and SAR techniques leads to the development of a small, lightweight and cost-effective high resolution imaging sensor.

SAR techniques have been successfully applied in combination with coherent pulse radars. Also the concept of synthetic aperture with FMCW sensors has already been put forward in literature, and some experimental systems have been described. However, the practical feasibility of an *airborne FMCW SAR was not evident*; the experimental sensors described in literature were, in fact, radars mounted on rail supports operating in ground SAR configurations and at short distances. The FMCW radars could perform measurements in each position of the synthetic aperture and then be moved to the next one. As in conventional pulse SAR systems, the stop-and-go approximation could be used; such an approximation assumes the radar platform stationary during the transmission of the electromagnetic pulses and the reception of the corresponding echoes. For airborne FMCW radars, however, the stop-and-go approximation can be not valid anymore because the platform is actually moving while continuously transmitting. A complete model for the deramped FMCW SAR signal *was missing in the literature.*

In addition to the particular signal aspects relative to the combination of FMCW technology and SAR techniques, the use of FMCW radars for long range high resolution applications

was not evident. In practical FMCW sensors, specially when using cheap components, the presence of unwanted non-linearities in the frequency modulation severely degrades the radar performances for long distances. Again, proper processing methods to overcome such limitation due to frequency non-linearities *were not available* to the scientific community.

Therefore, the area of FMCW SAR airborne observation and related signal processing aspects was a very novel field of research. At the International Research Centre for Telecommunications and Radar (IRCTR) of the Delft University of Technology, a project was initiated to investigate the feasibility of FMCW SAR in the field of airborne earth observation and to develop proper processing algorithms to fully exploit the capability of such sensors.

Within the framework of the project, the following novelties and main results have been reached and are presented in the thesis:

Non-linearities correction. The author has developed a very novel processing solution, which completely solves the problem of the presence of frequency non-linearities in FMCW SAR. It corrects for the non-linearity effects for the whole range profile at once, and it allows a perfect range focussing, independently of the looking angle. The proposed method operates directly on the deramped data and it is very computationally efficient.

A complete FMCW SAR signal model. The author has proposed a detailed analytical model for the FMCW SAR signal in the two-dimensional frequency domain. Based on this model, proper algorithms have been developed which guarantee the best performance when processing FMCW SAR data.

Moving Target Indication (MTI) with frequency modulated CW SAR. Two SAR MTI methods are proposed. The first is based on the frequency slope diversity in the transmitted modulation by using linear triangular FMCW SAR, while the second makes use of the Doppler filtering properties of randomized SFCW modulations.

First demonstration of an X-band FMCW SAR. A flight test campaign has been organized during the last part of 2005. The results were very successful. The feasibility of an operational FMCW SAR based on cheap components has been proved under practical circumstances. Thanks to the special algorithms developed, FMCW SAR images with a measured 45 cm times 25 cm resolution (including windowing) were obtained for the first time.

Samenvatting

In het veld van airborne aardobservatie is er bijzondere aandacht voor compacte, rendabele, hoge resolutie beeldvorming sensoren. Deze sensoren zullen in de toekomst een belangrijke rol spelen in kleine remote sensing toepassingen, zoals het controleren van dijken, waterwegen of snelwegen. Tevens zijn zulke sensoren interessant voor militaire doeleinden; verkennings taken kunnen worden uitgevoerd met kleine onbemande vliegtuigen, hiermee wordt het gevaar voor de eigen troepen verkleind.

Om het mogelijk te maken om zulke systemen te besturen vanuit kleine, zelfs onbemande vliegtuigen, moeten deze weinig energie verbruiken en klein genoeg zijn om aan de strikte laadvermogens eisen te voldoen. Tevens moet het rendabel zijn voor de niet-militaire markt.

Frequency Modulated Continuous Wave (FMCW) radar systemen zijn over het algemeen compact en betrekkelijk goedkoop om aan te schaffen en te exploiteren. Ze verbruiken weinig energie en tengevolge van het feit dat ze constant in gebruik zijn, kunnen ze maar een bescheiden vermogen uitzenden, die deze systemen heel interessant maakt voor militaire operaties. Derhalve is FMCW radar technologie interessant voor airborne aard observatie toepassingen, speciaal in combinatie met hoge resolutie *Synthetic Aperture Radar* (SAR) technieken. De vernieuwende combinatie van FMCW technologie en SAR technieken leidt tot het ontwikkelen van een kleine, lichtgewicht en rendabele hoge resolutie beeldverwerkingssensor.

SAR technieken zijn succesvol toegepast in combinatie met coherente puls radars. Ook is het concept van synthetic aperture met FMCW-sensoren reeds behandeld in de literatuur en zijn er enkele experimentele systemen beschreven. De praktische haalbaarheid van een luchtmobiele FMCW SAR *was echter niet direct duidelijk*; de experimentele sensoren die in de literatuur beschreven werden, waren in feite radars gemonteerd op 'rail supports', opererend in grondgebonden SAR-configuraties en op korte afstanden. De FMCW radars konden in elke positie van de 'synthetic aperture' metingen verrichten en daarna verplaatst worden naar de volgende. Zoals bij conventionele puls SAR systemen kon de stop-and-go benadering gebruikt worden; zo'n benadering neemt aan dat het radarplatform niet beweegt gedurende het uitzenden van de elektromagnetische pulsen en het ontvangen van de corresponderende echos. Echter, voor luchtmobiele FMCW-radars kan de stop-and-go benadering niet meer geldig zijn, omdat het platform in werkelijkheid beweegt terwijl het continu uitzendt. Een compleet model voor het deramped FMCW SAR signaal *ontbrak in de literatuur*.

Naast de specifieke signaalaspecten met betrekking tot de combinatie van FMCW tecnologie en SAR technieken, was het gebruik van FMCW radars voor lange afstands hoge

resolutie toepassingen niet vanzelfsprekend. In praktische FMCW sensoren, in het bijzonder wanneer goedkope componenten worden gebruikt, doet de aanwezigheid van ongewenste non-lineariteiten in de frequentie modulatie ernstige afbreuk aan het resultaat van de radar op lange afstanden. Ook in dit geval waren goede verwerkingsmethoden om zulke beperkingen als gevolg van frequentie non-lineariteiten op te heffen *niet beschikbaar* in de wetenschappelijke gemeenschap.

Dus, het gebied van FMCW SAR airborne observatie en aanverwante signal processing aspekten was een heel nieuw veld van onderzoek. In het International Research Centre for Telecommunications and Radar (IRCTR) van de Technische Universiteit in Delft, is een project geinitierd om de uitvoerbaarheid van FMCW SAR te onderzoeken op het gebied van airborne aard observatie.

In het kader van het project zijn verscheidene innovatieve signaalverwerkingstechnieken en een gedetailleerd FMCW SAR signaalmodel ontwikkeld. Deze technieken en het model worden uitgebreid beschreven in dit proefschrift.

Methode om niet-lineariteiten te corrigeren. De auteur heeft een nieuwe methode ontwikkeld waarmee het probleem van niet-lineariteiten in de frequentiezwaai voor FMCW systemen opgelost kan worden. Met deze methode kan een afstandsprofiel in één keer gecorrigeerd worden en is perfecte focusering van het afstandsprofiel mogelijk, onafhankelijk van de invalshoek van de radarbundel. De gepresenteerde methode werkt direct op de gedemoduleerde afstandsdata en vergt weinig rekenkracht.

Gedetailleerd FMCW SAR signaalmodel. De auteur heeft een gedetailleerd analytisch FMCW SAR signaalmodel ontwikkeld in het twee-dimensionale frequentiedomein. Met behulp van dit model zijn nieuwe SAR signaalverwerkingsalgorithmen uitgewerkt speciaal toegespitst op FMCW SAR data.

MTI met frequentie gemoduleerde CW SAR. Er worden twee SAR MTI methoden voorgesteld. De eerste is gebaseerd op de 'frequency slope diversity" in de uitgezonden modulatie door gebruik te maken van lineaire driehoekvorm FMCW SAR, terwijl de tweede gebruik maakt van de Doppler filtering eigenschappen van 'randomized' SFCW modulatie.

Eerste demonstratie van een X-band FMCW SAR. Een meetcampagne, om onder praktische omstandigheden de toepasbaarheid van een operationele, met standaardcomponenten gebouwde, FMCW SAR te testen, was uitgevoerd in 2005. De resultaten waren erg goed. Door toepassing van speciale algoritmes konden voor het eerst beelden worden verkregen met een nauwkeurigheid van 25 bij 45 cm.

Author's publications

Patent

[1] A. Meta, P. Hoogeboom and L.P. Ligthart, "Range Frequency non-linearity correction for FMCW SAR", European Patent Application No. 06076057.6, May 2006.

Journals

[2] A. Meta, P. Hoogeboom and L.P. Ligthart, "Signal Processing for FMCW SAR", in *IEEE Trans. Geoscience Remote Sensing*, submitted.

[3] J.J.M. de Wit, A. Meta and P. Hoogeboom, "Modified Range-Doppler Processing for FM-CW Synthetic Aperture Radar", *IEEE Geoscience and Remote Sensing Letters*, vol. 3, no. 1, Jan. 2006, pp. 83-87.

Conferences

[4] A. Meta, P. Hoogeboom and L.P. Ligthart, "Non-linear Frequency Scaling Algorithm for FMCW SAR Data", in *Proc. European Radar Conference EuRAD'06*, Manchester, UK, Sep. 2006, in press.

[5] A. Meta, P. Hoogeboom and L.P. Ligthart, "Range non-linearities correction in FMCW SAR", in *Proc. IEEE Int. Geoscience and Remote Sensing Symp. IGARSS'06*, Denver, CO, USA, July 2006.

[6] A. Meta, P. Hakkaart, F. van der Zwan, P. Hoogeboom and L.P. Ligthart, "First demonstration of an X-band airborne FMCW SAR," in *Proc. European Conf. on Synthetic Aperture Radar EUSAR'06*, Dresden, Germany, May 2006.

[7] A. Meta, P. Hoogebbom and L. P. Ligthart, "Correction of the effects induced by the continuous motion in FMCW SAR," in *Proc. IEEE Radar Conf. '06*, Verona, NY, USA, Apr. 2006, pp. 358-365.

[8] A. Meta, P. Hoogeboom and L. P. Ligthart, "Moving Target Indication enhancement in FMCW SAR using deramped randomized stepped-frequency signals," in *Proc. Waveform Diversity and Design Conf. WDDC'06*, Lihue, HI, USA, Jan. 2006.

[9] A. Meta, J.F.M. Lorga, J.J.M. de Wit and P. Hoogeboom, "Motion Compensation for a High Resolution Ka-band Airborne FM-CW SAR," in *Proc. European Radar Conf. EuRAD '05*, Paris, France, Oct. 2005, pp. 391-394.

[10] A. Meta and P. Hoogeboom, "Signal Processing for High Resolution FMCW SAR and Moving Targets," in *Proc. Int. Radar Symp. IRS '05*, Berlin, Germany, Sep. 2005, pp. 127-132.

[11] J.F.M. Lorga, A. Meta, J.J.M. de Wit, P. Hoogeboom and J.A. Mulder, "Airborne FM-CW SAR and Integrated Navigation System Data Fusion," in *Proc. AIAA Guidance, Navigation, Control Conf. GNC'05*, San Francisco, USA, Aug. 2005, pp. 201-205.

[12] A. Meta and P. Hoogeboom, "Signal Processing Algorithms for FMCW Moving Target Indicator Synthetic Aperture Radar," in *Proc. IEEE Int. Geoscience and Remote Sensing Symp. IGARSS'05*, Seoul, Korea, July 2005, pp. 316-319.

[13] A. Meta and P. Hoogeboom, "Development of Signal Processing Algorithms for High resolution Airborne Millimeter Wave FMCW SAR," in *Proc. IEEE Int. Radar Conf. '05*, Arlington, U.S.A., May 2005, pp. 326-331.

[14] P. Hoogeboom, J.J.M. de Wit, A. Meta and J. Figueras i Ventura, "FM-CW Based Miniature SAR Systems for Small UAV's," in *Proc. NATO SET-092 Symposium on Advanced Sensor Payloads for Unmanned Aerial Vehicles*, Lisboa, Portugal, May 2005, pp. 26.1-26.12.

[15] A. Meta, J.J.M. de Wit and P. Hoogeboom, "Development of High Resolution Airborne Millimeter Wave FM-CW SAR," in *Proc. European Radar Conf. EuRAD'04*, Amsterdam, The Netherlands, Oct. 2004, pp. 209-212.

[16] A. Meta and P. Hoogeboom, "High Resolution Airborne FMCW SAR: Preliminary Results," in *Proc. European Conf. on Synthetic Aperture Radar EUSAR '04*, Neu-Ulm, Germany, May 2004, vol. 1, pp. 183-186.

[17] J.J.M. de Wit, A. Meta and P. Hoogeboom, "First Airborne FM-CW SAR Campaign: Preliminary Results," in *Proc. Int. Radar Symp. IRS '04*, Warszawa, Poland, May 2004, pp. 165-170.

[18] A. Meta and P. Hoogeboom, "Time Analysis and Processing of FM-CW SAR signals," in *Proc. Int. Radar Symp. IRS'03*, Dresden, Germany, Sept. 2003, pp. 263-268.

[19] A. Meta and P. Hoogeboom, "High Resolution Airborne FM-CW SAR: Digital Signal Processing Aspects," in *Proc. Int. Geoscience and Remote Sensing Symp. IGARSS '03*, Toulouse, France, July 2003, vol. VI, pp. 4074-4076.

Acknowledgements

I would like to express my gratitude to all those who helped to make this Ph.D. thesis possible.

First of all, I would like to thank my supervisors Prof. Peter Hoogeboom and Prof. Leo Ligthart for having given me the possibility of working on the FMCW SAR project.

At IRCTR, I am very grateful to Jacco de Wit for the nice time we had working together and for all he did in designing and assembling the acquisition and controlling part of the FMCW SAR system within the frame of his Ph.D. Additionally, his dissertation was a valuable starting point for the writing of this thesis. The technical assistance received by Paul Hakkaart and Fred van der Zwan in building the FMCW front-end is very appreciated. Without this in-house work, most of the results of the thesis would not have been reached.

At TNO Defence, Securety and Safety I would like to acknowledge Matern Otten, Wim van Rossum and Wouter Vlothuizen for the time they spent with me in very useful discussions about SAR related subjects.

Hartmut Winter, pilot of Stemme company, is gratefully thanked for his help during the preparation of the test campaign. During the measurements, I certainly liked the experience of being his passenger in the Stemme S10 motor glider.

I want to thank Jose Lorga from Aerospace faculty of TU Delft for having provided the motion sensors he was working on. Although the IMU-FMCW SAR joint experiment failed to produce good results during the 2004 flight campaign, it provided very good experience.

I would like to express my gratitude to my colleagues at IRCTR. I enjoyed working in the nice, international and stimulating atmosphere they contribute to create. The weekly IRCPR is certainly a good memory I have of these four years in Delft.

I appreciate the assistance provided by Laura Bauman, Mia van der Voort and Dominique Meijer. They have been always very kind in helping me with all administrative matters.

Outside the working hours, I was never alone and for this I thank all the friends of Delft, particularly Marco Pausini and George Papaefthymiou for having agreed to serve as "paranimf" during my Ph.D. defense. And, of course, my friends from Roccasecca, which were (and are!) always close to me in spite of the distance.

Finally, I am indebted to Verena for her understanding and for all the time I stole from her. The future with our little Andrea is a long journey; sometimes it will be difficult, but no great and challenging experience is easy.

Adriano Meta
Delft, 8 August 2006

About the author

Adriano Meta was born in Pontecorvo, Italy, on August 8, 1978. He received his Laurea degree in Telecommunication Engineering from University of Rome "La Sapienza", Italy, in 2002, completing the whole programme in four years and an half with the maximum grade, within the best 0.5% of the students. In 2000, he spent a fruitful academic year at Gent University of Technology, Belgium, within the framework of the Erasmus project.

He joined the International Research Centre for Telecommunications and Radar at Delft University of Technology, The Netherlands, in 2002 where he started working towards his Ph.D. degree. Adriano Meta is author of almost 20 papers on FMCW SAR signal processing for some of which he was awarded the Best Student Paper prize. A patent application is pending on the FMCW SAR frequency non-linearity correction he developed.

He has attended the post lauream Aerospace School, University of Rome "La Sapienza", Italy.

He is currently employed at the DLR (Deutsches Zentrum für Luft und Raumfahrt - German Aerospace Center) in Oberpfaffenhofen, Germany, where is involved in the TerraSAR-X project.

Awards

Best Student Paper Award, European Conf. on Synthetic Aperture Radar EUSAR'06, Dresden, Germany, May 2006.
Awarded for the article entitled: *"First demonstration of an X-band airborne FMCW SAR"*.

Second Student Paper Award, IEEE Int. Geoscience and Remote Sensing Symp. IGARSS'06, Denver, CO, USA, July 2006.
Awarded for the article entitled: *"Range non-linearities correction in FMCW SAR"*.

Best Student Paper Award, Waveform Diversity and Design Conf. WDDC'06, Lihue, HI, USA, Jan. 2006.
Awarded for the article entitled: *"Moving Target Indication enhancement in FMCW SAR using deramped randomized stepped-frequency signals"*.